Sensitive and High-throughput Detection, Separation and Analysis of Circulating Tumor Cells

Mengxia Zhao

A dissertation

submitted in partial fulfillment of the

requirements for the degree of

Doctor of Philosophy

University of Washington

2013

Reading Committee:

Daniel T. Chiu, Chair

Robert E. Synovec

Qinghua Feng

Program Authorized to Offer Degree:

Department of Chemistry

University of Washington

Abstract

Sensitive and High-throughput Detection, Separation and Analysis of Circulating Tumor Cells

Mengxia Zhao

Chair of the Supervisory Committee:

Professor Daniel T. Chiu

Department of Chemistry

This dissertation describes novel methods to detect, separate and analyze circulating tumor cells (CTCs) from peripheral blood, with a high sensitivity and throughput. The ensemble-decision aliquot ranking (eDAR) platform is a new method for isolating CTCs from cancer patients with a recovery ratio of 93% and a zero false positive rate. We have validated this method by analyzing the samples from breast, pancreatic and lung cancer patients. The capability to perform downstream analyses on the isolated CTCs were also tested and integrated into the eDAR platform. We developed a method that can monitor eight protein markers, using a sequential staining and photobleaching procedure. Single-cell isolation and culture of the trapped CTCs were also tested. Based on these, we re-designed the eDAR platform by applying a new active cell sorting scheme and a new further purification method. Because many applications in the CTC area are focused on the enumeration, we also developed an automated method for counting tumor cells in whole blood samples. This enumeration method was validated by a side-by-side comparison with CellSearch, the only FDA approved method at present, in 90 metastatic breast cancer patient samples. These tools facilitate fundamental investigation of rare cells, as well as developing non-invasive biopsy to improve the clinical treatment.

Dedicated to my parents, Wei Zhang and Wuxin Zhao,

and my wife, Yuanhua Cheng.

Acknowledgement

It has been my fortune to be guided and helped by excellent people through my life as a graduate student in University of Washington. My advisor, Prof. Daniel Chiu, has been a remarkable advisor for his far sighted scientific vision as well as experienced practical lab advice. I would never have finished the project without his expert guidance, valuable suggestions, constructive criticism and persistent supervision. He provided me with the independence, flexibility and funds to work on some really challenging projects reported here.

It is an honor to work with the past and present group members, especially the people working with me in the CTC project. I would like to thank Dr. Jason Kuo and Dr. Perry Schiro, who worked with me from the very beginning of this project and taught me so many things for optics, fluidics and electronics. I also shared the credit of my work with Dr. Wyatt Nelson, who is an excellent scientist, especially for micro-fabrication. This project was fueled by many research groups collaborating with us. I wish to thank Prof. Daniel Sabbath, Prof. Qinghua Feng, Prof. Samuel Whiting, Prof. Keith Eaton, and Prof. Hubert Vesselle for their collaboration, academic advice and insightful opinions contributed to my dissertation. Furthermore, I cannot find words to express my gratitude to all the patients who enabled the studies, as well as all the clinical coordinators who smoothed the projects dramatically.

My education has been guided by a series of excellent teachers and researchers. I wish to express the special thanks to my undergraduate and master advisor, Prof. Xinrong Zhang in Tsinghua Univ., who gave me the first opportunity to work in a research lab, taught me how to play with analytical instruments and fueled my love for science.

My parents, Wei Zhang and Wuxin Zhao, have always been there for me with unconditional love and support. It is impossible to complete this work without their love and understanding. I give the most special thanks to my wife, Yuanhua Cheng for her love, encouragement, patience, and tolerance of my occasional childish mood throughout this journey.

Table of Contents

Dedication i

Acknowledgement ii

List of Figures vi

List of Tables ix

Chapter 1 Introduction ..... - 1 -

1.1 Cancer Metastasis and Circulating Tumor Cells (CTCs) ..... - 1 -

1.2 Current Technologies for CTC analysis ..... - 4 -

1.2.1 Technological challenges ..... - 4 -

1.2.2 CTC Methods Based on Physical Properties ..... - 6 -

1.2.3 CTC methods based on biological properties ..... - 7 -

1.3 Project Overview ..... - 8 -

Chapter 2 Detection and Isolation of CTCs Using Ensemble Decision Aliquot Ranking (eDAR) ..... - 12 -

2.1 Introduction ..... - 12 -

2.2 Results and Discussion ..... - 13 -

2.2.1 Overview of System ..... - 13 -

2.2.2 Individual Components of eDAR ..... - 14 -

2.2.3 Overall Performance of eDAR ..... - 24 -

2.2.4 Isolation of CTCs from Metastatic Breast, Lung and Pancreatic Cancer Patients using eDAR ..... - 26 -

2.3 Materials and Methods ..... - 31 -

2.3.1 Chip Fabrication and Multi-layer Structure Integration ..... - 31 -

2.3.2 Biological Material and Blood ..... - 33 -

2.3.3 Sample Preparation and Antibody Labeling ..... - 34 -

2.3.4 Electronics and Program Control for eDAR ..... - 36 -
2.4 Conclusion ..... - 38 -
Chapter 3 Subsequent Analyses and Manipulation of Single CTCs Captured on eDAR Platform ..... - 40 -
3.1 Introduction ..... - 40 -
3.2 Results and Discussion ..... - 42 -
3.2.1 CTCs Isolated by eDAR ..... - 43 -
3.2.2 General Scheme for the Sequential Immunostaining and Photobleaching Process ..... - 45 -
3.2.3 Characterization and Optimization of the Photobleaching Process ..... - 47 -
3.2.4 Sequential Immunostaining and Photobleaching Tests ..... - 48 -
3.2.5 Single-Cell Manipulation and Culture of captured CTCs ..... - 51 -
3.3. Materials and methods ..... - 53 -
3.3.1 Microfluidic Components and Line-confocal Optics ..... - 53 -
3.3.2 Biological materials and eDAR process ..... - 53 -
3.3.3 Sequential Immunostaining and Photobleaching Process ..... - 55 -
3.3.4 Safety Consideration for the Photobleaching Process. ..... - 56 -
3.4. Conclusion ..... - 57 -
Chapter 4 The Second Generation of eDAR with a Simplified Structure and an Improved Performance ..... - 58 -
4.1 Introduction ..... - 58 -
4.2 Results and Discussion ..... - 60 -
4.2.1 Redesigned Hydrodynamic Switching Scheme ..... - 60 -
4.2.2 On-chip Purification Component Based on Microslits ..... - 66 -
4.2.3 Characterization and Analytical Performance ..... - 69 -
4.3 Materials and Methods ..... - 76 -
4.3.1 Design and Fabrication of the Microfluidic Chips ..... - 76 -

4.3.2 Biological Materials and Patient Samples ..... - 77 -
4.3.3 Sample Preparation and eDAR Analysis ..... - 78 -
4.4 Conclusion ..... - 79 -
Chapter 5 An Automated and High-throughput Counting Method for CTCs ..... - 81 -
5.1 Introduction ..... - 81 -
5.2 Results and discussion ..... - 82 -
5.2.1 General Description of the System and Data Analysis ..... - 82 -
5.2.2 Background Level of Detected CTCs from Healthy donors and the Recovery Performance of the Flow Counting Method ..... - 86 -
5.2.3 Alternative Labeling and Detection Schemes ..... - 89 -
5.2.4 Results of Clinical Samples ..... - 91 -
5.3 Materials and Methods ..... - 98 -
5.3.1 Design and Fabrication of Microfluidic Devices ..... - 98 -
5.3.2 Biological and clinical materials ..... - 98 -
5.3.3 Line-confocal Detection Scheme ..... - 99 -
5.4 Conclusion ..... - 102 -
Chapter 6 Conclusion and Perspective ..... - 104 -
References ..... - 105 -
Vita ..... - 113 -

List of Figures

Figure 1.1 General strategies for isolating CTCs. - 6 -

Figure 2.1 Schematic and images showing the general concept of eDAR. - 15 -

Figure 2.2 Aliquot detection system. - 17 -

Figure 2.3 Signal to noise ratio of the line-confocal detection scheme. - 18 -

Figure 2.4 General scheme of the Aliquot sorting. - 20 -

Figure 2.5 The effectiveness of the aliquot sorting. - 21 -

Figure 2.6. Aliquot sorting efficiency. - 22 -

Figure 2.7 The cell capture chamber of eDAR. - 23 -

Figure 2.8 Recovery and false positive performance of eDAR. - 25 -

Figure 2.9 Clinical results for CTCs isolated from blood samples drawn from breast cancer patients. - 27 -

Figure 2.10 CTCs from pancreatic and lung cancer patients analyzed by eDAR. - 29 -

Figure 2.11 The six layers of the final eDAR chip - 32 -

Figure 2.12 Photograph of an eDAR chip. - 33 -

Figure 2.13 Blood preparation. - 36 -

Figure 2.14 The electonics and information flow of eDAR. - 37 -

Figure 2.15 Optimization of the applied air pressures to the side buffer channels. - 38 -

Figure 3.1 Cells captured by eDAR for downstream analysis. - 43 -

Figure 3.2 General scheme and procedure of the sequential immunostaining and photobleaching tests. - 46 -

Figure 3.4 Sequential immunostaining and photobleaching results for six cancer cells trapped on an eDAR chip. - 49 -

Figure 3.5 Fluorescence images of the four cancer cells captured on eDAR with Her2+/MUC1- character. ..... - 50 -
Figure 3.6 Single-cell removal on eDAR platform. ..... - 52 -
Figure 3.7 Single-cell culture of captured CTCs. ..... - 52 -
Figure 4.1 Summary of the 8 hydrodynamic switching schemes. ..... - 61 -
Figure 4.2 Microfluidic chip and hydrodynamic switching scheme of eDAR. ..... - 64 -
Figure 4.3 Switching time for the current fluidic scheme recorded by high speed camera. .... - 66 -
Figure 4.4 Micro-slits and multi-color fluorescence imaging of captured CTCs. ..... - 67 -
Figure 4.5 Transit time of the sorted CTCs. ..... - 70 -
Figure 4.6 Sorting efficiency and recovery performance of eDAR. ..... - 72 -
Figure 4.7 A CTC cluster with low EpCAM expression from a pancreatic cancer sample (No. 20). The scale bar is 100 μm. ..... - 75 -
Figure 4.8 The distribution of control and pancreatic patient samples analyzed by eDAR. .... - 76 -
Figure 4.9 The process flow the micro fabrication steps. ..... - 77 -
Figure 5.1 Schematic and data illustrating the flow-detection platform. ..... - 83 -
Figure 5.2 Sigmoidal burst filtering to improve the S/N. ..... - 85 -
Figure 5.3 The distribution of signal-to-noise ratio (S/N) of a breast-cancer sample analyzed by the EpCAM/cytokeratin/CD45 method. ..... - 86 -
Figure 5.4 False positive and recovery performance. ..... - 87 -
Figure 5.5 Example of APD data for the detection scheme using EpCAM, Her2 and CD45 as biomarkers. ..... - 90 -
Figure 5.6 The distribution of signal-to-noise ratio (S/N) of a breast-cancer sample analyzed by EpCAM\Her2\CD45 method. ..... - 90 -

Figure 5.7 Clinical results from the CTC flow counting system and CellSearch. ..... - 94 -

Figure 5.8 Side-by-side clinical results for regular CTCs and circulating cells with EpCAM+ / CD44+ / CD24- expression from the CTC flow detection system and CellSearch. ..... - 95 -

Figure 5.9 Comparison of the CTC enumeration results from the same set of patients using eDAR and flow detection system. ..... - 96 -

Figure 5.10 Fluorescence background levels in PE (phycoerythrin) detection channel ..... - 101 -

List of Tables

Table 2.1 eDAR and CellSearch results obtained for 20 breast-cancer patient samples. ..... - 30 -

Table 2.2 Characterization of fluorescence and concentration of antibodies. ..... - 35 -

Table 3.1 Experimental details of the four rounds of immunostaining and photobleaching. . - 56 -

Table 4.1 Summary of the fluidic configuration and performance of the 8 sorting schemes. - 63 -

Table 4.2 Raw data of the healthy control (n=15) and the pancreatic cancer samples (n=26). - 74 -

Table 5.1 High-throughput flow detection and CellSearch results obtained for 90 breast-cancer patient samples. ..... - 98 -

Chapter 1 Introduction

1.1 Cancer Metastasis and Circulating Tumor Cells (CTCs)

Cancer, the uncontrolled growth and spread of cells, is a leading cause of human deaths worldwide [1-2]. Metastasis is generally considered the most important clinical indicator of cancer [3-4]. Over 90% of deaths associated with cancer are directly attributable to metastasis [5]. During metastatic process, cancer cells are released from primary tumor, and then follow the two steps sequentially: (1) Cells from the primary tumor are physically translocated to the distant organs; and then (2) invade the microenvironment and proliferate to a secondary tumor [6].

The release of cancer cells from the primary tumor may happen at very early stages of the disease [7-8], which is the basis for the later development of metastasis. Circulating tumor cells (CTCs), defined as the cancer cells shed into the bloodstream from the primary tumor [9-11], are thought to be an important part of cancer metastasis in the "seed and soil" theory [12-13]. In this theory, secondary tumor will be developed when the tumor cells survive in circulation and seed in the host environment (the "soil").

CTCs have been found in the peripheral blood of all major carcinomas [14], such as breast [11, 15-16], lung [17-18], pancreatic [19-20], prostate [21-22], liver [23] and colon [24-25]. Detection and analysis of CTCs can benefit the early diagnosis of cancers [26-27], management of clinical treatment of cancer patients [15], development of personalized medicine [28], and exploring the

mechanism of metastasis [4-5, 9], which is thought to be the most poorly understood component of cancer pathogenesis [6].

Many studies proved that the number of CTCs directly correlates with the clinical outcome in metastatic patients, providing valuable prognostic information that can be helpful to manage the clinical care of these patients [29-30]. Cristofanilli *et al.* indicated that the presence of CTCs in peripheral blood from metastatic breast cancer patients has an adverse prognostic value [31]. The analysis of 177 patients showed the increased number of CTCs at baseline predicted a short progression free survival (PFS), and median overall survival (OS) time (2.7 and 10 months, respectively), compared to the low or negative CTCs corresponding to PFS and OS of 7 and more than 18 months. This result was further confirmed by a multi-center study, showing that the number of CTCs can predict the effect of treatment on metastatic breast cancer patients statistically [32]. Similarly, the clinical usefulness of CTC enumeration has been demonstrated in other types of metastatic cancers, such as the lung [33], colorectal [34] and prostate cancer [22].

For non-metastatic patients, the enumeration of CTCs was also proved to be valuable for the prognosis. After analyzing the CTCs from 302 non-metastatic breast cancer patients, Lucci *et al.* showed that the detection of CTCs predicted both decreased PFS and OS [35]. Another study performed by Pierga *et al.* reported that CTC enumeration for early stage breast cancer patients before chemotherapy was an independent prognostic factor for OS [36].

The presence and absence of CTCs determined during the follow-up of patients receiving the treatment has been proved informative for response evaluation, which may be helpful to

personalize the therapy on each patient [37]. Previous study demonstrated that the number of CTCs in breast cancer patients at four weeks after the start of chemotherapy was a more robust and earlier predictor of survival, compared to imaging studies before and after a median of 10 weeks from the beginning of the chemotherapy [38]. Another work confirmed that the CTC counts in patients with breast cancer were correlated with radiological signs of disease progression as well [39].

Although most of the CTC technologies focus on the enumeration, more and more studies showed that the genetic and molecular analyses of CTCs may be more important than simple enumeration [40]. These analyses can help us to understand the characteristics of CTCs compared to primary tumor, and explore the genes associated with the migration of cancer cells and the development of secondary tumor. Yu *et al* analyzed the RNA sequence of CTCs from a genetically engineered mouse model, and suggest that the non-carnonical WNT signaling pathway may contribute to metastasis in human pancreatic cancer [41]. Downstream analysis on CTCs can also verify some biological and clinical hypotheses by studying the expression of biomarkers on CTCs. For example, a recent study demonstrated that the epithelial-mesenchymal transition (EMT) plays an important role in the blood-borne dissemination of breast cancer, by analyzing the expression of epithelial and mesenchymal markers on CTCs [42].

1.2 Current Technologies for CTC analysis

1.2.1 Technological challenges

CTCs were first reported about 150 years ago [43], however, studies on this type of rare cells only emerged in large numbers in the last decade [10]. This was due to several technological challenges. The first challenge is the very low concentration of CTCs (typically 1 to 10 cells per 1 billion of blood cells) [44-45], which would require a high sensitivity on single-cell level with an acceptable throughput. For example, some traditional methods, such as flow cytometry, have a sensitivity on single-cell level, however, the throughput is too low for CTC analysis (> 24 h per 1 mL of whole blood) [46]. To overcome this challenge, most present CTC methods would require an initial enrichment step to improve the sensitivity and throughput, and the enrichment ratio determines to a large extent their analytical performance and potential applications. The throughput of these methods varies considerably, and fluorescence imaging, which is used in most CTC technologies, usually takes a long time and requires manual confirmation of cells.

The second challenge comes from the heterogeneity of cancer cells, whose physical and biological attributes can vary significantly within CTC populations and over time. Many present methods are positive selections based on a biological property, such as the widely used surface antigen, epithelial cell adhesion molecule (EpCAM) [47], or a physical property, e.g. the size or density of CTCs [48]. However, simply replying on one factor may lose the subpopulation of CTCs, which is negative to that marker. For example, filtration method is widely used to capture CTCs, however, due the heterogeneity of cancer cells, CTCs with a small size might be lost. For example. previous

study showed that the average size of CTCs from lung cancer patients captured by two different methods, immune-magnetic separation and filtration, differed significantly [49].

Negative selections [50-52], usually the removal of blood cells, could also isolate CTCs, however, the low purity limits the application of this type of method [48]. Therefore, in this dissertation I will focus on the methods based on positive selections, which can be generally summarized as two groups, selections based on physical or biological properties (Figure 1.1).

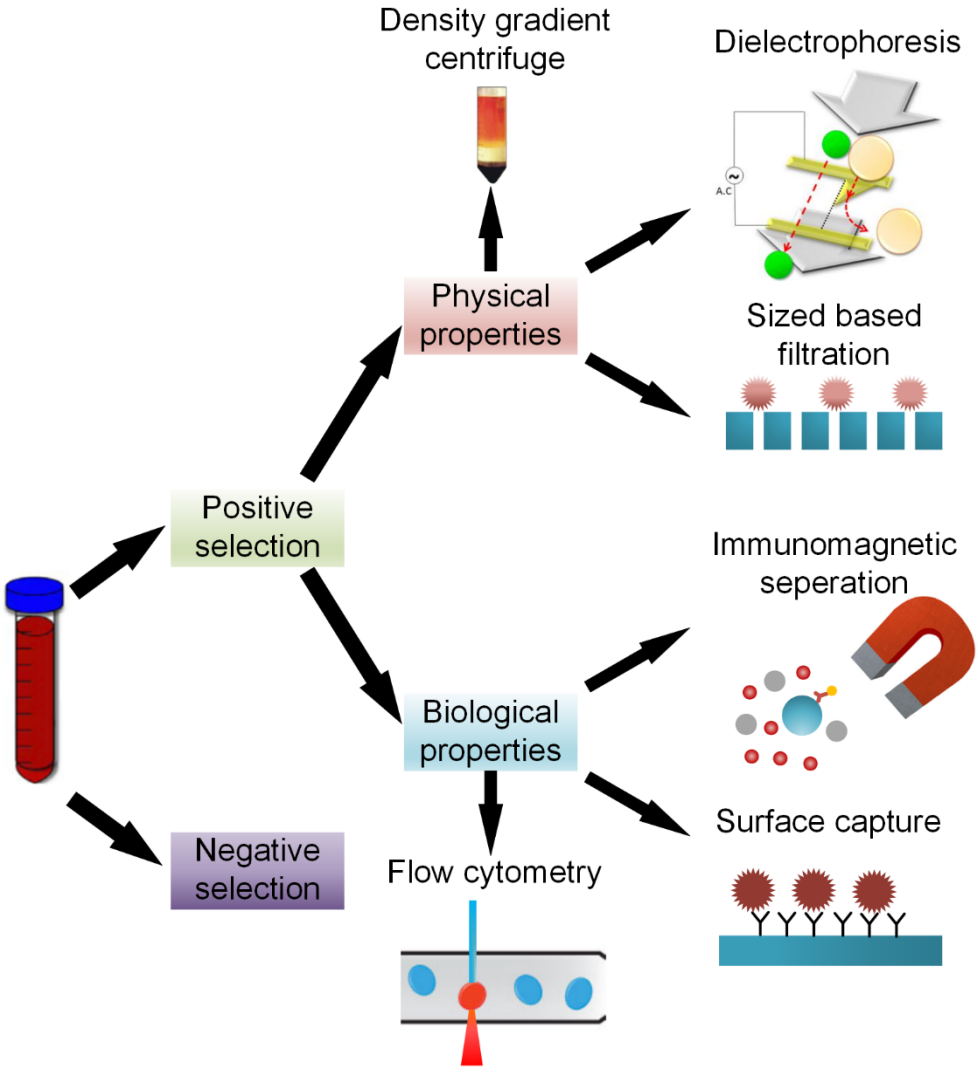

Figure 1.1 General strategies for isolating CTCs. The isolation of CTCs is based on either positive selection or negative selection. The positive selection methods are based on either a physical property or a biological property. RNA based enumeration methods are not included in this figure, because it is generally not considered as a cellular method, and cannot physically isolate CTCs.

1.2.2 CTC Methods Based on Physical Properties

Tumor cells are often considered bigger than blood cells, so a lot of CTC enrichment methods were performed using filtration. Traditional filters, such as the track etched plastic filter, could be directly used to capture CTCs. Isolation by size of epithelial tumor cells (ISET) utilized track etched polycarbonate filter with 8-μm diameter pores to trap CTCs [53]. Other types of filters, especially the ones made by micro-fabrication, have a more uniform pattern of micro-slots, which were also used for CTC isolation [54-57]. Generally, filtration based method has a high throughput, and does not depend on any particular bio-markers, however, there is always a chance to lose small cells, and the purity of CTCs could be low.

Other physical properties were also used to isolate CTCs, such as the density, electric properties, or deformability. Density gradient centrifugation, a standard protocol used to separate mononuclear cells from peripheral blood, was also applied in some CTC methods [58]. However, considering this method could not separate CTCs from white blood cells (WBCs), another enrichment or characterization method was often required [59]. Many technologies separate CTCs based on dielectrophoresis, which usually has a high throughput but a relatively low capture efficiency [60]. Deformability-based CTC enrichment methods was also reported recently [61]. CTC methods based on physical properties were generally considered as "label free" techniques, and usually has a higher throughput [62].

1.2.3 CTC methods based on biological properties

Surface antigens are frequently used to separate and characterize CTCs, and EpCAM is the most widely used one in this area [47, 63]. Depending on what the antibodies are conjugated with, there are usually two types of schemes for the isolation of CTCs, magnetic separation and affinity chromatography like method.

When cells are labeled with antibodies conjugated with magnetic beads, they could be separated from the majority of the blood cells if a magnetic field is applied. The only U.S Food and Drug Administration (FDA) approved method at present, CellSearch system, is actually based on this scheme [14, 64]. The captured CTCs were further labeled with one more epithelial marker, cytokeratin, a negative control marker (CD45), and a nuclear stain marker (4',6-diamidino-2-phenylindole, DAPI) to define and enumerate the cells. This system has been proved for its prognostic potential, however, several studies showed that it only detected CTCs from a fraction of metastatic patients with a low sensitivity [32]. Other methods based on immuno-magnetic separation were also reported [65].

If the antibodies are immobilized onto a surface, they can capture CTCs when the blood sample flows through that surface, which is similar to traditional antibody affinity chromatography methods [66-68]. These methods are able to analyze unprocessed whole blood, with excellent detection of CTCs in cancer patients, and are friendly for downstream analysis. The captured CTCs, however can be difficult to remove from the surface without cleaving cell surface proteins (e.g. with Trypsin) and thus potentially stressing the cells. Subsequent imaging of the captured CTCs can also be time consuming, owing to the large area over which images must be taken.

Therefore, the throughput is usually limited (> 1 mL per 2 hours) in these affinity chromatography like methods.

It is worth to point out that, methods based on biological properties could be further enhanced by the incorporation with another method based on physical properties. For example, in surface capture methods, it is important to increase the probability of CTCs collision with the antibodies immobilized on the surface, so a higher capture efficiencies could be achieved. However, increasing this collision probability for all sample cells will increase the chance of non-specific binding as well. Gleghorn *et al* reported a microfluidic device coated with a monoclonal antibody to selectively increase the chance of cell–surface collisions for prostate CTCs, rather than all cells in the blood [69].

For biological property based methods, there is a chance for them to be limited by the usage of bio-markers. Surface antigens such as EpCAM are widely used to select CTCs [47, 63], however, previous studies show that simply relying on one biomarker may not be adequate to define the whole population of CTCs. It has been proved that the tumor cells with low EpCAM expression have more mesenchymal characteristics [70], and might correlate with cancer progression closely. Other studies showed that, a method based on EpCAM (CellSearch), could not detect the CTCs with low or non EpCAM expression [63, 70].

1.3 Project Overview

This dissertation summarizes my research from January 2009 to June 2013 as a Ph.D, candidate in the Department of Chemistry at University of Washington. The project focused on the

development of analytical methods for CTCs, aiming at providing an "all-in-one" platform to analyze such rare cells. It can be divided into four parts, from chapter 2 to 5.

Chapter 2 focuses on the first CTC method I developed, ensemble-decision aliquot ranking (eDAR). In eDAR, a blood sample is first broken up into nanoliter volumes in a microfluidic device. Each aliquot is ranked based on whether or not a rare cell is present in the ensemble of cells within the aliquot. After sorting the aliquots, the rare cells are isolated from the collected aliquots using an on-chip filtration system. eDAR is well-suited for the enrichment of CTCs, because it can rapidly and efficiently reduce sample complexity by over a million fold. It had a recovery efficiency of over 93% for cultured cancer cells in healthy donor whole blood with a zero false positive rate. I applied eDAR in isolating CTCs from 20 breast-cancer patient samples and carried out a side-by-side comparison between eDAR and CellSearch, which is currently the only system approved for enumerating CTCs by FDA. CellSearch did not identify any CTCs in 12 out of 20 patient samples and found more than 2 CTCs in only 4 samples; eDAR isolated CTCs from all 20 patient samples with a range of 11 to 105 CTCs. Furthermore, we were able to detect cancer stem cells, as determined by CD^{44+} / $CD^{24-/low}$, within the isolated CTCs from these patients. Blood sample from patients with pancreatic and lung cancer were also tested on this platform. Importantly, eDAR isolated the rare cells within a small field-of-view (<1 mm^2), and provided direct easy access to individual live CTCs.

The third chapter focuses on the methodological development of subsequent analyses on CTCs, including two parts. The first part is to image protein markers in CTCs captured by eDAR using sequential immunostaining and photobleaching. eDAR is a high-throughput method that allows

the isolation of the CTCs from the whole blood with a high recovery and a zero false-positive rate. Coupling a CTC separation and capturing method, such as eDAR, with a downstream immunostaining test provides information about the cell's expression of certain protein biomarkers. We developed a semi-automated system for sequential immunolabeling and photobleaching based on the eDAR platform. With this new technique, we were able to evaluate the expression of eight different biomarkers on isolated CTCs. The second part of this chapter focuses on the manipulation of single CTCs captured by eDAR. We could selectively pick up single CTCs, deliver them to a new reservoir, and then culture them.

Chapter 4 reports a re-designed microfluidic platform of eDAR with an improved performance. In this method, the microfluidic chip was simplified by using a functional area for subsequent purification based micro-slits fabricated by standard lithography method. We also designed a new active sorting scheme, providing a fast performance with an improved reproducibility. Using this generation of eDAR, we were able to analyze 1 mL of whole blood sample in 12.5 min, with a 95% recovery ratio and a zero false positive rate (n=15). The recovery ratio was greater than 88% when we used bio-markers other than EpCAM to select CTCs, including the intracellular markers, such as green fluorescence protein (GFP). CTCs were detected in 8 of 10 patients with metastatic pancreatic cancer, and the clinical performance was not significantly different than the first generation of eDAR applied on the same type of patients.

The fifth chapter introduces an automated high-throughput enumeration method for CTCs based on microfluidics and line-confocal microscopy. Peripheral blood was directly labeled with multiple antibodies, each conjugated with a different fluorophore, pneumatically pumped through

a microfluidic channel and interrogated by a line-confocal microscope. Based on the fluorescence signals and labeling schemes, the count of CTCs was automatically reported. Due to the high flow rate, 1 mL of whole blood can be analyzed in less than 30 minutes. I applied this method in analyzing CTCs from 90 stage IV breast-cancer patient samples, and performed a side-by-side comparison with the results of the CellSearch assay, which is the only method approved by U.S. Food and Drug Administration (FDA) at present for enumeration of CTCs. This method has a recovery rate for cultured breast cancer cells of 94% (n=9), with an average of 1.2 counts/mL of background level of detected CTCs from healthy donors. It detected CTCs from breast-cancer patients, ranging from 15 to 3375 counts/7.5 mL. Using this method, I also demonstrate the ability to enumerate CTCs from breast-cancer patients that were positive for Human Epidermal Growth Factor Receptor 2 (Her2) or CD44+/CD24-, which is a putative cancer stem cell marker. This automated method can enumerate CTCs from peripheral blood with high throughput and sensitivity. It could potentially benefit the clinical diagnosis and prognosis of cancer.

At the end of this dissertation, I would give a brief summary and discussion on potential future studies.

Chapter 2 Detection and Isolation of CTCs Using Ensemble Decision Aliquot Ranking (eDAR)

2.1 Introduction

The challenge of enriching and isolating rare cells is often a stumbling block for research in CTCs in peripheral blood [71], fetal cells in maternal blood [72-73], and cancer stem cells [74-75]. An ideal method for isolating rare cells, such as CTCs, should be: (1) highly sensitive, with the ability to detect and isolate 1 CTC/mL of blood; (2) capable of easily recovering live CTCs with minimal stress on the cells, which is important for downstream molecular analysis [44] or cell culture; (3) capable of high throughput so it can process milliliters of blood within tens of minutes; and (4) robust and economical to operate. To meet this challenge, we describe an approach that is different from what has been so far explored in this area of research and which we believe offers significant advantages.

Our method is based on positive selection, where cell-surface markers are labeled with fluorescent antibodies, ranked by aliquots, and sorted. We call this process ensemble-decision aliquot ranking (eDAR), because we perform the ranking by looking at an ensemble of cells within each aliquot [76]. In our method, we break down a blood sample into nanoliters of aliquots that get rapidly ranked for the presence or absence of CTCs; the ranking helps us to decide which aliquots of cells are worth closer investigation. Our current microfluidic platform can routinely analyze 1 mL of whole blood in 20 minutes with a recovery efficiency of greater than 93% and a false positive rate of zero. Most importantly, this platform concentrates CTCs into a small field-of-view (< 1mm^2)

for microscopic imaging and allows easy isolation of and access to individual live CTCs for further downstream analysis and culture. This feature of concentrating live CTCs within a small and easily accessible area is lacking in existing methods but is important for translation into the clinical application, because it circumvents the long image acquisition times (hours) required in existing techniques. This feature is also important for accessing the isolated CTCs for downstream single-cell manipulations (e.g. culture) and analysis (e.g. molecular profiling).

2.2 Results and Discussion

2.2.1 Overview of System

eDAR is operationally similar to flow cytometry but with important differences. The throughput of traditional flow cytometry is limited by the sequential analyses of individual cells in a single-file format; the process may take over 24 hours for 1 mL of blood containing 5 billion blood cells. [46] To greatly increase throughput, eDAR probes for rare cells in nanoliter aliquots of blood that each contain thousands of cells. Once the aliquots containing CTCs have been collected, blood cells, especially RBCs, are removed from the CTCs by an on-chip filtration system. The isolated CTCs can then be imaged on the filter or selectively removed for additional single-cell studies. The filtration area (<1 mm^2) is comparable to the field-of-view of a microscope (e.g. with a 10× objective), which facilitates subsequent analysis. The filtration area is open at the top and can be directly accessed, for example with a micropipette, for cell removal.

In comparison with flow cytometry, there are some key advantages and disadvantages of eDAR. A main advantage of eDAR is the 3 to 4 orders of magnitude improvement in throughput. For

example, our current system breaks down a blood sample into 2-nL aliquots, a volume that contains a total of ~ 10,000 blood cells. At an interrogation rate of 1 ms per aliquot, it takes ~ 8 minutes to process 1 mL of blood. Unlike existing approaches, subsequent imaging of the isolated CTCs takes mere seconds. eDAR is extremely efficient at enriching rare cells: If there are 5 CTCs in 1 mL of blood, eDAR will discard 99.999% of the blood volume and present a combined 10 nL of blood within a small accessible area of the filter.

However, the ensemble ranking process limits eDAR to the isolation of rare cells and prevents it from working well for target cells that are abundant. In exchange for the vast improvement in throughput of isolating rare cells, eDAR is limited to obtaining only fluorescence information because there are many cells within the detection volume that cause scattering. In flow cytometry, where each cell is detected in a single-file format, it is possible to obtain both fluorescence and light-scattering information so cell size and morphology can be determined. For the isolation of rare cells, the lack of light-scattering information is not important because the targeted cells are captured downstream for imaging and individual analysis. Another advantage of eDAR is reduced hydrodynamic-induced cell stress. In eDAR, a volume containing thousands of cells flows past the interrogation region, resulting in a linear flow rate up to 50 times lower than in flow cytometry, which minimizes shear stress on the cells. Preserving the viability of each isolated cell is particularly important for these rare cells.

2.2.2 Individual Components of eDAR

Generation of Aliquots. Figure 2.1A schematically depicts our eDAR system. The first step in eDAR is to generate or define an aliquot. We initially focused on aliquoting blood into droplets

[77-78]; Figure 2.1B shows a continuous stream of aliquots defined by droplets surrounded by an immiscible phase. We had presumed that encapsulation of the cells in a droplet may protect the cells from flow and associated stresses outside of the droplet. We have since found this assumption may be too simplistic because re-circulation flow present within droplets can generate significant hydrodynamic shear stresses on cells. In addition, we found droplets had other disadvantages. First, because droplets were spaced apart by immiscible oils, the throughput was reduced by at least half at a given flow rate through the interrogation region. Second, the generation and stability of the droplet stream was highly sensitive to flow conditions, an unwanted characteristic that compromised the operational robustness of the system. And finally, droplets were incompatible with the on-line filtration that we used to isolate the targeted CTCs from the other blood cells.

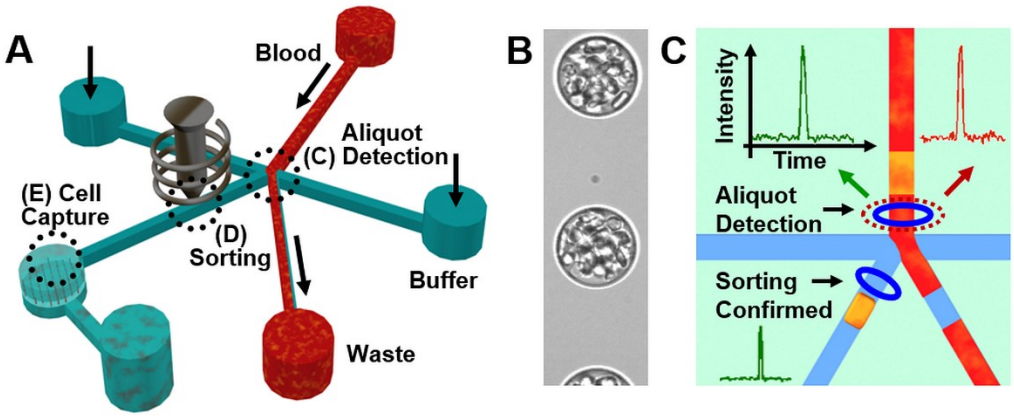

Figure 2.1 Schematic and images showing the general concept of eDAR. (A) Overview of the microfluidic chip. Whole blood labeled with fluorescent antibodies flows through the main channel of the microfluidic chip with desired aliquots actively sorted into the cell capture chamber. (B) A high-speed camera image of whole blood aliquoted into a continuous stream of droplets surrounded by silicone oil. (C) Laser-induced fluorescence triggers the sorting of an aliquot containing a rare cell (shown in yellow) to the collection microchannel and cell capture chamber.

Rather than creating physically isolated aliquots with droplets, we next pursued the notion of virtual aliquots. Here, each aliquot was defined by a combination of the laser illumination volume, the bin time of the detection system, and the switching time of the solenoid. We found this approach offered the highest throughput and operational robustness. In our current system, 2-nL aliquots were the optimal compromise between detection sensitivity and throughput at a flow rate of 50 μL/min.

Aliquot Ranking. Once we defined an aliquot, we ranked the aliquot based on the presence or absence of rare cells by sequentially interrogating aliquots of blood in a flow-through format (Figure 2.1C). To detect rare cells in an aliquot, we labeled the cells with fluorescent antibodies against cell-surface markers characteristic of CTCs. For breast cancer cells, for example, characteristic cell-surface markers are EpCAM and Her2 (all patients in this study were Her2 positive). Once labeling was complete, we introduced blood into the microfluidic chip at rates up to 80 μL/min. As an aliquot of blood passed through the detection region in the microfluidic channel, a laser illuminated it and excited any fluorescence tags that were present in the aliquot (Figure 2.1C). For each aliquot, the resulting fluorescence could be simultaneously collected at several (typically 3) wavelengths using fiber-coupled avalanche photo diodes (APDs) to determine the contents of the aliquot. If the aliquot contained a target cell, the fluorescence emission triggered the sorting of that aliquot into the collection channel.

To detect a single CTC in a background of nanoliters of blood, we developed a line-confocal detection scheme [79] with a probe volume that spanned the width (150 μm) and height (50 μm) of the main blood channel. Our system had two lasers at 488 nm and 633 nm, whose outputs were

shaped by cylindrical lenses and focused into a 20× objective to form a 200 µm by 5 µm line (Figure 2.2A). Fluorescence from this region was collected through a rectangular confocal aperture and a series of dichroics and filters to fiber-coupled APDs operating in the single-photon counting mode. In our current setup, APD1 detected the yellow fluorescence (560-590 nm) from the monoclonal antibody anti-EpCAM labeled with phycoerythrin (PE); APD2 was used as a negative control for the green wavelength range (500-550 nm) to eliminate false positives from broadly emitting fluorescent contaminants; and APD3 detected anti-Her2 labeled with Alexa-647 in the red wavelength band (640-690 nm). A second excitation region using only the 488-nm laser was located immediately after the sorting junction (Figure 2.1C); yellow fluorescence (560-590 nm) was collected in this spatially distinct detection region through a separate confocal a blood aliquot with the target cell.

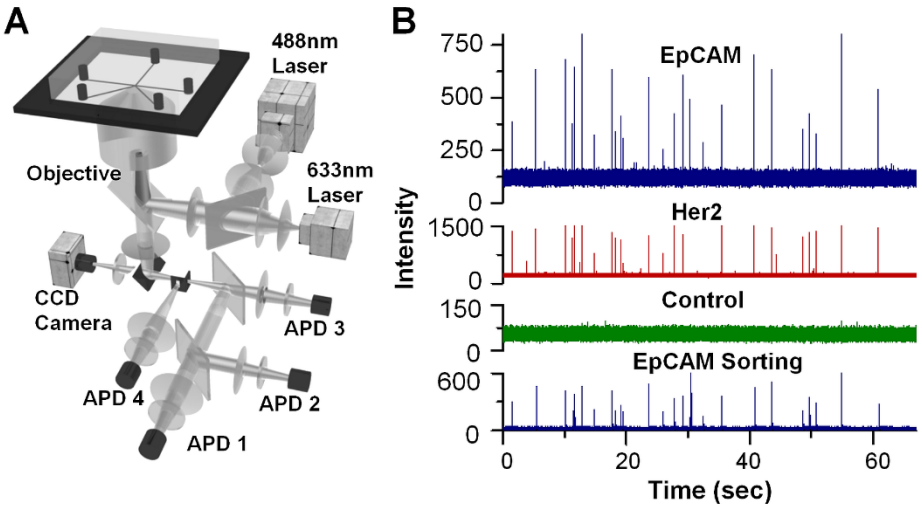

Figure 2.2 Aliquot detection system. (A) The setup for aliquot detection is comprised of two excitation lasers and four APDs. APDs 1, 2, and 3 collect fluorescence at three different wavelength regions (560-590 nm, 500-550 nm, 640-690 nm) from the aliquot to determine the presence of a CTC. APD 4 confirms the sorting of the desired aliquot. (B) A segment of the APD trace at the three different colors from clinical sample number 16 showing aliquots positive for the antibody markers EpCAM (top trace) and Her2 (second trace) that were correctly sorted (bottom trace).

Figure 2.2B shows a portion of the data trace from a metastatic breast cancer patient sample (#16). The CTCs were readily detected in the 2-nL aliquots of blood with an average signal-to-noise (S/N) ratio of 32 for the EpCAM marker and 64 for the Her2 marker (Figure 2.3A). The S/N ratio was highly dependent on the flow rate of the cells as they went through the detection region as well as the detection bin time (Figure 2.3B). Faster flow rates resulted in fewer photons detected from the CTC and a higher background from the surrounding blood. With our current system, the maximum flow rate that still allowed for an average S/N above 20 was 133 µL/min. For these experiments, the optimal bin time was 0.1 ms, which was comparable to the transit time of a CTC through the detection region.

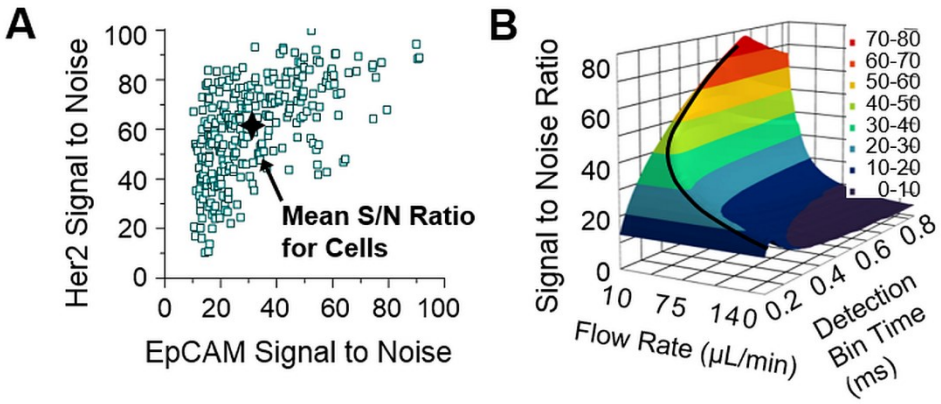

Figure 2.3 Signal to noise ratio of the line-confocal detection scheme. (A) The S/N ratio for each single cell detected in an aliquot of blood for both antibody labels from clinical sample number 16. The mean S/N ratio was 32 for EpCAM and 64 for Her2. (B) S/N ratio for EpCAM-labeled single cells as a function of flow rate and signal bin time. The black curved line shows the optimal parameters with a maximum flow rate of 133 µL/min for a S/N ratio above 20.

For this study, we simply ranked the aliquots as zero (no CTCs) or one (containing CTCs), but we envision more sophisticated rankings will be beneficial in the future, for instance for aliquots with

different types of rare cells. In comparison to the antibody-based surface capture of rare cells [67-68], aliquot ranking offers more flexible logical operations. For example, we can collect aliquots based on the presence of EpCAM and Her2 and absence of fluorescence in the green channel; in antibody-based surface capture, cells that express either EpCAM or Her2 will be retained. Surface capture can only employ the "OR" logical operation while eDAR can make more complex logic decisions.

Aliquot Sorting. To sort and collect the aliquots that contained CTCs, we used an externally actuated solenoid piston valve that sat above the elastomeric polydimethylsiloxane (PDMS) microchannel (Figure 2.4). When an aliquot containing the target cell was detected, the solenoid piston was released to direct flow through the collection microchannel. The flow rate in the two side buffer channels was balanced by air-pressure regulators so that when the collection channel was open, the entire aliquot of blood containing the target cell was directed towards the cell-capture chamber. After a predefined interval, the solenoid piston was reengaged and the blood again flowed to the waste outlet.

The raw photon counts from the APDs were sent to the sorting processor and simultaneously graphed in real time and saved by a computer. At a rate of 10,000 Hz, the dedicated circuit compared the intensity count at each time point to a threshold value defined by the blood's background signal. If a time bin contained a signal higher than the background threshold value, the solenoid piston was released by switching the voltage from high (22 volts) to low (0 volts). The elastomeric collection channel reverted to its native open state, forcing the solenoid piston up. After the aliquot was sorted, the voltage was re-applied to the solenoid to close the collection channel.

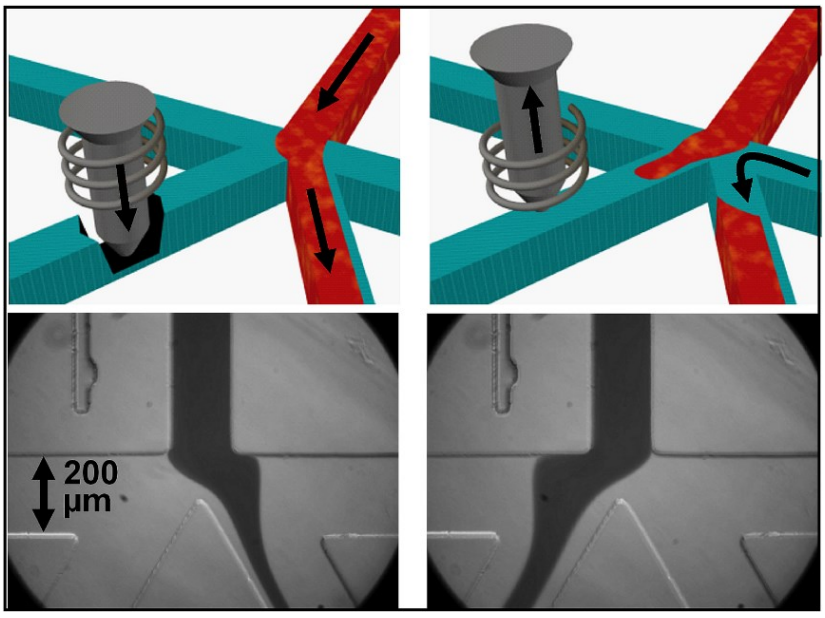

Figure 2.4 General scheme of the Aliquot sorting. The solenoid piston is released to allow flow through the collection channel; images at bottom show the flow of whole blood when the collection channel is closed (left) and opened (right).

To test the effectiveness of the solenoid piston at preventing unwanted aliquots from being collected, we prepared a sample using healthy donor blood to which we added SKBr-3 cells and anti-EpCAM-PE antibodies (Figure 2.5). We used the fourth APD (Figure 2.2A) positioned in the collection channel to monitor the performance of the eDAR system (red bottom APD trace). As expected, when the sorting processor was configured to not release the solenoid, we found that none of the aliquots that contained SKBr-3 cells (top black APD trace in Figure 2.5A) were detected in the collection channel. When the sorting processor was operating in the normal triggering mode (Figure 2.5B), each aliquot containing a labeled SKBr-3 cell that was detected by the main APD (black) was also detected by the collection APD (red), confirming successful sorting. The two traces appear to almost overlap, but the time difference between the signals can be used

to determine the minimum amount of time that the solenoid needs to remain open to collect the entire aliquot.

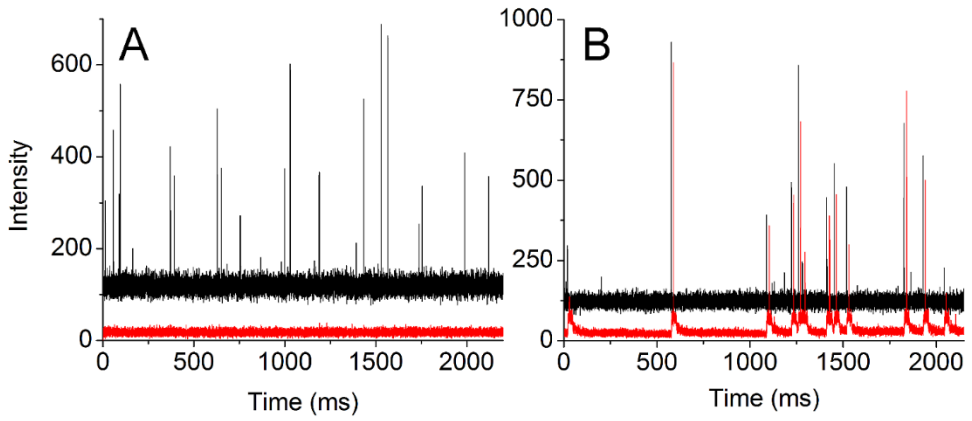

Figure 2.5 The effectiveness of the aliquot sorting. (A)When the sorting scheme was configured as "off", APD traces from the first detection area (black) and the second detection area (red) show that no cells were collected. (B) When the sorting scheme was applied, APD traces from the first detection area (black) and the second detection area (red) show that all the cells were collected.

To test the performance of eDAR, we spiked cultured breast cancer cells (SKBr-3) into whole blood and labeled them with fluorescent anti-EpCAM-PE. The blood was introduced into the microfluidic chip using a syringe pump with flow rates varying between 10 and 80 µL/min. We avoided any issues with dead volumes by mounting the syringe pump vertically with the tip of the syringe pointing down.

The sorting efficiency was defined as the number of aliquots triggered to be sorted compared to the number of cells detected as they entered the collection channel (Figure 2.6B). At slow flow rates (25 µL/min and below), we got 100% sorting efficiency as the entire volume of each aliquot was collected (Figure 2.6A). At the fastest flow rate of 80 µL/min, only a portion of each aliquot was captured, resulting in a reduced sorting efficiency of 85%. The loss was caused by the

collection channel not being completely open before the aliquot arrived because the solenoids do not have reproducible timing below 2 ms. There are several design improvements that could be made to increase the throughput, including increasing the distance between the detection region and the sorting junction, using a solenoid with sub-millisecond response times, and changing the channel dimensions. Figure 2.6C shows high-speed camera images of the blood flow as it completely switched to the collection channel in less than 2 ms once the solenoid piston was released.

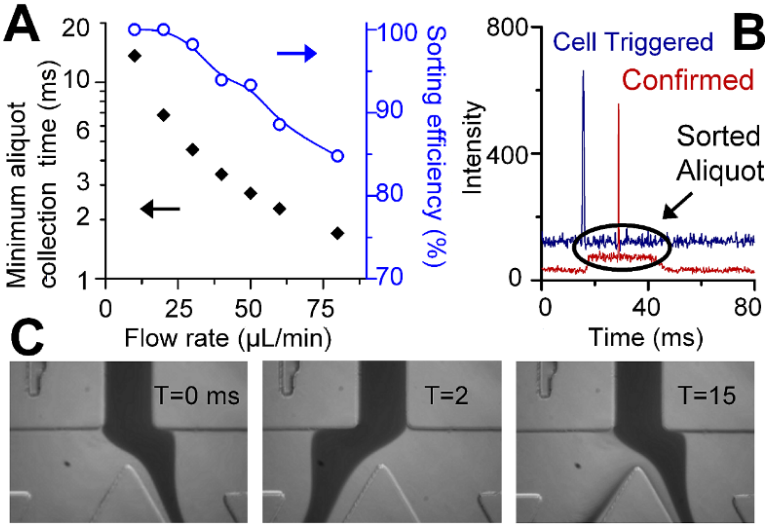

Figure 2.6. Aliquot sorting efficiency. (A) A plot showing the minimum amount of time required to collect a desired aliquot of blood as a function of flow rate. The collection time was ~ 2.7 ms for 50 µL/min. The plot of sorting efficiency versus flow rate shows highly accurate sorting (up to 100%). (B) Fluorescence trace from a CTC showing the triggering (blue) and successful sorting (red) of an aliquot of blood. (C) High-speed camera images of the sorting junction before and after the release of the solenoid piston that show complete flow switching within 2 ms. The final image shows flow returning to the waste channel after the completion of the aliquot sorting.

Aliquot Collection and Further Isolation of CTCs via Filtration. Sorted aliquots flowed to the cell capture chamber where the target cells were retained by a filter. The majority of blood cells, including all RBCs and many small WBCs, passed through the filter (Figure 2.7). The filter was

a transparent, track-etched, polycarbonate membrane with 5-µm pores that spanned the 1-mm diameter chamber. With such a small volume of blood coming into the collection chamber, the capacity of the ~1,000 pores was more than adequate. Captured cells, which clogged the pores once trapped, did not significantly increase the pressure of the system, unlike bulk blood filtration systems where capacity issues are a primary concern [54, 62, 80]. The small size of the filtration chamber allowed for complete high-magnification imaging with just a few fields of view. Alternatively, the entire chamber could be imaged in a single frame using a 10× objective and a camera with a large CCD sensor.

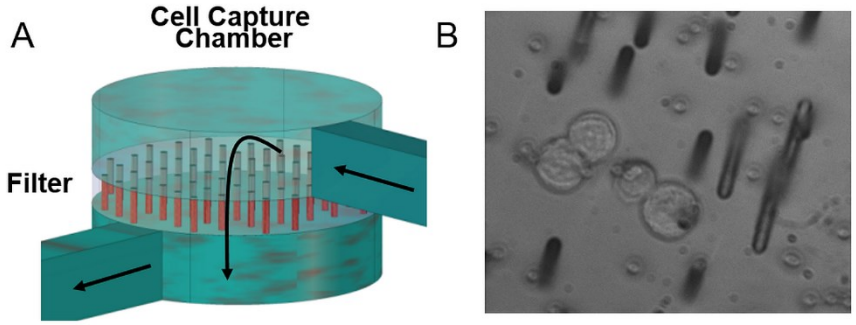

Figure 2.7 The cell capture chamber of eDAR. (A) The schematic drawing shows the structure of the cell capture chamber, which can trap the cells and further purify it by removing red blood cells (RBCs) and most of the white blood cells (WBCs). (B) The bright field image shows the 4 MCF-7 cells captured on the polycarbonate filter.

The chamber was open and easily accessible from the top. Additional reagents, such as antibodies against various cellular targets, could be pipetted onto the filter and perfused over the targeted cells. Micropipettes could also be positioned above the filter to remove individual CTCs for analysis or culture. With a 5-µm pore size, some WBCs were also retained on the filter. But with highly enriched CTCs, these WBCs were present in comparable numbers to CTCs and were easily distinguishable from CTCs with anti-CD45 antibodies specific for WBCs. A wide range of pore

sizes are available and the filter can easily be varied depending on the final requirements of the application.

2.2.3 Overall Performance of eDAR

Cell Recovery. Among the many reasons why recovery rates are typically low for rare cells is the loss or damage of cells during the preparation process. Depending on the technique, these losses can be caused by mechanical or chemical lysis or cell adhesion to the tubing and vials during multiple transfer steps. Our process was optimized to include a minimum of sample preparation steps that didn't involve lysing. The blood processing consisted of labeling with antibodies, dilution with buffer, followed by centrifugation and removal of the supernatant containing the free antibodies.

Recovery experiments were conducted with two breast cancer cell lines, MCF-7 and SKBr-3. A known quantity of cells ranging from 5 to 311 was spiked into a tube containing 1 to 2 mL of healthy donor blood. Typically, cell recovery experiments are conducted by calculating the concentration of cells using a hemocytometer or flow cytometer prior to serial dilution. For the low cell numbers that are the most interesting in rare-cell isolation experiments, the statistics for serial dilution break down and are inaccurate. For our studies, the number of cells was counted individually using a capillary cell-spiking method that we previously published [81]. This method allowed us to investigate the recovery rates conveniently for as few as 5 cells rather than the tens to thousands range that is typically reported.

The isolated cells were enumerated in the filtration area using laser excited epi-fluorescence imaging of anti-EpCAM (Figure 2.8B) and anti-Her2 (Figure 2.8C). From nine separate recovery experiments using a flow rate of 50 μL/min, we determined the average recovery efficiency of the whole system was better than 93% (Figure 2.8A). This flow rate was used for the false positive experiments as well as for all the clinical samples.

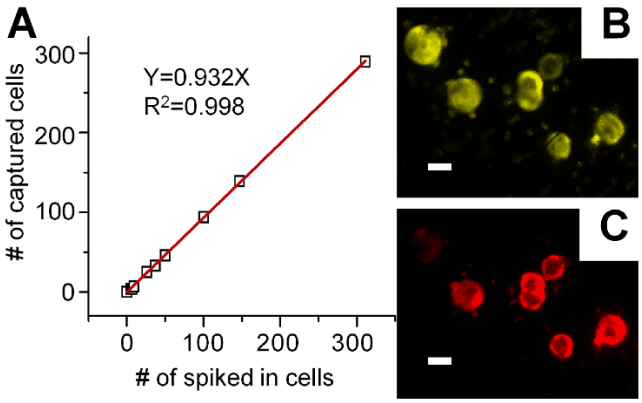

D Control run #	1	2	3	4	5	6	7	8
# of cells captured	0	0	0	0	0	0	0	0

Figure 2.8 Recovery and false positive performance of eDAR. (A) Captured cells were counted at the end of each run and compared to the number initially spiked into the sample. The average recovery efficiency for the nine runs is higher than 93% (flow rate was 50 μL/min). Fluorescence images of the captured cells on the filtration membrane labeled with (B) anti-EpCAM and (C) anti-Her2. The scale bar is 20 μm. (D) Negative controls showing 8 control runs using healthy donor blood with zero false positives.

Equally important is the potential for false positives. We performed negative control experiments using healthy donor blood. One milliliter of blood was labeled with anti-EpCAM and anti-Her2 antibodies and run through our system using the same protocol as used for the cell-recovery experiments and for processing clinical samples from breast cancer patients. Figure 2.8D shows the results from eight experiments, all of which found no target cells, yielding a false positive rate of zero.

2.2.4 Isolation of CTCs from Metastatic Breast, Lung and Pancreatic Cancer Patients using eDAR.

To better understand the performance of eDAR, we carried out a side-by-side comparison between eDAR and the FDA-approved CellSearch assay using clinical samples. Patients with Stage IV metastatic breast cancer had peripheral blood drawn in an outpatient cancer clinic as a part of their office visit. Multiple tubes of venipunctured blood were collected in each draw. The first tube was not used for cell analysis because of the potential for contamination from epithelial cells during the venipuncture process. Of the remaining tubes, one was drawn into a Veridex CellSave tube for enumeration using the Veridex CellSearch system. A second sample from the same draw was collected in a Vacutainer tube containing K3EDTA and delivered to our laboratory for analysis with eDAR. The samples were run independently: CellSearch was performed by a clinical technologist as part of routine clinical testing, and eDAR was carried out by our lab. The results of the CellSearch analysis were unknown to us until after we had completed the analysis of our samples. This arrangement allowed for a direct head-to-head comparison between the two systems.

For each clinical sample, we processed between 1 and 2 mL of whole blood with a total sample preparation time of 40 minutes. Each sample was run using a new disposable PDMS chip to prevent contamination. Aliquot sorting was triggered by the presence of anti-EpCAM-PE fluorescence. EpCAM was chosen because it is the primary marker used in the CellSearch system. For a 1-mL sample with a flow rate of 50 μL/min, each run took 20 minutes. The captured cells at the end of the run were imaged and analyzed using multi-color epi-fluorescence.

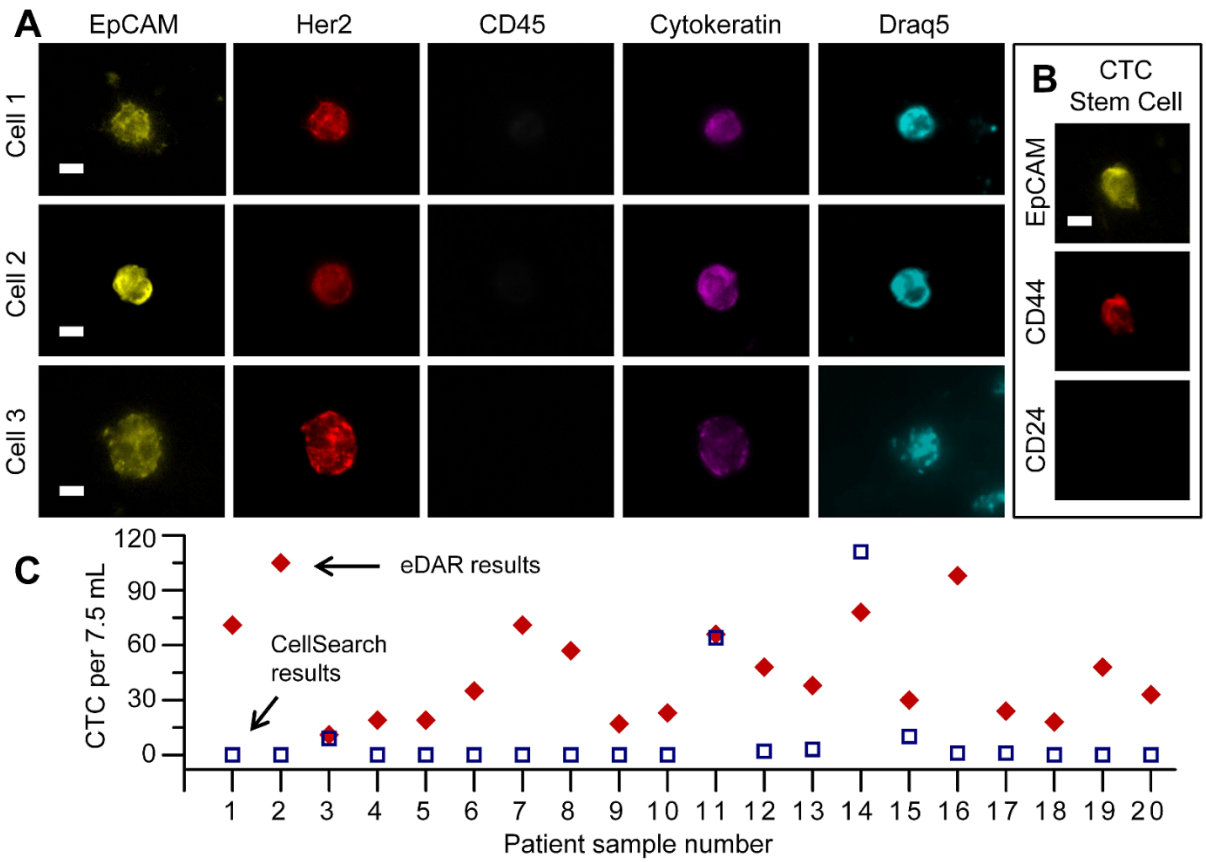

Figure 2.9 Clinical results for CTCs isolated from blood samples drawn from breast cancer patients. (A) Images of three CTCs isolated from clinical sample number 16; scale bar is 20 µm. (B) Images from a CTC labeled with fluorescent antibodies against the breast cancer stem cell marker ($CD44^+/CD24^-$). (C) Side-by-side comparison of clinical results from 20 breast cancer patient samples ran with CellSearch and eDAR.

To confirm the presence of anti-EpCAM-PE, images were collected in the yellow wavelength region, 560 to 590 nm, by excitation with a 488-nm laser. To test for anti-Her2-Alexa 647's presence, images were also collected in the red wavelength region, 650 to 690 nm, using a 633-nm laser. To count the number of CTCs, additional labeling with anti-CD45 and anti-cytokeratin was performed by directly pipetting the reagents onto the cells and washing the cells retained on the filter through the open top of the cell-capture chamber. For this secondary labeling step, the cells were first fixed with paraformaldehyde and permeabilized with a surfactant to allow binding

of antibody to cytokeratin. The presence of CTCs was confirmed if they were labeled by anti-EpCAM and anti-cytokeratin but not anti-CD45, which is present on leukocytes. After this secondary labeling, the cells were further labeled with the nuclear stain DRAQ5 to confirm that the cells were intact. Figure 2.9A shows 3 cells from clinical sample number 16 that were positively labeled with EpCAM, Her2, cytokeratin, and DRAQ5 but were negative with the CD45 antibody.

eDAR affords us the versatility of having the captured cells isolated in a small open area and retained by the filter where multiple analyses can be performed. Captured and labeled CTCs from clinical sample number 23 were first photobleached and then labeled with the stem cell markers anti-CD24- fluorescein isothiocyanate (FITC) and anti-CD44-Alexa-647 (Figure 2.9B). A study has shown that in breast cancer, the cell subpopulation that expresses the cell surface markers CD44+ and CD24-/low exhibits stem-cell characteristics; less than 200 of these cells were sufficient to form tumors when implanted in mice [74]. In contrast, more than 20,000 cells isolated from the same tumor that did not exhibit this marker (i.e. CD44+ and CD24-/low) were unable to form tumors when implanted in mice [74]. Furthermore, these CD44+ and CD24-/low cells were shown to form tumor mammospheres in vitro, a property that was described for mammary stem/progenitor cells [16, 82-84]. Using eDAR, we were able to detect the presence of this subset of cells within the isolated CTCs from breast cancer patients.

Figure 2.9C summarizes the results from 20 clinical samples analyzed both by eDAR and CellSearch. The number of CTCs found by eDAR ranged from 11 to 105 for a normalized volume of 7.5 mL, with an average of 45. The CellSearch results from the same patient samples ranged

from 0 to 111, with an average of 10. CellSearch found 0 cells in 12 of the patient samples, with only 4 samples containing more than 2 CTCs. eDAR, in comparison, identified CTCs in all samples. The average of 10 CTCs enumerated by CellSearch is skewed by clinical sample 14. If we omit this sample from the analysis, CellSearch detected 0 to 64 CTCs with an average of 5, while eDAR recovered 11 to 105 CTCs with an average of 44 (Table 1). This comparison clearly illustrates the improved sensitivity offered by eDAR.

In another clinical study, we validated the reported method by analyzing 16 samples from patients with metastatic pancreatic cancer and 9 samples from patients with metastatic lung cancer (Figure 2.10). CTCs were found in 87% of the pancreatic cancer samples in the range from 2 to 183 cells/mL. The average counts of pancreatic CTCs were 21 cells/mL with a median value of 7 cells/mL. In the group of lung cancer CTCs were found in 90% of the samples (n=9) in the range from 1 to 147 cells/mL. The average number of lung CTCs were 20 cells/mL with a median concentration of 4 cells/mL. These results proved that our method can detect CTCs from patients with other types of cancer, with a high sensitivity and efficiency.

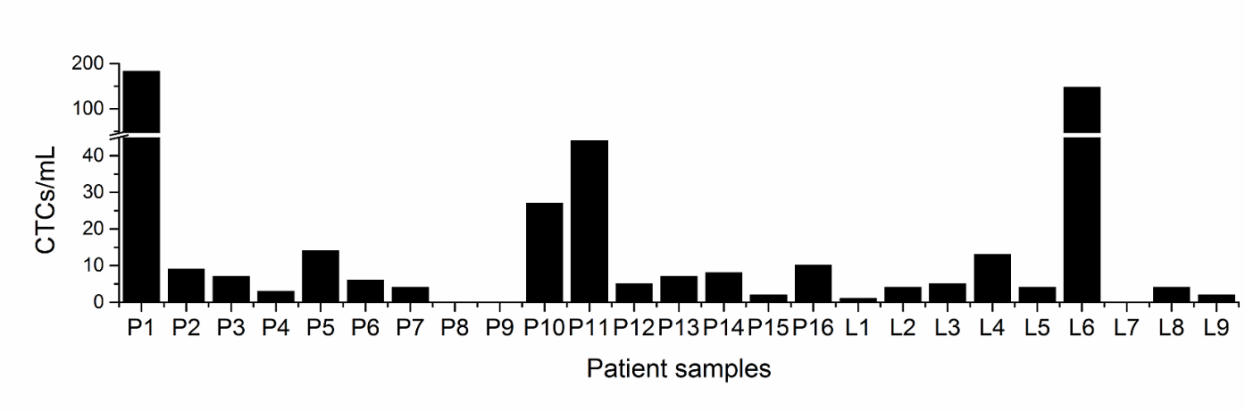

Figure 2.10 CTCs from pancreatic and lung cancer patients analyzed by eDAR. Samples P1 to P16 are pancreatic cancer samples; samples L1 to L9 are the blood samples from lung cancer patients.

Sample ID	Sample Volume (mL)	Raw number of CTCs captured by eDAR	Normalized CTCs captured by eDAR (/7.5 ml)	CTCs counted by CellSearch (/7.5 ml)
1	2.00	19	71	0
2	1.00	14	105	0
3	2.00	3	11	9
4	2.00	5	19	0
5	2.00	5	19	0
6	1.50	7	35	0
7	2.00	19	71	0
8	1.70	13	57	0
9	1.80	4	17	0
10	1.00	3	23	0
11	1.25	11	66	64
12	1.25	8	48	2
13	1.00	5	38	2
14	1.25	13	78	111
15	1.00	4	30	10
16	1.00	13	98	1
17	1.25	4	24	1
18	1.25	3	18	0
19	1.25	8	48	0
20	0.90	4	33	0

Table 2.1 eDAR and CellSearch results obtained for 20 breast-cancer patient samples. The head-to-head comparison between the commercial CellSearch system and our eDAR platform using blood draws from Stage IV metastatic breast cancer patients.

2.3 Materials and Methods

2.3.1 Chip Fabrication and Multi-layer Structure Integration

The microfluidic channels were developed by photolithography methods described previously [85-86]. Briefly, features were designed in AutoCAD and written to a transparency mask (FineLine imagining, Colorado springs, CO, USA). Master silicon wafers were created with SU-8 3050 (MicroChem, Newton, MA, USA) with a feature height of 50 μm and a silanization layer of tridecafluoro-1,1,2,2-tetrahydrooctyl-1-trichlorosilane (Sigma–Aldrich, St. Louis, MO, USA). A thin layer of PDMS was spun to a final height of 150 μm on the master wafers and baked at 75 °C for 1 hour.

To integrate the solenoid (S-10-38-H-40, Magnetic sensor systems, Van Nuys, CA), a threaded mount made of cured PDMS was positioned above the collection channel and fresh PDMS was poured in and allowed to cure [87]. The device was then removed from the silicon master wafer and pre-cleaned before it was combined with the filter and bottom collection channel. The bottom outlet collection channel underneath the filtration area was cut out of a PDMS film with a thickness of 250 μm before sealing to a 0.5 mm thick cover glass using plasma oxidation. A small piece of polycarbonate filter membrane (Millipore, Billerica, MA, USA) was then sandwiched between the upper collection channels and the outlet channel and sealed using Polymethylhydrosiloxane (PMHS) assisted plasma oxidation [88]. Finally, the solenoid was integrated into the device by screwing it into the integrated threaded PDMS mount.

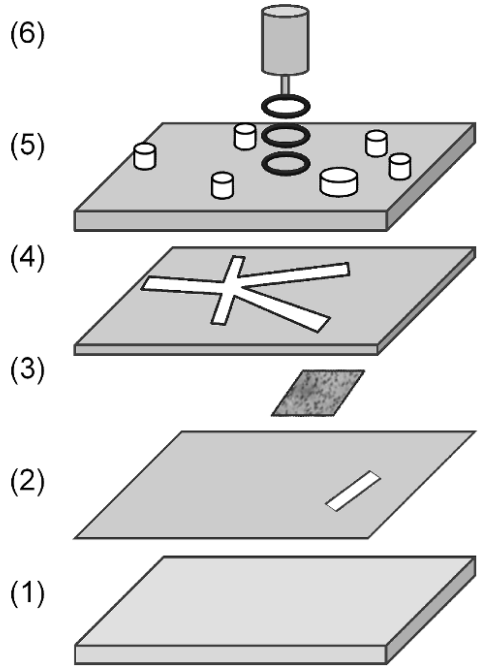

Figure 2.11 The six layers of the final eDAR chip: (1) cover glass, (2) PDMS membrane with outlet collection channel, (3) membrane filter, (4) main channel network, (5) solenoid threaded mount with inlet and outlet ports for the blood and buffer, and (6) solenoid with piston.

The final microchip had six distinct layers (Figure 2.11): (1) 500-µm thick cover glass; (2) 250-µm thick PDMS membrane with a 2 mm × 6 mm channel in it; (3) polycarbonate filter with 5-µm pores; (4) 150-µm thick PDMS membrane with the channel network; (5) PDMS slab with a threaded mount for the solenoid as well as inlet and outlet ports for the blood sample and buffer; (6) Solenoid with piston. The final device is approximately 5 × 3.5 × 0.5 cm, with the solenoid protruding an additional 4 cm above the device (Figure 2.12).

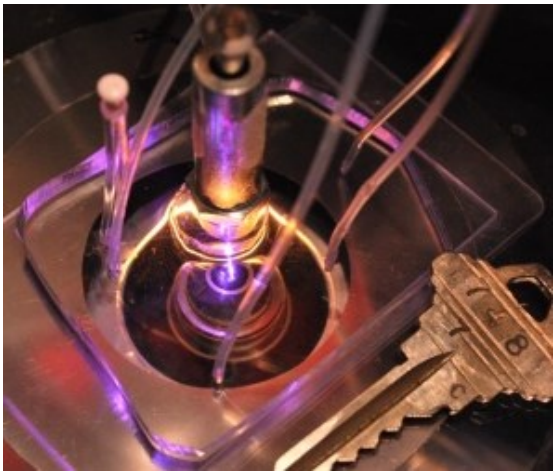

Figure 2.12 Photograph of an eDAR chip.

2.3.2 Biological Material and Blood

Two breast cancer cell lines, MCF-7 and SKBr-3 (American Type Culture Collection), were used to characterize and optimize eDAR. Cells were maintained in the recommended culture media (McCoy's 5A or EMEM) containing 2 mM L-1 glutamine, 10% fetal bovine serum, and 50 μg/mL penicillin/streptomycin at 37 °C with 5% CO_2 in a humidified environment. Isoton (Beckman Coulter, Miami, FL) was used as the buffer for all experiments. Whole human blood, individually drawn from healthy donors, was provided by Plasma International (Everett, WA). Each 20-mL draw was collected into five Vacutainer tubes containing K_3EDTA, stored at 4°C upon arrival, and used within 72 h of the draw. The first tube of each draw was discarded to avoid potential contamination from skin fragments.

Patients with Stage IV metastatic breast cancer were recruited according to the protocol approved by the University of Washington's Institutional Review Board. Peripheral blood samples were drawn at the Seattle Cancer Care Alliance as a part of the subjects' office visits. Multiple tubes of

venipuncture blood were collected in each draw. One tube was collected in a Veridex CellSave tube for enumeration of CTCs by Veridex's CellSearch test. A second tube was collected in a Vacutainer tube containing K_3EDTA for analysis by eDAR. The sample was stored at 4°C after the draw and delivered to our laboratory within 4 h. Patients with metastatic lung and pancreatic cancer patients were recruited according to the protocols approved by Fred Hutchinson Cancer Research Center's institutional review board. Blood was collected into a 10-mL Vacutianer tube containing K_3EDTA for analysis by eDAR.

2.3.3 Sample Preparation and Antibody Labeling

For clinical samples, 0.90 to 2.00 of blood were transferred to a 15-mL polypropylene conical centrifuge tube (Becton Dickinson, Franklin Lakes, NJ, USA). The blood sample was typically incubated with 120 µl of PE-anti-EpCAM (BioLegend, San Diego, CA, Catalog # 324206) and 20 µl of Alexa-647-anti-Her2 (BioLegend, San Diego, CA, Catalog # 324412) in the dark at room temperature for 30 min. Antibodies were centrifuged (20,000× g, 5 min) to remove any aggregates before labeling. Optimal parameters for antibody labeling were investigated and are shown in Table 2. The labeled blood was diluted to 14 mL with Isoton and centrifuged to remove the free antibodies (Figure 2.12). The final volume was controlled to be the same as the initial volume. All control and clinical samples were prepared using the same protocol. For the recovery experiments, the cultured cancer cells were spiked into whole blood prior to antibody labeling.

Antibody	Manufacturer	Stock Concentration (μg/ml)	Normalized Fluorescence Intensity (a.u.)
EpCAM - Phycoerythrin	Biolegend	5	100
Her2 - Alexa 647	Biolegend	Not reported	833
Cytokeratin - Alexa 647	Cell Signaling	50	304
CD45 - FITC	Biolegend	Not reported	47
DRAQ5	Cell Signaling	Not reported	220
CD24 - FITC	Biolegend	100	262
CD44 - Alexa 647	Biolegend	500	385

Table 2.2 Characterization of fluorescence and concentration of antibodies. For each batch of antibodies, we conducted cell-labeling experiments to optimize the fluorescence intensity. These experiments were also a quality-control check to monitor concentration changes between the purchased batches. The fluorescence intensity was normalized to the EpCAM-phycoerythrin antibody.

After the sample was run through the microfluidic chip, cells trapped on the filter could be labeled again to further identify their characteristics. To fix the captured cells, 2% paraformaldehyde (Electron Microscopy Sciences, Hatfield, PA) and 0.5% Surfactant 465 (Air Products and chemicals, Allentown, PA) were pipetted directly into the cell capture chamber and incubated for 15 min. A mixture of PE-anti-EpCAM, Alexa647-anti-cytokeratin (pan-Keratin (C11)) (Cell Signaling technologies, Danvers, MA, Catalog #4528), and FITC-anti-CD45 (BioLegend, San Diego, CA, Catalog # 304006) was then added and incubated in the dark at room temperature for 20 min. Cells could also be labeled with a nuclear staining dye such as DRAQ-5 (Cell Signaling technologies, Danvers, MA).

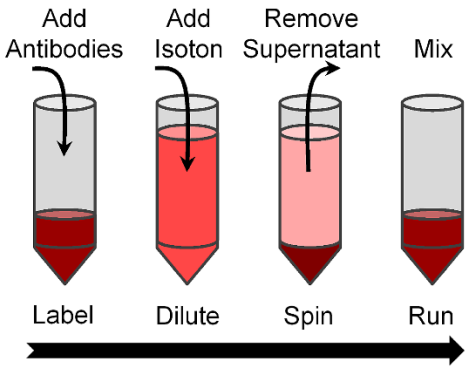

Figure 2.13 Blood preparation. Typically 2 mL of blood were incubated on a rocker at room temperature for 30 minutes with the chosen antibodies. After incubation the blood was diluted to 14 mL with Isoton buffer and centrifuged at 500× g for 10 minutes. The supernatant containing unbound antibodies was removed, leaving 2 mL of the blood for processing with eDAR.

For cancer stem cell labeling, a mixture of PE-anti-EpCAM, Alexa 647-anti-CD44 (BioLegend, San Diego, CA, Catalog #103018) and FITC-anti-CD24 (BioLegend, San Diego, CA, Catalog #311104) was added. Before each additional antibody incubation step, labeled fluorophores on the cells were photobleached to avoid spectral interference. This photobleaching step was carefully optimized to avoid cellular damage.

2.3.4 Electronics and Program Control for eDAR

Because computer processors are not designed for high speed timing and synchronization, we used an independent dedicated logic circuit processor that was preprogrammed with input parameters by LabVIEW software. Figure 2.13 shows the data flow between the APDs, sorting logic processor, and the computer as well as the feedback to the solenoid used for sorting. The fluorescence intensity detected by the APDs is output as 50-ns TTL pulses, which are integrated for a predefined interval of typically 100 µs by both a computer using a PCI data acquisition card

(PCI 6602, National Instruments, Austin, TX) and a dedicated sorting processor. The sorting processor is needed to precisely trigger the solenoid because computer timing is typically inconsistent below a couple ms. The sorting processor is preconfigured using LabVIEW software to change the voltage applied to the solenoid. The logic mode that triggers sorting can be configured to respond to any combination of signals from the different APDs. The computer simultaneously graphs the fluorescence intensity readout from the 4 APDs for user monitoring.

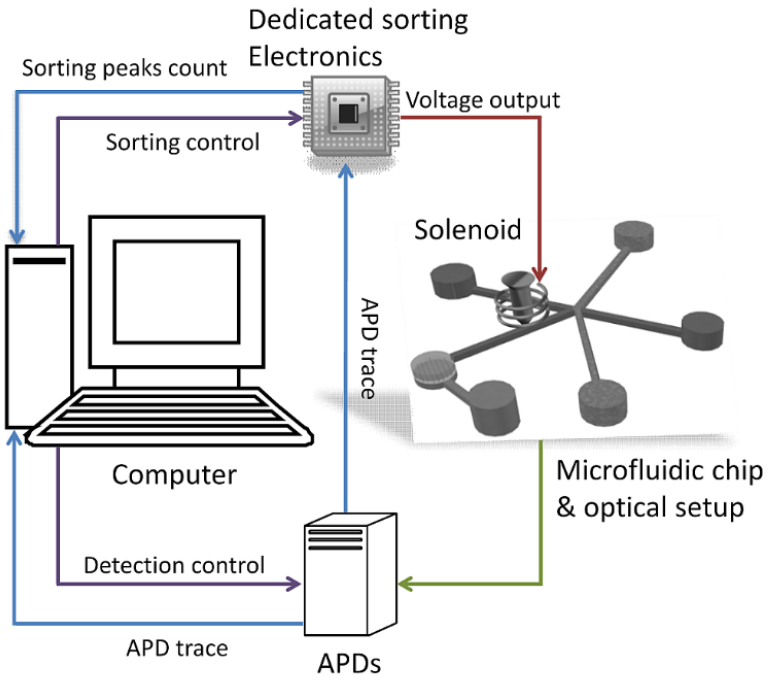

Figure 2.14 The electonics and information flow of eDAR. Green line shows the optical signal; blue lines show the electrical signal of the APD detectors and sorting controller. Purple lines are the command that set up the experimental parameters; red line is the DC voltage output.

2.3.5 Air Pressure on the Two Buffer Lines

The buffer flowing in the two side channels were driven by compressed air. The air pressure was used to regulate the hydrodynamic switching of the blood flow when the "positive" aliquot was

collected. Figure 2.14 shows the optimized pressure on both sides, which corresponded to the highest sorting recovery at different flow rates. Prior to each experiment, the air pressures applied to the side sorting channels were adjusted to optimize sorting. The air pressure for each side channel is controlled independently by pressure regulators. The pressure needed to achieve proper sorting depends on the flow rate of the main blood channel. Typically, the flow rate in the right buffer channel is twice the flow rate of the main blood channel, which in turn is twice the flow rate of the left buffer channel.

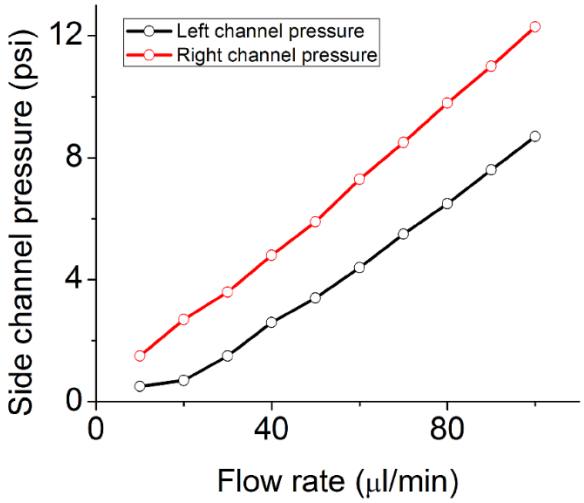

Figure 2.15 Optimization of the applied air pressures to the side buffer channels.

2.4 Conclusion

Cancerous tumors are diverse in their molecular and cellular composition. Because cancer is a very heterogeneous disease, a given patient may have many types of cancer cells with different phenotypes and genetic profiles. eDAR represents a different approach than other techniques demonstrated thus far for enumerating rare cells like CTCs. We believe it has the unique capability

of recovering individual live CTCs with high efficiency, throughput, and minimal stress; eDAR's feature of concentrating the isolated rare cells within a small easily assessable area bypasses the long imaging times that plague most other existing techniques and greatly increases its throughput. At present, we are applying sensitive single-cell techniques, such as single-cell gene-expression, proteomic, and pathway analysis, for studying CTCs so we can gain a better understanding of the physiology and diversity of these rare but deadly cells. This new understanding will facilitate the development of more accurate diagnostic and prognostic markers as well as more effective personalized therapies to eradicate these cancer cells. We believe eDAR will also find use in the isolation of other rare cells besides CTCs.

Chapter 3 Subsequent Analyses and Manipulation of Single CTCs Captured on eDAR Platform

3.1 Introduction

Many new technologies—immunomagnetic separation, affinity chromatography like separation methods, negative selection, and various other microfluidic approaches [89]—only aim to count CTCs. Indeed, the only method currently approved by FDA, the CellSearch system, is entirely based on the enumeration. It should be noted that CTC methods are often considered to be akin to a non-invasive and real-time biopsy.

As discussed previously, more studies are showing that the cellular and molecular analyses of CTCs may be more important than simple enumeration [71]. These analyses can potentially verify some biological and clinical hypotheses by studying the expression of many biomarkers on CTCs and comparing them to the biomarker expression profile of the primary tumor. For example, a recent study revealed the marked heterogeneity in the expression of stem cell and mesenchymal markers, by analyzing the gene profile of 15 single CTCs from a prostate cancer patient [90]. Downstream analysis post-enumeration can also improve our understanding of the mechanisms of metastasis. Some studies showed that cancer stem cells can be found in the population of CTCs [16, 59], and may also correlate with the disease progression.

Among various potential genetic and molecular analyses, analyzing protein biomarkers may be an easy and important starting point to perform in the downstream analyses of CTCs for several

reasons. First, some protein markers are direct targets of anti-tumor drugs, such as Her2 [64] or epidermal growth factor receptor [18, 91]. By studying these biomarkers, more molecular details can be revealed, which may benefit the prognostic evaluation. Second, some protein markers can clearly define the sub-populations of CTCs, such as epithelial CTCs, mesenchymal CTCs or CTCs with stem-cell characteristics, which may provide more biological details about the metastatic tumor biomarker. Third, no matter what enrichment method is used, most of the current CTC-methods count and verify CTCs using immunostaining and fluorescence imaging techniques. These techniques are fully compatible with subsequent protein biomarker analysis after CTC enumeration. Therefore the immunostaining and fluorescence analyses of CTCs can be readily done once the cells are captured with minimum additional sample preparation or transfer processes.

In chapter 2, I described a high-throughput and sensitive method for detecting and isolating CTCs in human blood called eDAR [76]. The detection, separation and analysis were integrated into a single microfluidic chip, aiming for an "all-in-one" platform for the analysis of CTCs. eDAR took less than 20 min to analyze 1 mL of whole blood. The method had a 94% recovery rate and a zero false-positive value, demonstrating that eDAR has high throughput, sensitivity, and accuracy. We believe eDAR is an ideal platform for capturing CTCs and performing the subsequent analysis of the expression of protein markers for two reasons: First, cells are captured and enriched into a small area on the microfluidic chip so the imaging process can be done much faster than accomplished by other techniques. The small area also minimizes the usage of secondary antibodies. Second, eDAR has an open-access design, which can facilitate the manipulation of single cells, such as picking up a cell of interest or delivering certain reagents to a cell.

Another potential important application of eDAR is the manipulation of the single CTCs captured by this method. Because of the open access design and the very small area where the CTCs were enriched, it is very easy to pick up a single CTC trapped on the polycarbonate filter, or deliver specific reagents onto that cell. After picking up the cell, various downstream analysis could be performed, such as the cell culture or gene analysis.

In this chapter, two types of subsequent analyses are reported. First, I developed and optimized a simple and semi-automatic method to perform the downstream analysis of the expression of protein markers on trapped CTCs. I designed an inline immunostaining and photobleaching system which allowed us to perform labeling and fluorescence imaging tests on selected CTCs with a group of antibodies conjugated with different fluorophores followed by the photobleaching and re-labeling with different fluorescent antibodies against another group of biomarkers. This process can be repeated multiple times to study groups of protein biomarkers. In our experiment, two protein markers of interest, combined with a positive control marker (nuclear stain) and a negative control marker (CD45), are studied in each round. As proof of principle, I performed four rounds of the immunostaining and photobleaching process to look at the expression of eight protein markers of interest. Second, I designed and built a device to selectively pick up or manipulate single CTCs trapped on eDAR microchip. Using cultured cancer cells spiked into human blood, we were able to pick up the CTC and then deliver it to another reservoir for cell culture.

3.2 Results and Discussion

3.2.1 CTCs Isolated by eDAR

Before running the eDAR test, whole blood sample was pre-labeled with the antibodies conjugated to fluorophores and then introduced to the microchip. In many applications, EpCAM was used as the biomarker for the positive selection. However, our method can be flexible in using a different or more complicated selection logic. As summarized in chapter 2, eDAR has three major components: the line-confocal detection scheme, the hydrodynamic sorting scheme and the subsequent purification and analysis area [76] (Figure 3.1).

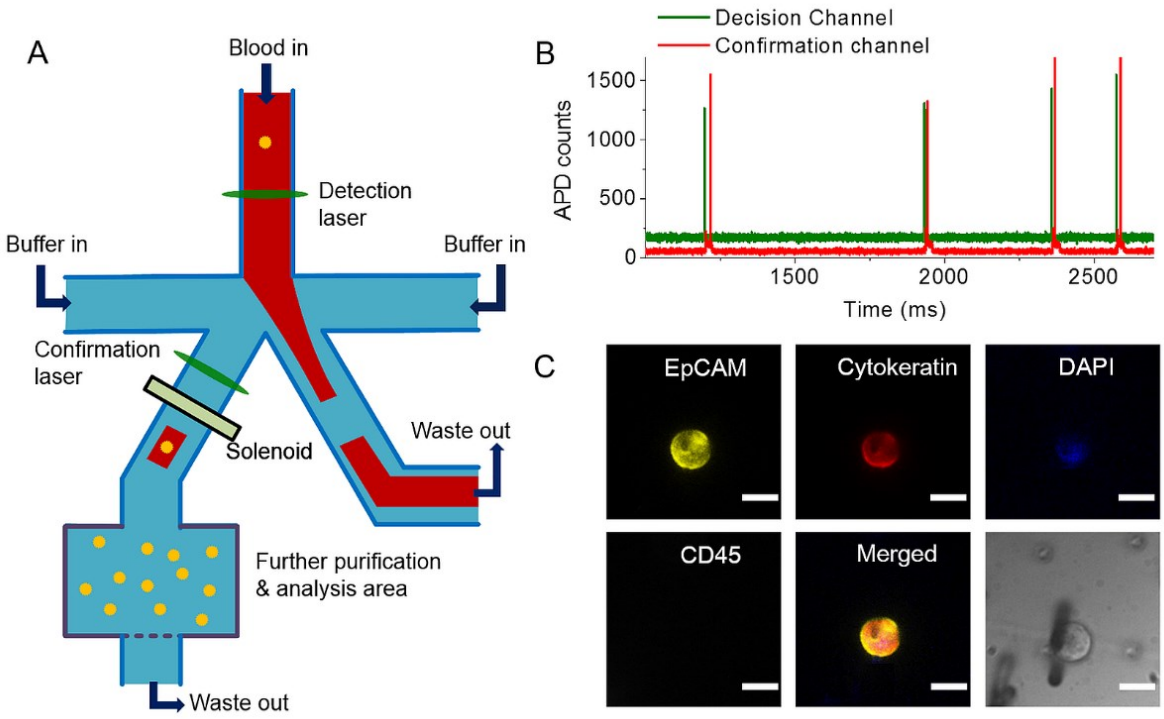

Figure 3.1 Cells captured by eDAR for downstream analysis. (A) The general scheme of eDAR. The two yellow dots in the top channel and the left collection channel show cancer cells in blood labeled with antibodies. (B) An example of the APD traces, which control the aliquot ranking (data in green), and confirm the cells are actually sorted (data in red). (C) A cancer cell captured on the polycarbonate filter

and labeled with anti-EpCAM-PE, anti-Cytokeratin-Alexa647, anti-CD45-FITC, and DAPI. Merged fluorescence and the bright field images are also shown here. All the scale bars are 20 μm.

In eDAR, a virtual aliquot was first defined by a combination of the laser detection beam, the volumetric flow rate, and the sorting speed. Based on these factors, the labeled blood sample was virtually divided up into half a million aliquots per 1 mL with 2 nL per an aliquot. The line-confocal detection method detected the fluorescence emission with single-cell sensitivity [92]. As a result, these virtual aliquots were ranked based on the primary labeling schemes as "positive" or "negative". Because of the very low concentration of CTCs, more than 99.999% of the aliquots were discarded (Figure 3.1A), which resulted in a greater than 1-million-fold enrichment ratio.

Based on the results of the aliquot ranking, an automatic feedback mechanism was applied to trigger a hydrodynamic switch of the blood flow so that the "positive" aliquots could be collected and transferred to an area for further purification and analysis. A solenoid was placed in the CTC collection channel in the closed mode on the left (Figure 3.1A) so the "negative" aliquots only flowed into the waste channel on the right. There was also a pressure drop between the two side channels where the buffer flowed, which switched the blood flow from the waste channel to the collection side when the solenoid was open. A second line-confocal detection window was also placed on the collection side to monitor the efficiency of the hydrodynamic switching in real time. Figure 3.1B shows a small part of the data from a sample taken from a lung cancer patient. In this figure, the green signal shows the APD traces from the first detection area which controlled the aliquot sorting; the signal in red was the APD counts from the second detection area confirming that the aliquots were actually sorted.

These sorted aliquots were transferred to an area where CTCs could be trapped and most of the blood cells discarded (Figure 3.1A). Although there are many possible ways to further purify the captured cells, we usually incorporated a small piece of polycarbonate filter (5 μm pore size) onto the eDAR chip. The trapped cells were imaged and further labeled with more biomarkers on the chip to determine their identities. For example, figure 3.1C shows a cancer cell trapped on the eDAR microchip, which was positive against EpCAM, cytokeratin, and the nuclear stain but negative against CD45. This cell was also observed by bright-field microscopy, which provided the morphological information.

3.2.2 General Scheme for the Sequential Immunostaining and Photobleaching Process

We developed an inline staining and washing system coupled with the current eDAR platform in order to minimize the dead volume; decrease the amount of antibodies used; avoid introducing air bubbles; and automate the process. As shown in figure 3.2A, two ports on the eDAR microchip were left open to perform the perfusion labeling and washing steps while all the other three ports were completely closed. A peristaltic pump delivered the washing buffer and labeling reagents to the eDAR microchip and was coupled with the pressurized buffer source via a six-way valve. The other three ports on this valve were completely blocked to prevent any possible leakage or contamination. When running the eDAR experiment, the six-way valve was turned to the pressurized buffer side to provide a stable control of the hydrodynamic switching. It could be switched to the peristaltic-pump side to inject accurate amounts of reagents to the microchip without introducing any air bubbles. Using this scheme, a few nanograms of the antibodies were

introduced to the trapped cells in less than 5 min; a typical incubation step took less than 20 min (Figure 3.2B).

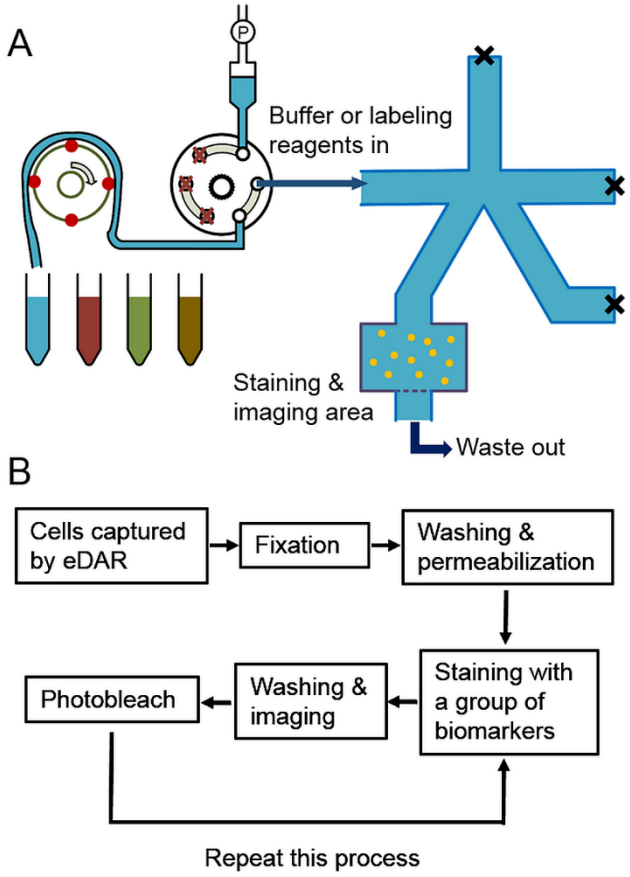

Figure 3.2 General scheme and procedure of the sequential immunostaining and photobleaching tests. A) The inline labeling system coupled to the current eDAR system. A peristaltic pump delivered the labeling reagents and washing buffer. The cross bars on this figure mean the corresponding ports were closed during the experiments. B) The general process flow of the sequential immunolabeling and photobleaching experiment.

If there was a need to perform intracellular marker testing, the captured cells could be fixed and permeabilized on the chip prior to the test. Then multiple rounds of the staining, washing, imaging and bleaching experiments could be performed sequentially. In each round, four colors of

fluorescence — yellow (PE), red (Alexa 647 or APC), green (FITC), and blue (nuclear stain) — were monitored.

3.2.3 Characterization and Optimization of the Photobleaching Process

There are two critical factors that could determine the efficiency of the photobleaching step—exposure power and time. We carefully characterized and optimized them to improve the efficiency and throughput while ensuring that the cells were not damaged by potential heating. The photobleaching curve under different exposure powers was studied first (Figure 3.3A). MCF-7 cells were labeled with anti-EpCAM-PE, and placed on a No.2 coverslip. We bleached the labeled single cells with three different power settings. The bleaching curves show that the exposure time could be controlled under 10 min to get a more than 95% bleaching efficiency when the exposure power was higher than 2 mW.

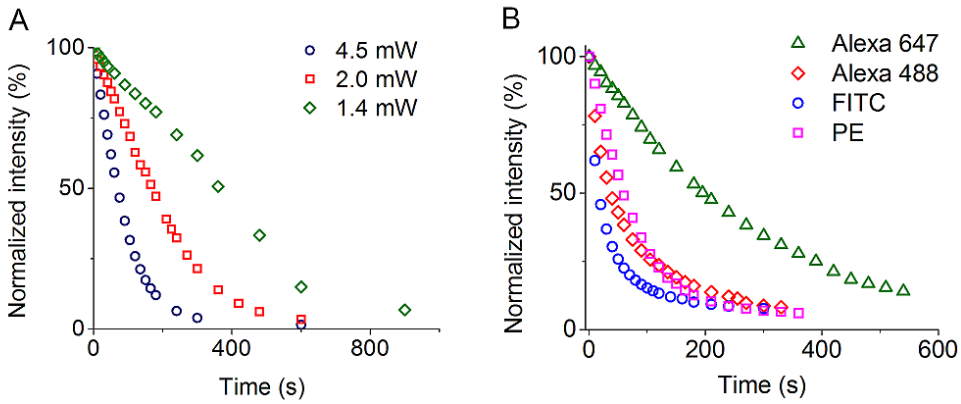

Figure 3.3 Optimization of the photobleaching process. (A) Photobleaching curves for the MCF-7 cells labeled with anti-EpCAM-PE exposed to different powers of the light source. (B) Photobleaching curves for the MCF-7 cells labeled with anti-EpCAM conjugated with Alexa 647, Alexa488, FITC and PE.

Based on this, we studied the bleaching curves of the four fluorophores, PE, FITC, Alexa 488 and Alexa 647, which could be directly applied in our scheme. Figure 3.3B shows that the fluorescent emission of PE, FITC and Alexa 488 could be bleached to less than 10% in less than 5 min; the photobleaching times for Alexa 647 took longer, partly because the power of the light source between 610 to 660 nm (red excitation) was lower than that in the range of yellow and green excitation. As a result, we set the bleaching time as 15 min to get a high bleaching efficiency with an acceptable throughput. This could be further improved by raising the power of the light source; however, it might increase the risk of heating and cellular damage.

3.2.4 Sequential Immunostaining and Photobleaching Tests

For this part of the study, we designed an assay for the expression of protein markers on captured CTCs based on four rounds of sequential immunostaining and photobleaching processes. We monitored four different makers in each round through four individual channels using epi-fluorenscence microscopy. Each set of markers had a nuclear stain (Hoechst) as a positive control marker, CD45 conjugated with FITC as a negative control marker, and two protein markers conjugated with PE or Alexa 647. Our system was designed not to bleach the Hoechst stain for two reasons: First, because the stain was used as a positive control marker, we could not keep track of it if we photobleached it. Second, it would require a UV exposure to bleach the stain, which could cause significant cellular damage [93]. CD45 is widely expressed on many types of white blood cells (WBCs), which are considered to be the biggest interferences in the separation of CTCs. Therefore, they are frequently used as negative control markers.

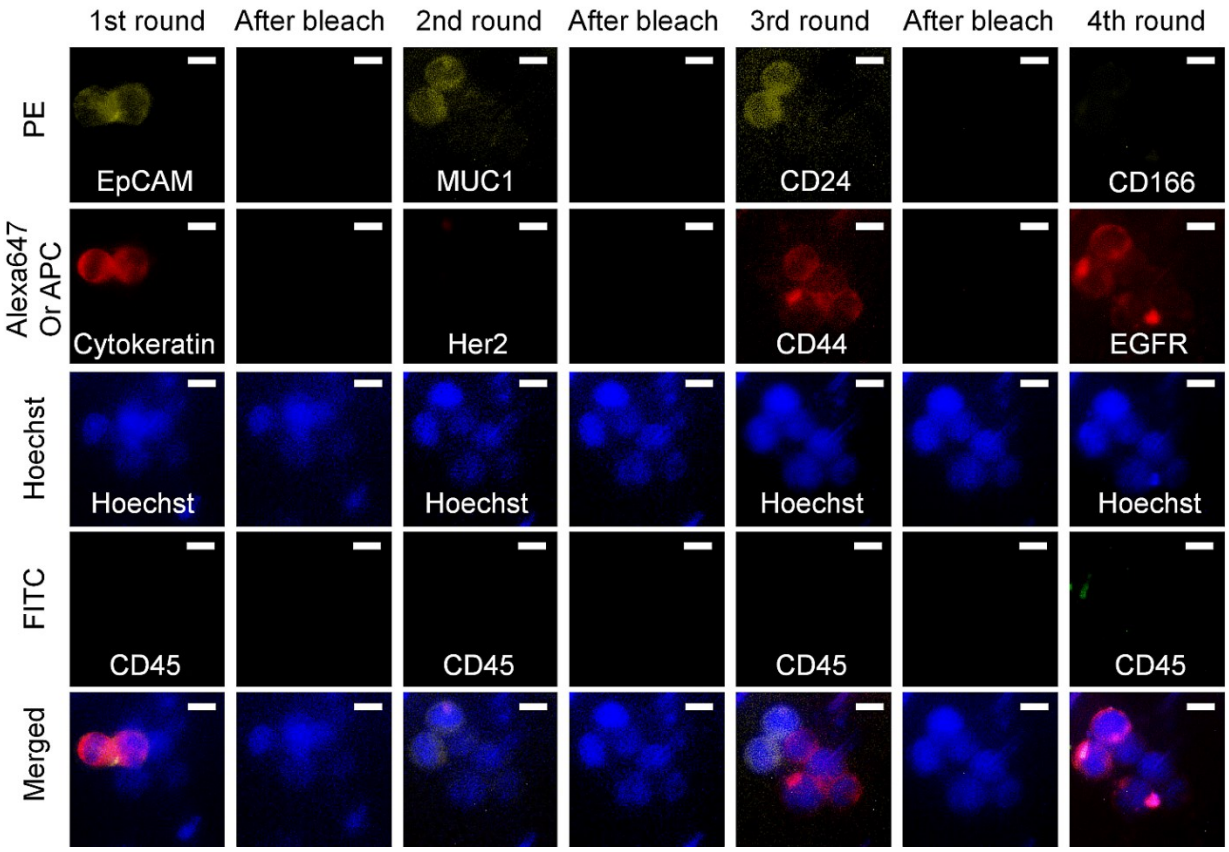

Figure 3.4 Sequential immunostaining and photobleaching results for six cancer cells trapped on an eDAR chip. The Hoechst nuclear stain was used as a positive control marker and CD45 was used to exclude the potential interference from WBCs. Eight protein markers were studied, including EpCAM/Cytokeratin, MUC1/Her2, CD44/CD24 and CD166/EGFR. Scale bar represents 20 μm.

Many protein markers could be tested on CTCs but as a proof of concept, we selected eight antigens and divided them into four groups (Figure 3.4). The first set had EpCAM and cytokeratin, which are the most widely used markers to identify CTCs [47, 63]. We applied this immunostaining test set right after the capture of CTCs by eDAR to further confirm and enumerate the CTCs with epithelial biomarkers. Figure 3.4 shows that there were six tumor cells trapped on the eDAR chip, which are positive to the Hoechst stain but negative to CD45. Two of them had a strong expression of EpCAM and cytokeratin, which implied the cells had epithelial characteristics.

The second set was designed to investigate other epithelial markers which are important for clinical and biological studies. We selected Her2 and MUC1 as the two protein markers for this set since these two biomarkers play important roles in the cancer pathogenesis and resistance to drugs [64, 94]. They are also potential targets of the anti-tumor drugs and immunotherapy. The second round of labeling in figure 4 shows that part of the cells trapped on the eDAR-chip had MUC1 expression but all of them were really low in their Her2 expression. However, in other experiments, we did observe cells expressing Her2 strongly (Figure 3.5)

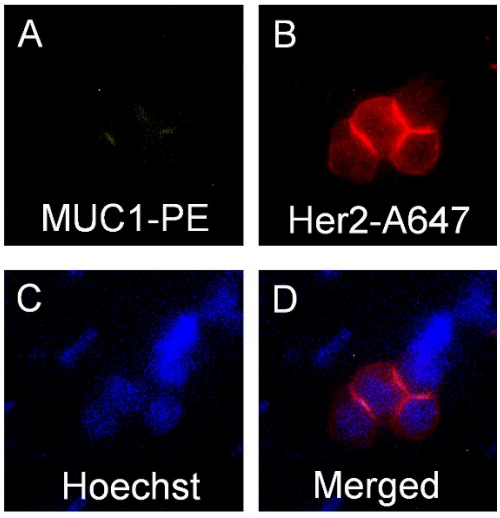

Figure 3.5 Fluorescence images of the four cancer cells captured on eDAR with Her2+/MUC1- character. A) shows a very dim yellow emission from PE, which was conjugated with MUC1, B) shows a strong red emission from Alexa 647, which was conjugated with Her2, C) shows the results of Hoechst stain, and D) is the merged image of the above three.

Cancer stem cells have been shown to play important roles in tumor progression and have been observed in the population of CTCs [82]. The third set of markers had two cancer stem cell antigens, CD44 and CD24. They are extensively studied as stem cell markers for breast cancer and possibly for other types of cancers as well [84]. Figure 3.4 shows that 4 cells had a strong

expression of CD44+/CD24-, and the other two are CD44-/CD24+. Other stem cell markers, such as CD133 and CD105, could also be used in this group based on the type of primary cancer.

The last set of markers in figure 3.4 was designed to look at the expression of EGFR and CD166 to demonstrate the mesenchymal characteristics of tumor cells. EGFR has been shown to be associated with the EMT process [95], and CD166 was used to define mesenchymal stem cells in bone marrow [96]. Other related markers, such as vimentin and cadherin, could be used in this group as well [40, 52].

3.2.5 Single-Cell Manipulation and Culture of captured CTCs

One important advantage of eDAR is its ability to easily access the isolated CTCs that are concentrated and retained within a small area on a filter. To demonstrate this point, we spiked cultured breast cancer cells (MCF-7) into whole blood, ran the blood through the chip, isolated the spiked MCF-7 cells on the filter, inserted a micropipette into the open volume and removed a single MCF-7 cell from the filter (Figure 3.6A). We transferred this MCF-7 cell into a culture dish containing cell culture media and cultured the cell for one week. Figures 6B and 6C show the selective removal of a targeted MCF-7 cell from other MCF-7 cells retained on the filter. We believe this capability will allow researchers to go beyond simple enumeration of CTCs and to perform single-cell molecular profiling and manipulation of individual isolated CTCs.

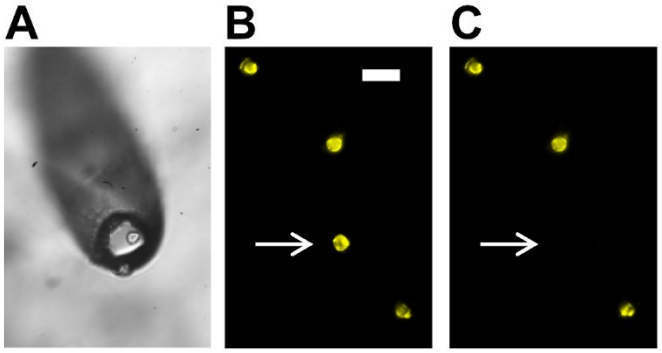

Figure 3.6 Single-cell removal on eDAR platform. (A) Photograph of the pulled capillary used for selecting a single cell for removal and further analysis. (B) Fluorescence image of EpCAM-labeled MCF-7 before and (C) after removal of the select cell from the filter. The scale bar is 40 µm.

After picking up the selected CTC, we could deliver that cell to another reservoir for cell culture and proliferation studies. Figure 3.7A shows that the same MCF-7 cell removed in figure 3.6 was delivered into the plastic reservoir sealed with a coverslip having photo-etched grids. After that, cell culture medium was added into this reservoir and placed in an incubator for cell culture. Figure 3.7B and 3.7C show the cell in figure 3.7A after 2 and 4 days, respectively. Those proliferated cells could be washed out of that surface and then labeled with antibodies, such as EpCAM, showing that this single-cell culture experiment did not change the function of the captured CTC.

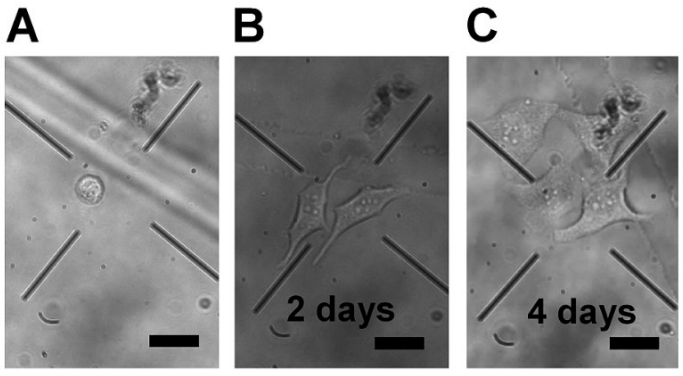

Figure 3.7 Single-cell culture of captured CTCs. (A) The image of a MCF-7 cell that was isolated using eDAR from whole blood, and then delivered on the single cell culture chip. (B, C) shows the cell in (A) after 2 days (B). and 4 days (C) of culture. The scale bar is 40 µm.

3.3. Materials and methods

3.3.1 Microfluidic Components and Line-confocal Optics

Briefly, the features were designed using AutoCAD (AutoDesk, San Rafael, CA), and then written on a transparency mask by Fineline Imaging (Colorado Springs, CO). Micro-features were fabricated on a silicon wafer using SU-8-3050 (Micro-Chem Corp., Newton, MA) as a negative photoresist; the feature height was controlled to be 50 μm. Once the features were developed, uncured PDMS was poured onto the silicon master, incubated at 75 °C for 2 hours, peeled off and then bonded to a glass coverslip using the plasma oxidation method.

Earlier, we had developed the line-confocal detection scheme where two laser sources, 488 and 633 nm, were used to form the two detection windows using a series of dichroic mirrors, cylindrical lens and beam splitters. The first detection window, having the two laser beams overlapped at the same time, was used to detect the fluorescence signals from the labeled CTCs, and then controlled the sorting automatically. The second detection window was used to confirm the sorted aliquots and monitor the sorting efficiency.

3.3.2 Biological materials and eDAR process

Isoton (Beckman Coulter Inc., Chino, CA) was used as the buffer for all the experiments unless otherwise specified. The breast cancer cell lines MCF-7, SKBr-3 and MDA-MB-231 (American Type Culture Collection (ATCC), Manassas, VA) were used to characterize the system. Cell culture was performed under the conditions recommended by the vendor, and harvested once a

week. MCF-7 was cultured in Eagle's Minimum Essential Medium (EMEM); SKBr-3 cells were cultured in McCoy's 5; and MDA-MB-231was cultured Dulbecco's Modified Eagle's Medium (DMEM) (ATCC, Manassas, VA). All media also contained 2 mM L-glutamine, 10% fetal bovine serum (FBS) (ATCC, Manassas, VA), and 50 μg/mL penicillin/streptomycin. Human whole blood drawn from healthy donors was purchased from Plasma Lab International (Everett, WA) and stored at 4°C upon arrival. Each 20-mL draw came in four 5-mL Vacutainer tubes coated with EDTA as an anti-coagulant. We discarded the first tube of each draw to avoid potential contamination from skin cells.

Antibodies were centrifuged for 5 min at 14,000 rpm to remove possible aggregates before any labeling procedure. Each blood sample was labeled with anti-EpCAM-PE (Abnova, Taipei City, Taiwan) in darkness and incubated at room temperature for 30 min. The labeled blood sample was washed and centrifuged (2,300 rpm for 10 min) to remove the free antibodies. The sample was immediately injected into the eDAR chip using a syringe pump. Typically, the flow rate was set to 50 μL/min for the operation of eDAR, although based on the previous optimization methods, it could be higher [76]. APD signal traces were collected by a PCI data acquisition card (PCI 6602, National Instruments, Austin, TX) and analyzed by a MATLAB (MathWorks, Natick, MA) script developed in-house. A home-built electronic box was programmed to give an automatic feedback control based on the detected APD signals, and apply a voltage on the solenoid (S-10-38-H-40, Magnetic sensor systems, Van Nuys, CA) connected to the microfluidic chip. More details about eDAR are described in chapter 2.

3.3.3 Sequential Immunostaining and Photobleaching Process

After washing the cells isolated by eDAR, main, side and waste channels were closed by turning off the inline valve. A 400-µL aliquot of cell fixation buffer (BioLegend, San Diego, CA) was introduced into the microchip by a peristaltic pump (Fisher Scientific, Pittsburgh, PA) at a flow rate of 15 µL/min. After washing with the buffer for 5 min at the same flow rate, the cells are permeablized by flowing through 250 µL of 2.5% surfynol 465 surfactant (Air Products and Chemicals Inc, Allentown, PA) for 15 min. After this step, four rounds of immunostaining and photobleaching of the cells are performed. For each round of staining, 220 µL of a staining solution with four biomarkers conjugated to four different fluorescent dyes were prepared. The details about the antibodies and nuclear stain used in each round are summarized in Table 3.1. After a centrifugation step (14,000 rpm for 5 min) to remove the aggregates, 200 µL of the supernatant was collected as the staining buffer. We injected it into the microchip at a flow rate of 20 µL/min. When the antibody solution filled the whole filtration area, the flow was stopped. Incubation took place for 20 min in dark to ensure all the trapped cells came into contact with the antibodies efficiently. After this step, the cells were washed for 10 min to remove any free antibodies and minimize the fluorescence background. Photobleaching was performed using a xenon arc lamp as the light source (Sutter instrument, Novato, CA). Each bleaching step took 15 min. A 20X objective was used for epi-fluorescence imaging and photobleaching. Fluorescence images were collected before and after the photobleaching step from 4 different emission channels: yellow (555 to 605 nm for PE), blue (435 to 485 nm for Hoechst), green (510 to 540 nm for FITC or Alexa 488) and red (665 to 695 nm for Alexa 647 or APC).

Round	1	2	3	4
Yellow channel	Anti-EpCAM-PE Lot# 515776 (1:50 dilution, Biolegend, San Diego, CA)	MUC1-PE Lot# B160021 (1:50 dilution, Biolegend, San Diego, CA)	Anti-CD24 PE Lot# B159732 (1:50 dilution, Biolegend, San Diego, CA	Anti-CD166 PE Lot# B139297 (1:10 dilution, Biolegend, San Diego, CA)
Red Channel	(PAN) Cytokeratin-AlexaFluro647 Lot# 4528S-14 (1:10 dilution, CellSignalling, Danvers, MA)	HER2-AlexaFluro647 Lot# B110523 (1:50 dilution, Biolegend, San Diego, CA)	Anti-CD44-AlexaFluro647 Lot# B124953 (1:66 dilution, Biolegend, San Diego, CA)	EGFR-APC Lot# B161059 (1:40 dilution, Biolegend, San Diego, CA)
Blue Channel	Hoechst Lot# 1249542 (1:500 dilution, Life technologies, Carlsbad, CA)	Hoechst Lot# 1249542 (1:500 dilution, Life technologies, Carlsbad, CA)	Hoechst Lot# 1249542 (1:500 dilution, Life technologies, Carlsbad, CA)	Hoechst Lot# 1249542 (1:500 dilution, Life technologies, Carlsbad, CA)
Green Channel	Anti-CD45-FITC Lot# B116314 (1:66 dilution, Biolegend, San Diego, CA)	Anti-CD45-FITC Lot# B116314 (1:66 dilution, Biolegend, San Diego, CA)	Anti-CD45-FITC Lot# B116314 (1:66 dilution, Biolegend, San Diego, CA)	Anti-CD45-FITC Lot# B116314 (1:66 dilution, Biolegend, San Diego, CA)

Table 3.1 Experimental details of the four rounds of immunostaining and photobleaching.

3.3.4 Safety Consideration for the Photobleaching Process.

To ensure safety when running the photobleaching tests, the highest power was locked to 10 mW. Certain protective methods should be considered when the sample is exposed to the light source, such as wearing protective goggles or covering the photobleaching area with a black box.

3.4. Conclusion

In this chapter, I report a semi-automatic inline injection system for our eDAR platform to perform sequential immunostaining and photobleaching tests. The expression of eight protein markers, as well as two control markers, was observed in four rounds of labeling and photobleaching. The experimental parameters were optimized to get a high bleaching efficiency and throughput. This downstream analysis method could be a complementary part of eDAR in the future to benefit studies of CTC subpopulations and quantitatively monitor the expression of multiple CTC protein markers. I also designed and tested the method which allowed us to selectively pick up the CTCs trapped by eDAR, and those cells could be delivered to another reservoir for further cell culture experiments.

Chapter 4 The Second Generation of eDAR with a Simplified Structure and an Improved Performance

4.1 Introduction

Many CTC analysis systems, including ours, utilize microfluidic components in order to overcome the technological challenges discussed in chapter 1, increase the sensitivity and improve the throughput [89]. Various systems have been built upon this principle, including the high-throughput line confocal detection method [92], flow counting method based on micro-Hall effects [97] and the conductometric detection platform [98-99]. Of course, many CTC analysis systems that do not involve microfluidics, instead relying on methods such as fiber optic array scanning [100] and immunomagnetic separation [31]. In fact, the only FDA-approved CTC analysis system, CellSearch, does not have microfluidic components, but rather selects and manipulates target cells via magnetic nanoparticles. A current trend, however, is to use the advantages brought by microfluidics – often in combination with nanotechnology – to build sensitive CTC methods [101-102]. Other types of microfluidic CTC systems include those which select/isolate target cells based on: (i) affinity chromatography like methods [67], (ii) size via micro-filtration [57], (iii) size, density, or permittivity via field flow fractionation [62], (iv) morphology via high-speed photography [103], and (v) size or density via Dean flow [61].

A recently reported CTC analysis method called ensemble-decision aliquot ranking, or eDAR (Chapter 2), combines the line-confocal fluorescence detection, an active sorting mechanism, a cell trapping and further purification process, and the ability to perform the identification and

subsequent analyses onto a single microfluidic chip. It has a high throughput, analyzing 1 mL of whole blood in 20 minutes, and the CTCs are captured onto a small area with a high enrichment ratio (more than a million fold). Due to the open access design of the cell trapping area, it is easy to manipulate and pick up single CTCs from the chip, aiming for possible downstream analysis.

Although eDAR has been proven to be a promising method, and more sensitive than the CellSearch method in detecting CTCs from metastatic breast cancer patients [76], the application of the original version is still limited by some design factors. First, the original microchip requires six individual layers (Figure 2.11), and four of them need to be assembled manually, which constrains the yield and efficiency of the chip production. Second, we used an on-chip solenoid to control the active sorting of CTCs, however, the drift of the piston in that solenoid was occasionally observed in some experiments, resulting in an unstable control of the hydrodynamic switching. Third, although the throughput of fluorescence imaging was improved significantly due to the very small area where CTCs were trapped on, the imaging quality might be affected by the track-etched polycarbonate filter, generating a non-uniform background.

To address these shortcomings, we reported the next generation of eDAR platform in this chapter, with a new active sorting scheme and a further purification component integrated into the micro-fabrication process. The re-designed microchip has only two layers, the PDMS feature and the glass substrate. We have evaluated multiple potential designs of the microfluidic chip and the hydrodynamic switching mechanisms, respectively, and optimized the analytical performance based on the best combination. The recovery efficiency was 95% with a zero false positive rate

(n=15), and the highest throughput tested was 4.8 mL of whole blood per an hour. We successfully applied this method on analyzing the samples from metastatic pancreatic cancer patients.

4.2 Results and Discussion

4.2.1 Redesigned Hydrodynamic Switching Scheme

In the first generation of eDAR, we designed a mechanical valve integrated onto the microchip, which was fast and robust compared to other reported active sorting mechanisms, such as the electro-osmotic flow [104] or the sole-gel transformation [105]. Although promising, some design factors may constrain the potential application of eDAR. To form such a mechanical valve on the chip, 3 individual structural layers were required, the solenoid, its PDMS thread, and the features of eDAR on a 150 μm PDMS film (Figure 2.11). This would make the chip preparation complicated and time consuming, resulting in a low yield, especially due to several manual alignment processes. Another shortcoming is the direct contact between the captured blood aliquots and the mechanical valve, which might increase the risk of the loss and damage of CTCs. During previous experiments, we also observed a slight drift of the solenoid's piston occasionally, and that would generate an inconsistent sorting performance. Moreover, during the eDAR process, the collection channel was closed at most of the time, which would limit the efficiency of the subsequent purification step, and increase the chance to form aggregates of cells on the polycarbonate filter.

In this work, we replaced the previous solenoid with an off-chip model, which are closed if no voltage was applied on, but can be opened in 3 to 4 ms when a 5V DC voltage is applied. Because

this in-line solenoid was not a part of the chip, the preparation of the microfluidic device was significantly simplified. It can be connected with the micro-channels very easily, resulting in many possible hydrodynamic switching schemes.

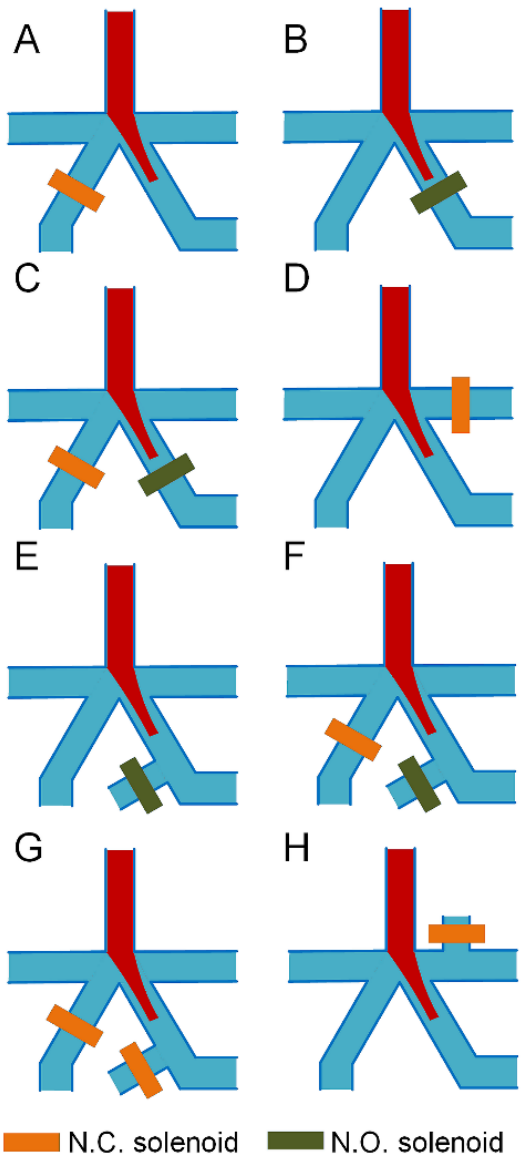

Figure 4.1 Summary of the 8 hydrodynamic switching schemes. The blood was injected from the main channel, shown as the red flow. Buffer flowed in the two side channels, CTCs were collected to the bottom left channel, and the waste was directed to the bottom right channel. The rectangular blocks represents

the solenoid. If the solenoid was set to be normally open (NO), the color of the block is set to green; if the solenoid was set to be normally closed (NC), the color is set to yellow.

We have designed and tested eight different schemes that can drive the fluidic switch. Figure 4.1 shows the basic configuration for each scheme. Depending on the normal state, number and location of the solenoids, their fluidic driving modes could vary, summarized in table 4.1. The solenoid's normal state was defined as the normal state, when the aliquots were ranked as "negative". If a 5V voltage was applied at that moment, the solenoid would work in a "normally open" mode, otherwise, it would work in a "normally closed" mode. Five of the schemes (Design A, B, D and H) used only one solenoid; the other three had two solenoids working either simultaneously (Design C and F) or sequentially (Design G). In six of the schemes (Design A, B, C, E, F and G), solenoids were connected with the two collection channels; in the other two schemes (Design D and H), the solenoid was connected with the side channel where buffer flowed.

Due to the structure of this type of solenoid and the elastic nature of PDMS, the performance of the fluidic switch varied notably. We evaluated this performance by analyzing the "switch over" and "switch back" time for each scheme, respectively. The "switch over" time was defined as the time for switched blood flow switched from the waste collection channel to the CTC collection side, which partly determined the throughput of this method. The "switch back" time was determined as the blood flow switched from the CTC collection channel back to the waste side, which was closely related to the size of the collected aliquot. Table 4.1 shows that design G and H had the best fluidic performance, 2 to 3 ms switch over and back time, respectively. However, scheme G requires a complicated procedure, having 4 individual steps in each cycle, which make this scheme hard to be utilized in practice (see table 4.1 for more information).

Scheme	Position	Normal state	Left pressure (psi)	Right pressure (psi)	Switch over time (ms)	Switch back time (ms)
A	Collection	Closed	Low	High	~2-3	~15-25
B	Waste	Open	High	Low	~15-20	~2-3
C	Collection Waste	Closed Open	Low	High	~4-5	~10
D	Right buffer	Close	Low	High	~3	~40
E	Waste	Open	High	Low	~25	~2
F	Collection Center waste	Closed Open	Low	High	~25	~5-6
G	Collection Center waste	Closed Closed	Low	High	~2-3	~2-3
H	Center right buffer	Closed	Low	High	~1-2	~2-3

Table 4.1 Summary of the fluidic configuration and performance of the 8 sorting schemes. Two solenoids were used in scheme C, E, and G. When there were two outlets or inlets on a single channel, the position of the solenoid was marked. For example in scheme F, the position of the second solenoid was "center waste", meaning that it was placed on the center outlet of the waste collection channel. In every scheme except (G), when the "positive" events were detected, the DC voltage applied on the solenoids were changed immediately to trigger the sorting, and after a certain period of time was changed back to the normal state. Scheme G utilized 4 individual steps to control the sorting. Initially, both solenoids were set to closed, and the blood would flow to the waste channel. When the sorting was triggered, only the solenoid on the collection side was opened to perform the switch over step; after the cell was collected, the other solenoid was opened to perform the switch back step. After the blood flow was completely switched back, both solenoids were closed at the same time, same as the normal state.

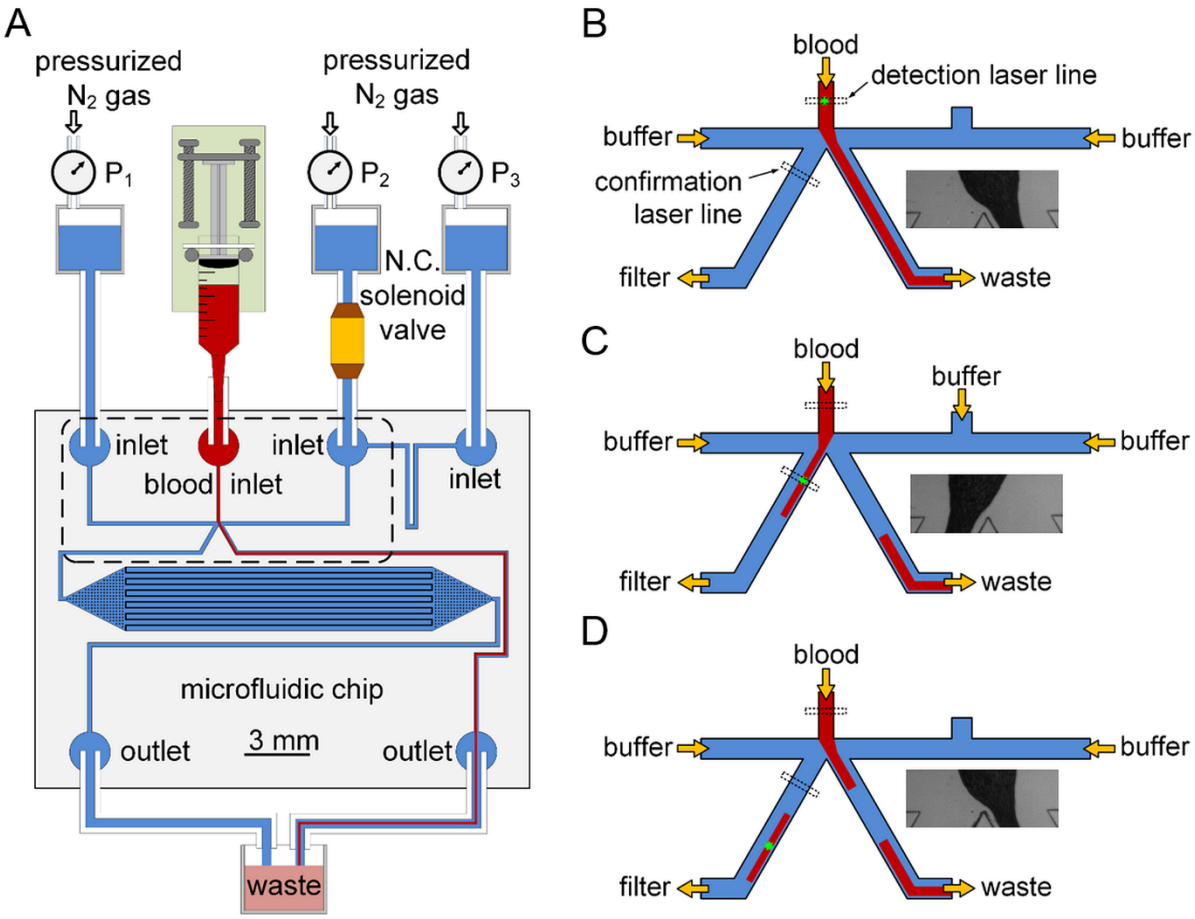

Figure 4.2 Microfluidic chip and hydrodynamic switching scheme of eDAR. (A) General structure of the microfluidic chip and the configuration of the eDAR platform. The bottom left channel was to collect sorted aliquots and transfer them to the subsequent purification area, which had 20,000 micro-slits. The area surrounded by dashed lines is further explained in B, C and D. B) The flow condition when no positive aliquot was ranked. (C) The blood flow was switched to the CTC collection channel, and the sorted aliquot was confirmed by the second APD. (D) The flow was switched back after the aliquot was sorted.

After the characterization and optimization, the following structure of the eDAR chip (Figure 4.2) and the corresponding scheme (Figure 4.1H) of the hydrodynamic switch were chosen for the reported generation of eDAR. The labeled blood sample was injected into the top channel of the microchip using a syringe pump (Figure 4.2A). Two side channels, where buffer driven by compressed nitrogen flowed through, were used to control the active sorting step. There were two

ports placed on the right side channel, and both of them were connected to a reservoir filled with pressurized buffer. The normally closed solenoid was connected to the port near the sorting junction to control the hydrodynamic switch. There are two channels after the sorting junction: the one on the left was used to collect "positive" aliquots and deliver them to the further purification area; the one on the right was the waste collection channel, where all the negative aliquots flowed through.

When those aliquots were ranked as "negative" (Figure 4.2B), there was no voltage applied on the solenoid, so it was closed. An initial pressure drop was set between the No.1 and 3 buffer sources in figure 4.2A, so the blood could only flow into the channel collecting the waste, which is shown in figure 4.2B. However, when a positive event was detected by the first detection window, a 5V DC voltage was immediately applied on the solenoid to introduce the buffer flow from the No.2 buffer reservoir. This would decrease of the flow resistance in right-side buffer channel, and thus generate a higher flow rate of buffer there. The blood flow would be pushed from the right side to the left, so the positive aliquot could be collected (Figure 4.2C). After this aliquot was collected and confirmed by the second detection window, the voltage was changed to 0V to close the solenoid and thus switch the blood flow back to the waste side (Figure 4.2D).

The time required for the switch over and back step was determined to be 1 to 2 ms and 2 to 3 ms, respectively (Figure 4.3, Table 4.1), which are close to the response time of this type of solenoid. This process was stable enough for eDAR even after more than 10^5 on-off cycles. The in-line solenoid was placed on the buffer line, so blood would not contact with the solenoid, which minimized the possibility of the blood coagulation and cross-contamination.

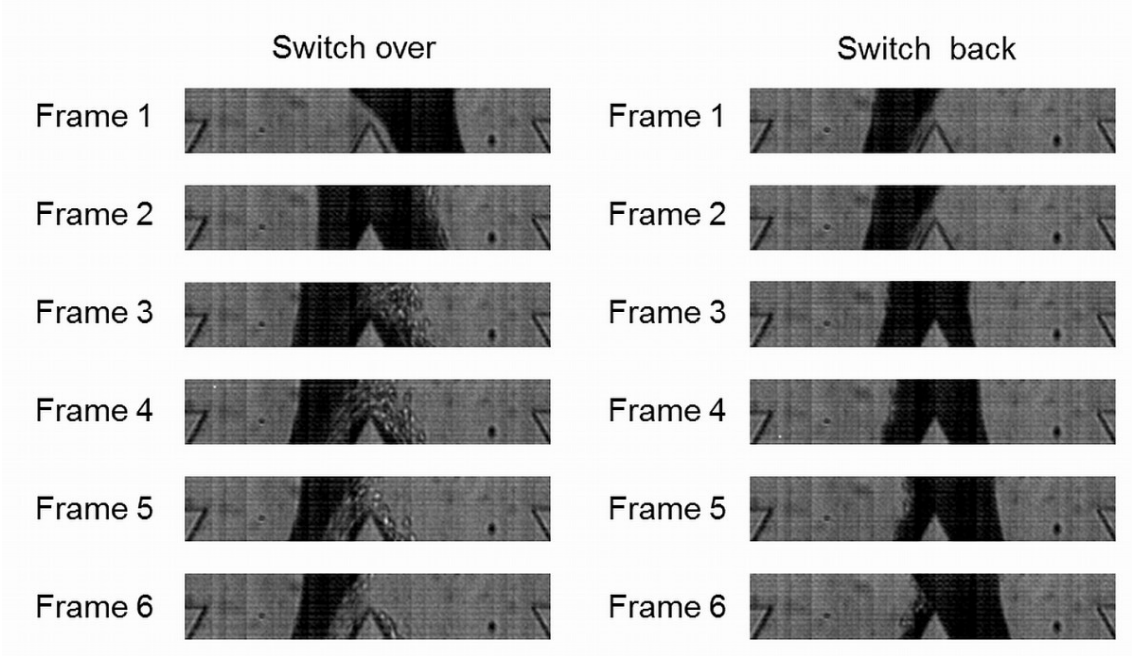

Figure 4.3 Switching time for the current fluidic scheme recorded by high speed camera. The frame rate was 1918 fps, so the average switch over time was 1 to 2 ms, and the switch back time was also 2 to 3 ms. It's worth to point out that in both steps we observed the back flow of a fraction of blood, which does not affect the sorting speed and efficiency.

4.2.2 On-chip Purification Component Based on Microslits

In the first generation of eDAR, we used a piece of tracked-etched polycarbonate filter to retain and purify the captured CTCs on the microfluidic chip. It required two additional layers to make this part, the polycarbonate filter and the waste removal layer, as well as a complicated procedure to assemble those layers. To bond the polycarbonate filter between two PDMS layers, a surface modification step using silicon compounds and multiple plasma assisted oxidation steps were often necessary. In this chapter, I report a new structure of the filtration unit consisting of micro-slits made of PDMS and does not require any additional layers assembled with the eDAR-feature.

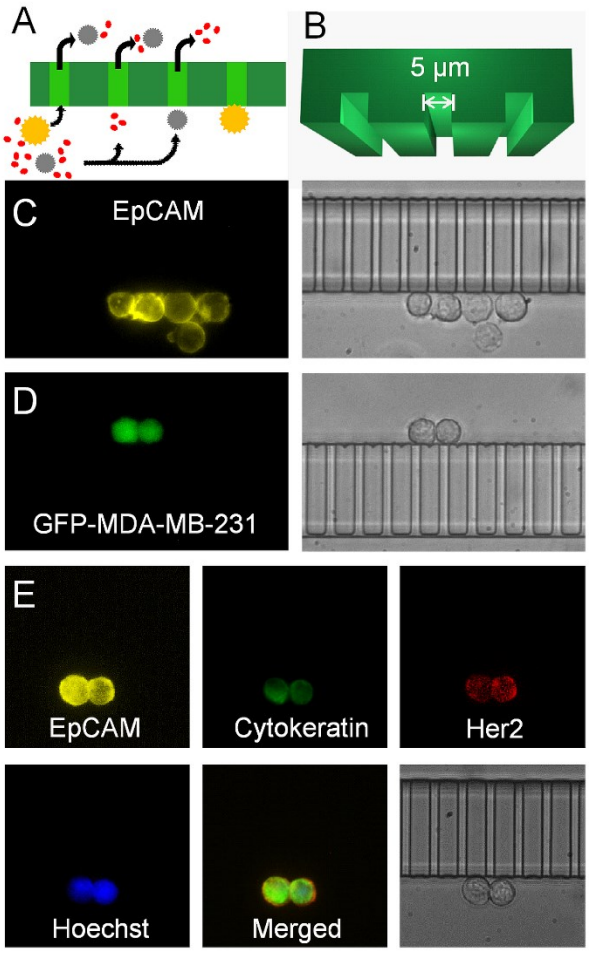

Figure 4.4 Micro-slits and multi-color fluorescence imaging of captured CTCs. (A) The sorted aliquots were further purified through the array of micro-slits. (B) The 3D model of the micro-slits with a 5 µm height and a 5 µm width. (C) Fluorescence and bright field images of five MCF-7 cells captured via eDAR. (D) Fluorescence and bright field images of two MDA-MB-231-GFP cells captured based on the GFP signal without any pre-labeling. (E) Two SKBr-3 cells were captured by eDAR, and further labeled with additional markers.

Figure 4.4A shows the basic structure of these PDMS filter. The microslits on the side of the flow would capture the CTCs without retaining any red blood cells (RBCs). The size of the slit was optimized to 5 µm tall and 5 µm wide (Figure 4.4B), so we would not lose any small CTCs. Due of the ultra-high enrichment ratio of eDAR (up to 1 million fold) [76], only a small amount of

WBCs would be isolated and retained on the filter with this size, which is smaller than most filters used to capture CTCs. Because this microfilter was made of PDMS and bonded with a piece of coverslip, the imaging quality was improved significantly (Figure 4.4C and D) compared to the polycarbonate filter, which is not fully transparent and may generate the scattering and aberration. Moreover, since the cells can only be trapped along the array of slits, they could be easily referenced and tracked, while in a lot other methods, the cells distributed randomly on the surface. This could make the imaging procedure faster and the results of enumeration more accurate.

It is also fast and efficient to perform the secondary labeling on the trapped CTCs, due to the fluidic design with a small internal volume. Figure 4.4E shows two breast cancer cells (SKBr-3) labeled with anti-EpCAM-PE captured by eDAR. We then fixed, permeabilzed and labeled them using anti-Cytokeratin-Alexa488, anti-Her2-Alexa647 and Hoechst. Fluorescence images shows the expression of these markers on these two cells clearly, and the bright-field image also confirmed their morphology. We also applied anti-CD45-Alexa700 as a negative control marker to exclude interference from WBCs, and did not find any signal in this channel.

To optimize the performance, we prepared and tested eDAR chips with 1000, 5000, and 20000 micro-slits, respectively. This number would determine the flow resistance across the filtration area, which could affect the hydrodynamic switching and the stress on the trapped cells. The eDAR-chip with 20000 slits would require a low pressure (< 4 psi) on the two side buffer channels to balance the switching step. The pressure drop across the filter was also lower compared to the other two designs, which would minimize the stress and deformation of the cell.

4.2.3 Characterization and Analytical Performance

The efficiency of the active switching step could be monitored in real time. For example, figure 4.5A shows a small portion of the APD data from a pancreatic cancer patient sample. The signals in blue were from the first detection window, ranking the aliquots and controlling the active sorting step. The two peaks at 978 and 1298 ms in this channel represented two CTCs labeled with anti-EpCAM-PE, which triggered the aliquot sorting, respectively. The two subsequent peaks in red showed there were two labeled CTCs flowing through the second detection window, which was located on the collection channel, confirming that the two positive aliquots were actually sorted. It is also worth to point out that the change of background in the second detector (Figure 4.5A) could also confirm that only a small portion of blood was collected in eDAR, resulting in a high enrichment ratio.

Because it took time for the labeled CTC to flow from the first detection window to the second one, we could observe a time difference between the decision APD trace and its conformational signal (Figure 4.5A). This time difference was defined as the transit time of the sorted CTCs to characterize the performance of the active sorting step in eDAR. The transit time of each sorted CTC varied a lot, because the CTCs could have different linear flow rates in the top channel. Figure 4.5B shows the distribution histogram of the transit time at the flow rate of 40 and 80 μL/min, respectively. Generally, a higher volumetric flow rate of the blood would resulted in a shorted transit time (Figure 4.5C). When the flow rate was 90 μL/min, the average transit time was lowered to 4 ms, close to the switch over time of the current active sorting scheme (Figure 4.3), which implied the limit of the throughput for the current design.

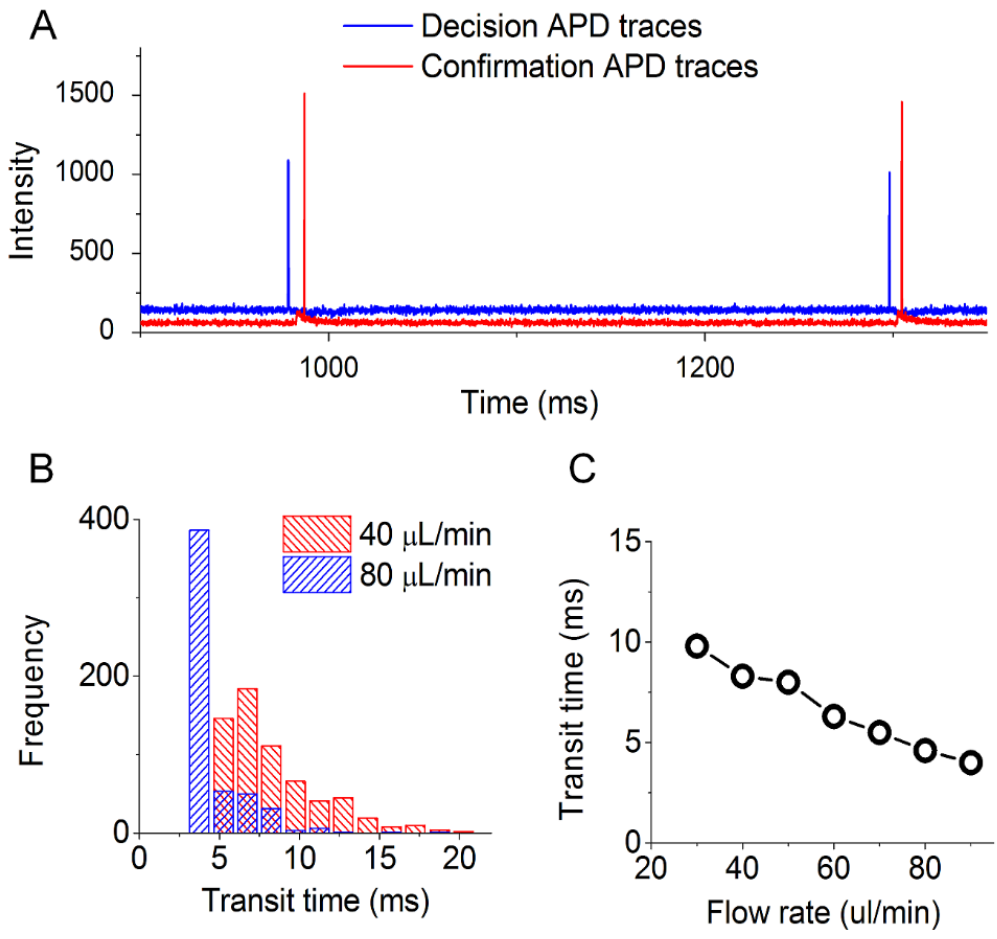

Figure 4.5 Transit time of the sorted CTCs. (A) The segment of APD data from a pancreatic cancer sample shows two events triggered the sorting and then confirmed by the second detection window. (B) The distribution of transit time at the flow rate of 40 and 80 μL/min, respectively. (C) A plot shows the fastest average transit time was about 4 ms when the flow rate was 90 μL/min.

If the transit time for a CTC was shorter than the hydrodynamic switching time, that cell could not be sorted on this platform. The sorting efficiency was thus defined as the number of collected events versus the total number of events that triggered the sorting. Figure 4.6A shows the values of sorting efficiency at the flow rate of 30 to 100 μL/min. When the flow rate was 30μL/min, the sorting efficiency was almost 100%, because the average transit time at that flow rate was around

10 ms (Figure 4.5C), which is long enough for the active sorting step to collect the CTCs. The sorting efficiency decreased to 90% at the flow rate of 80 μL/min, and then dropped to 49% when the flow rate was 90μL/min.

Figure 4.6A also shows the recovery efficiency of eDAR at different flow rates, which had a similar trend compared to the sorting efficiency. However, the recovery efficiency was defined as the number of spiked-in cells versus the number of recovered cells counted using multicolor fluorescence imaging on the eDAR chip. This performance is a combination of many factors, including the antibody labeling efficiency, the line-confocal detection efficiency, and the sorting efficiency. This explains the difference between the recovery and sorting efficiency at the same flow rate. As a result, for the reported generation of eDAR, the upper limit of the throughput in this generation was 80 μL/min (12.5 min for 1 mL of blood) with an 88% recovery ratio. Although this throughput is higher than most of the CTC technologies for the analysis of whole blood, it can be further improved by designing a wider blood inlet channel or moving the first detection beam up.

3 to 975 MCF-7 cells were spiked into 1 mL of healthy blood to analyze the recovery efficiency at the flow rate of 50 μL/min, respectively. To ensure of the accuracy of the cell numbers at the low end, we used a capillary counting method [81] to spike in cultured cells precisely, when the concentration was lower than 100 cells/mL. The average recovery efficiency was 95% with an R^2 value of 0.998 (Figure 4.6B), higher than that of the first generation of eDAR (93%) [76]. Because the concentration of CTCs are usually very low, the enumeration results could be affected by Poison distribution. In this case, the ability to analyze a larger volume of whole blood sample with

an acceptable throughput and recovery ratio would be very important. We spiked the same number of MCF-7 cells into 1, 5 and 10 mL of healthy blood, and then analyzed these 3 samples at the flow rate of 50 μL/min, respectively. There was no significant change in their recovery ratio (Figure 4.6C), which shows that our method is capable of running a large amount of whole blood sample with a high efficiency and throughput.

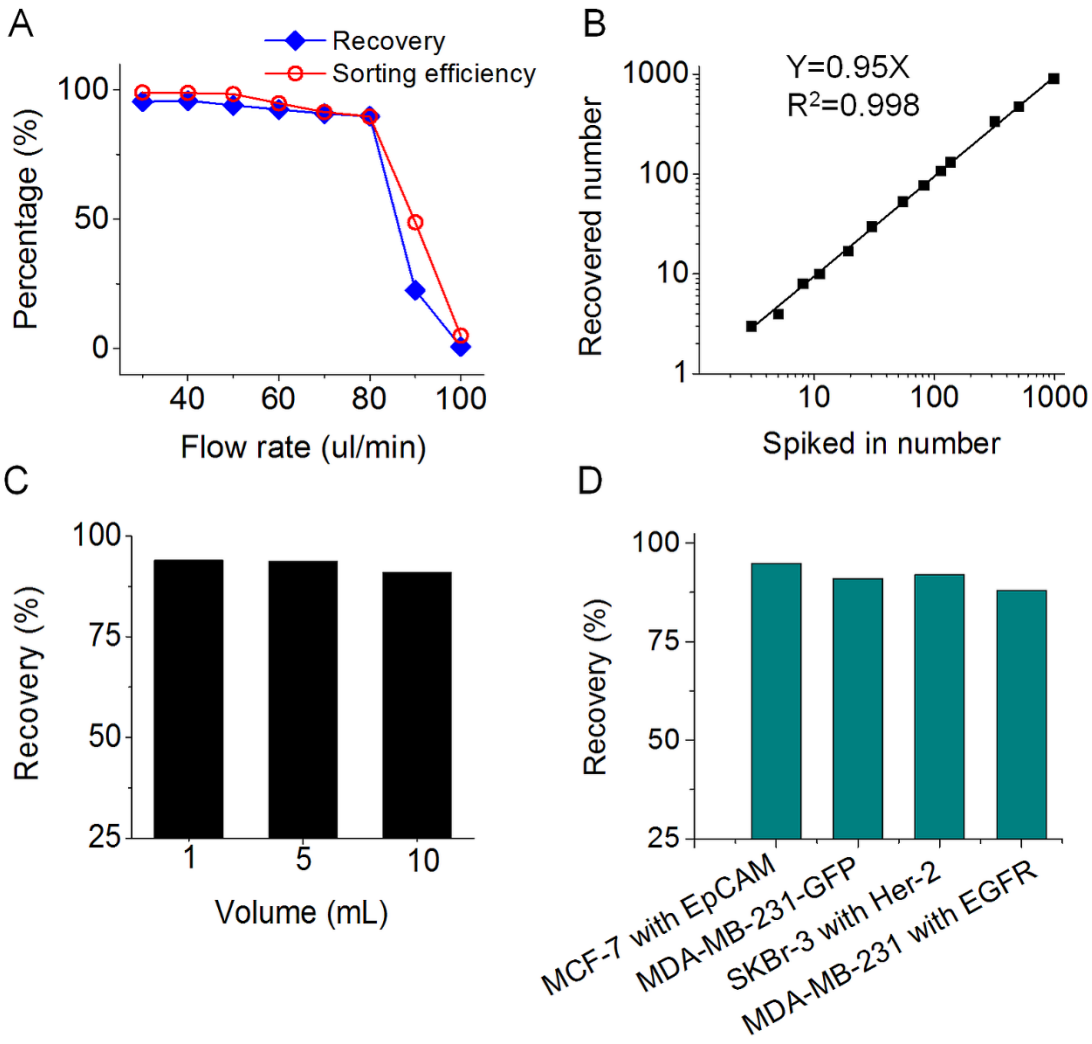

Figure 4.6 Sorting efficiency and recovery performance of eDAR. (A) The recovery and sorting efficiency value versus different flow rate. (B) The recovery ratio of MCF-7 cells spiked into whole blood. (C) The recovery ratio of 300 MCF-7 cells spiked into 1, 5 and 10 mL of whole blood, respectively. (D) The recovery ratio of 4 selection schemes of 4 breast cancer cell lines spiked into whole blood.

Although EpCAM was used in most of the CTC methods to select tumor cells, more and more studies reported that CTCs with a low EpCAM expression would have more mesenchymal characteristics and are more aggressive [70]. It is flexible to use any labeling scheme to select rare cells in eDAR, so we could select tumor cells based on biomarkers other than EpCAM. We designed three schemes to select different cultured cancer cell lines based on surface antibodies (Figure 4.6D). EpCAM was used to select MCF-7 cells, Her-2 was used to select SKBr-3 cells, and EGFR was used to select MDA-MB-231 cells. All these three schemes can separate and trap the targeted cells with a recovery ratio higher than 88%. Another unique and important feature of eDAR is the independence of the biomarker's location. Other technologies, for example, the surface capture methods, could only capture the cells based on the antigens on their surface, but our method can select cells based on an intracellular marker as well, such as GFP (Figure 4.4D). The recovery ratio of the MDA-MB-231-GFP cells spiked into whole human blood was 91% (Figure 4.6D). Since fluorescent proteins are widely used in animal model to study the progression and mechanism of metastasis [106], eDAR could be an ideal tool to select CTCs in these models without any additional labeling step.

4.2.4 eDAR Analysis of Blood Samples from the Patients with Pancreatic Cancer.

Blood samples from 15 healthy donors were used to evaluate the false positive ratio of this method, and no CTCs were found in any of them. We collected 26 blood samples from the patients with metastatic pancreatic cancer. 16 of them were analyzed using the first generation of eDAR, and the other 10 samples were analyzed using the new eDAR platform reported in this chapter. The

raw data of those clinical samples are summarized in table 4.2. Using this method, we detected CTCs in 80% (8 of 10) of the samples ranging from 2 to 872 cells/mL. CTC clusters, reported by previous studies [67], were also observed in patient blood. It is interesting to point out that many of the clusters observed in our experiments had a low EpCAM expression. Figure 4.7 shows a cluster of CTCs with a high expression of cytokeratin and a low expression of EpCAM.

Sample	Volume (mL)	CTCs counts	Sample	Volume (mL)	CTCs counts	Sample	Volume (mL)	CTCs counts
Control 1	1	0	Control 15	1	0	Patient 14	1	8
Control 2	1	0	Patient 1	1	183	Patient 15	1	2
Control 3	1	0	Patient 2	1	9	Patient 16	1	10
Control 4	1	0	Patient 3	1	7	Patient 17	1	872
Control 5	1	0	Patient 4	1	3	Patient 18	1	2
Control 6	1	0	Patient 5	1	14	Patient 19	1	5
Control 7	1	0	Patient 6	1	6	Patient 20	1	12
Control 8	1	0	Patient 7	1	4	Patient 21	1	22
Control 9	1	0	Patient 8	1	0	Patient 22	1	2
Control 10	1	0	Patient 9	1	0	Patient 23	1	0
Control 11	1	0	Patient 10	1	27	Patient 24	1	14
Control 12	1	0	Patient 11	1	44	Patient 25	1	0
Control 13	1	0	Patient 12	1	5	Patient 26	1	7
Control 14	1	0	Patient 13	1	7			

Table 4.2 Raw data of the healthy control (n=15) and the pancreatic cancer samples (n=26). Patient sample #1 to #16 were analyzed using the first generation of eDAR; patient sample #17 to #26 were analyzed using the second generation of eDAR.

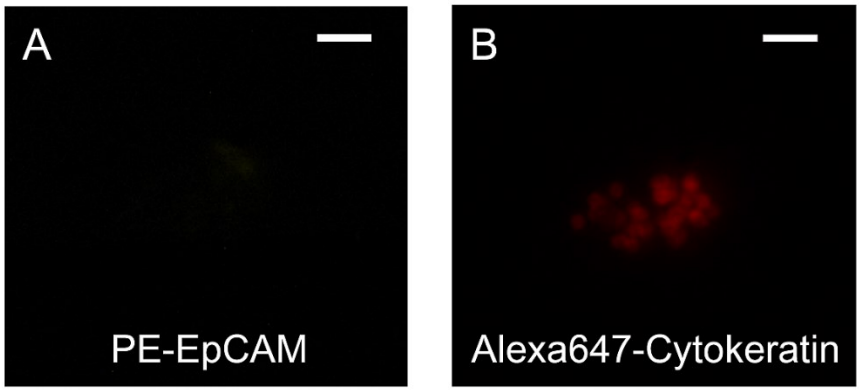

Figure 4.7 A CTC cluster with low EpCAM expression from a pancreatic cancer sample (No. 20). The scale bar is 100 μm.

Figure 4.8 also summaries the distribution of the three data sets for the healthy control blood samples analyzed by the reported method, pancreatic cancer samples analyzed by the first generation of eDAR, and the pancreatic cancer samples analyzed by this method, respectively. We compared the performance of the two generations of eDAR using the analysis of variance (ANOVA), which shows that the two data sets were not significantly different ($p=0.30$, $\alpha=0.05$).

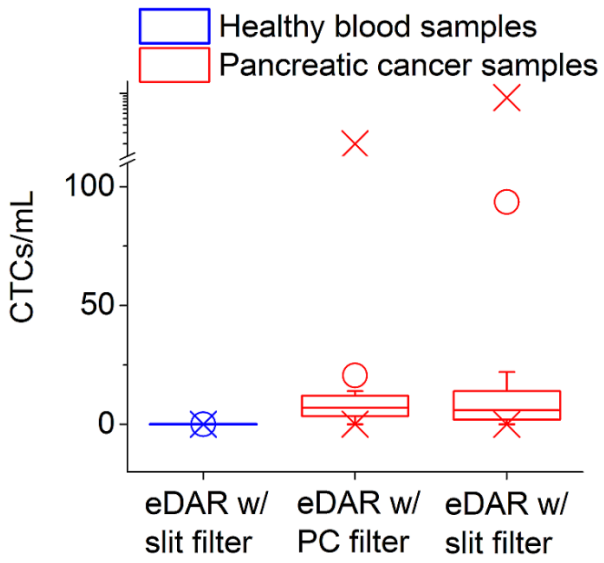

Figure 4.8 The distribution of control and pancreatic patient samples analyzed by eDAR. 15 control samples and 10 pancreatic cancer samples were analyzed by the reported method; 16 pancreatic cancer samples were analyzed by the first generation of eDAR.

4.3 Materials and Methods

4.3.1 Design and Fabrication of the Microfluidic Chips

The microfluidic chips had two functional areas integrated in the same design, eDAR sorting features and the filtration unit based on slit structures. The main channel in the sorting unit, which introduced the blood into the sorting junction, had a height and width of 50 and 150 μm, respectively; all the other 4 channels were 50 μm tall and 200 μm wide. The slit-filters were 5 μm tall and 5 μm width, and the maximum number of slits we tested was 20,000.

The silicon master was fabricated using two photolithography processes, which were summarized in figure 4.9. The features were designed using AutoCAD (Autodesk, San Rafael, CA), and written on a chrome mask (TRICR Corporation, SF, CA). Positive resist lithography and deep reactive ion etcher (DRIE) were chosen for forming the first layer, the micro-filter feature. AZ 1512 was used as a positive photoresist, which was provided by Micromanufacturing Facility (MMF) in University of Washington. DRIE process was optimized to achieve a depth in the range of 4.5-5 μm. The second layer of the eDAR feature was fabricated using the SU-8-3050 as a negative photoresist (MicroChem, Newton, MA), and the height of the feature was controlled to be 50 μm. After the master was silanized using tridecafluoro-1,1,2,2-tetrahydrooctyl-1-trichlorosilane (Sigma-Aldrich, St. Louis, MO), uncured PDMS was poured onto the silicon wafer and baked for 2 hours at 70°C. The piece of PDMS with the desired micro-feature was then peeled off from the

silicon master, and then bonded with a piece of cover glass using the standard process of plasma oxidation.

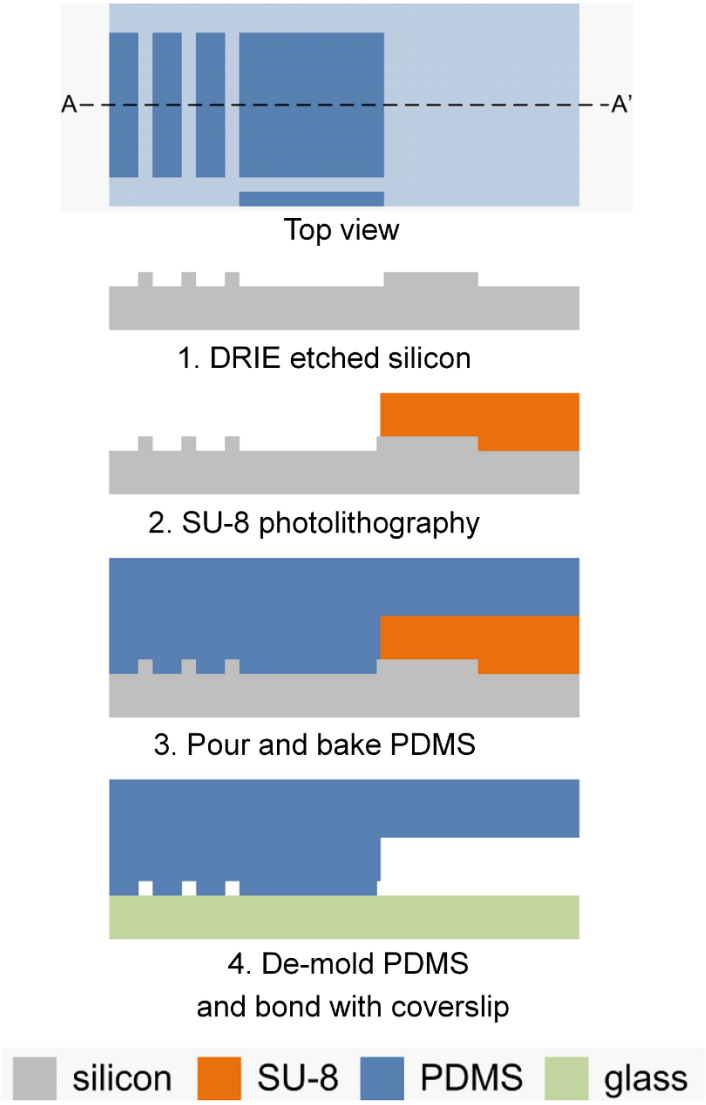

Figure 4.9 The process flow the micro fabrication steps.

4.3.2 Biological Materials and Patient Samples

Three breast cancer cell lines, SKBr-3, MCF-7, and MDA-MB-231 (American Type Culture Collection (ATCC), Manassas, VA) were used to characterize and optimize the eDAR system.

SKBr-3 cells were cultured in McCoy's 5, MCF-7 was cultured in Eagle's Minimum Essential Medium (EMEM), and MDA-MB-231 was cultured in Dulbecco's Modified Eagle's Medium (DMEM) (ATCC, Manassas, VA). All cell culture media also contained 2 mM L-glutamine, 10% fetal bovine serum (FBS) (ATCC, Manassas, VA), and 50 μg/mL penicillin/streptomycin (ATCC, Manassas, VA) at 37 °C with 5% CO2 in a humidified environment. The MDA-MB-231-GFP was provided by Prof. Gail Sonenshein in Tuffs University, and cultured in the DMEM medium with 10% FBS and 1 μg/mL puromycin (Life Technologies, Carlsbad, CA). Control blood from healthy donors was purchased from Plasma International Lab (Everett, WA), and the first tube of the blood draw was discarded to prevent any possible contamination from skin cells. Whole blood samples were drawn from patients with pancreatic cancer based on a protocol approved by Fred Hutchinson Cancer Research Center's institutional review board. Patient samples were collected in Seattle cancer care alliance (SCCA) using Vacutainer tubes (BD, Franklin Lakes, NJ) containing EDTA as an anti-coagulant, stored at 4 °C, and analyzed within 4 hours.

4.3.3 Sample Preparation and eDAR Analysis

Isoton (Beckman Coulter Inc., Chino, CA) was used as the buffer for all the experiments unless otherwise specified. For a typical experiment, 1 mL of whole blood samples were labeled with anti-EpCAM conjugated with PE (Lot No. 515776, Abnova, Walnut, CA) for 30 minutes at room temperature in dark. All the labeling parameters have been optimized based on our previous works [76]. The labeled samples was diluted to 14 mL and then centrifuged to remove the free antibodies. The final volume was adjusted to be as same as the initial volume. After that, the prepared sample was injected to the microfluidic chip using a syringe pump. Traces from fiber-coupled avalanche photodiodes (APDs) (Excelitas Technologies, Waltham, MA) were collected by a PCI data

acquisition card (PCI 6602, National Instruments, Austin, TX). The sorting process of eDAR was automatically controlled using a home-written LabVIEW (National Instruments, Austin, TX) script and a field programmable gate arrays (FPGA) device built in house. The hydrodynamic switching that collect the sorted aliquots were controlled by a solenoid (INKA1226212H) purchased from the Lee Company (Westbrook, CT).

After all the positive aliquots were collected onto the filtration area, isoton was used to quickly wash the filtration area in less than 1 minute. If any cytoplasmic markers are used for the secondary labeling, 4% of PFA was loaded into the filtration area to fix the cells. Surfynol® 465 (Air product, Allentown, PA) was used to peameablize the fixed cells. Anti-EpCAM-PE, anti-Cytokeratin-APC (Lot No. MAB5131, Abnova, Walnut, CA) and anti-CD45-FITC (Lot No. B116314, BioLegend San Diego, CA,) was typically used as the antibodies for the secondary labeling to confirm the identity of CTCs. Hoechst (Life Technologies, Carlsbad, CA) was also used as the nuclear stain to verify the labeled target is actually a nucleated cell.

4.4 Conclusion

eDAR has been proven as an "all-in-one" platform for analyzing rare cells in complicated biological matrix, such as CTCs in peripheral blood. In the reported work, we re-designed the eDAR platform by incorporating a micro-fabricated filter and a new hydrodynamic switching scheme. The structure of the microchip was simplified significantly, resulting in a higher yield and a better quality control of the chip preparation, as well as an ideal imaging quality to enumerate and analyze CTCs. The analytical performance was optimized, so we can analyze 1 mL of whole blood in 12.5 min with an average recovery ratio at 95% and a zero false positive rate (n=15). Bio-

markers other than EpCAM was also successfully applied to select different subpopulations of CTCs on this platform, including the intracellular markers, such as GFP. We have also validated this method by analyzing pancreatic cancer samples using this method. In summary, we believe this generation of eDAR platform is more sensitive, robust and flexible in analyzing CTCs from patient blood with a higher throughput, and it may potentially benefit the analysis of other types of rare cells as well.

Chapter 5 An Automated and High-throughput Counting Method for CTCs

5.1 Introduction

We recently developed a new method called ensemble-decision aliquot ranking (eDAR) to analyze rare cells from peripheral blood. The functions of detection, isolation, identification, and downstream analysis are integrated into one microfluidic chip. It is highly sensitive, with a detection limit close to 1 cell/mL, and the throughput is high enough for clinical applications (20 minutes for 1 mL whole blood) [76]. Due to the open-access design of the chip, it is easy to selectively extract captured cells and perform various downstream analyses. However, the whole process of eDAR still requires some manual manipulation, because cells trapped on the integrated filter need to be imaged and identified manually, and cell harvesting requires micro-pipetting by a skilled operator. This implies that eDAR might not be highly efficient for some special applications, such as a fast "coarse screening" of CTCs that may not require very detailed information of cellular and molecular profiles.

Actually, in clinical applications, CTCs are only enumerated; there is no additional analysis of CTCs beyond enumeration. For example, Veridex's CellSearch, which is the only FDA approved instrument at present, is solely for the enumeration of CTCs. As a result, we and our collaborators decided to determine if we can simplify eDAR for enumerating CTCs, which represents the majority of assays being run in the clinic that pertains to CTCs.

In this chapter, I report the development of a fast and automated screening method based on the multicolor line-confocal detection technique used in eDAR for CTCs. The sample processing and experimental procedures – which do not include any enrichment steps – were optimized to maximize throughput. Also, because labeled blood samples are simply flowed through the chip and not immobilized, destroyed, or physically bound to any substrate, this method is highly compatible with other downstream analysis techniques. Indeed, the same sample can be re-analyzed with eDAR or other techniques after this initial "coarse screening" for the presence of CTCs. The overall time of analysis for 1 mL whole blood can be less than 1 hour, including sample preparation, microfluidic detection, and data analysis. The average background level for healthy blood samples was 1.2 counts /mL, and the recovery rate of our method was high, at around 94% (n=9). 90 samples from stage IV breast cancer patients were analyzed using this method and compared side-by-side with the results of the FDA-approval CellSearch method. Based on the results, we believe the reported method represents a more effective approach to fast screening of CTCs for early detection and prognosis in cancer treatment.

5.2 Results and discussion

5.2.1 General Description of the System and Data Analysis

In order to detect CTCs, whole blood was directly labeled with antibodies, loaded into the microfluidic chip pneumatically, and analyzed by the line confocal detection system (Figure 5.1A). When the labeled blood flowed through the detection area, fluorescence was excited by the

combined two-color laser beam (488 nm and 633 nm), and detected by APDs. The collected APD traces were used to determine and enumerate cancer cells in the blood.

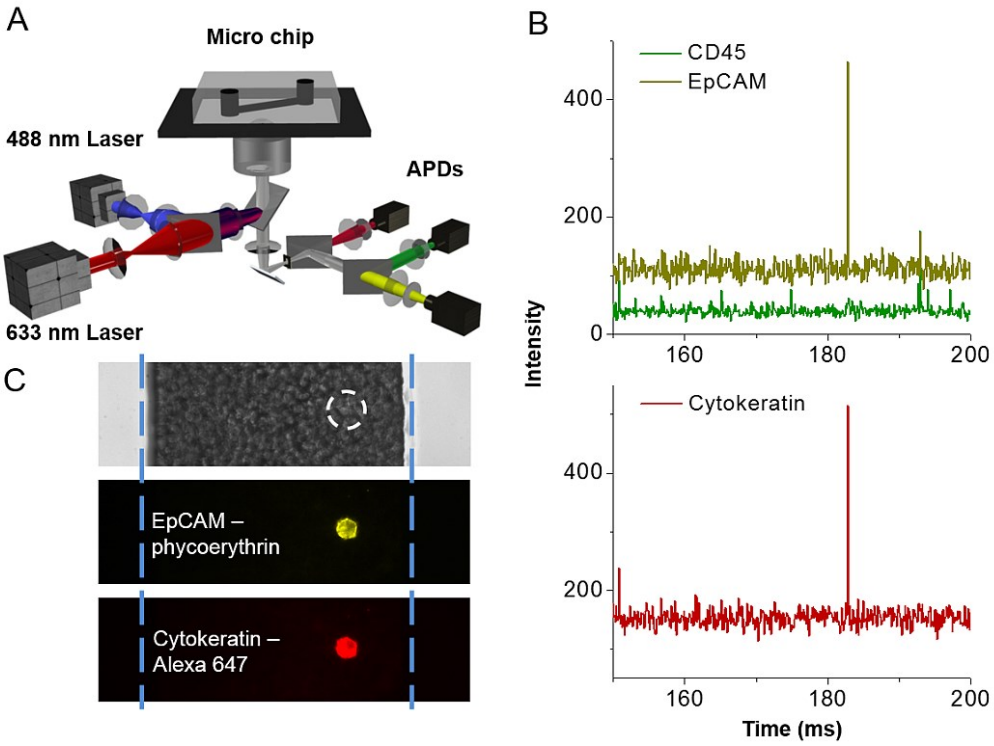

Figure 5.1 Schematic and data illustrating the flow-detection platform. (A) Depiction of the microfluidics and optics. (B) CTC detection and identification scheme using APD signals. A typical CTC event at 183 ms is positive for EpCAM (Yellow signal) and cytokeratin (Red signal), but negative for CD45 (Green signal). (C) A cultured MCF-7 cell imaged in the microfluidic channel filled with whole blood. The top panel shows a bright field image of the blood in the microchannel. The white dashed circle shows the location of the MCF-7 cell that is not visible beneath the many blood cells. The blue dashed lines show the location of the microchannel walls. Fluorescence images of the same location show the MCF-7 cell labeled with both anti-EpCAM and anti-Cytokeratin.

Surface markers such as EpCAM are widely used to select CTCs36; however, previous research has shown that simply relying on one biomarker may not be adequate to define the whole

population of CTCs. For example, normal-like breast cancer cells do not express EpCAM and thus would be missed by the CellSearch method that relies on EpCAM for CTC isolation [63]. As a result, a set of criteria is necessary to identify CTCs. The CellSearch assay defines a CTC as a cell that is EpCAM positive, cytokeratin positive, CD45 negative and nuclear stain positive, with a certain nuclear to cytoplasmic ratio and cell morphology character. In our approach, we followed these widely used criteria to enumerate CTCs in all patient samples, except that we did not use a nuclear stain, since we would need another APD detector. Whole blood was labeled with PE-anti-EpCAM, Alexa647-anti-pancytokeratin, and FITC-anti-CD45. Any cell deemed a CTC had positive fluorescence signals representing expression of both EpCAM and cytokeratin, but no signal associated with CD45. As an example, Figure 5.1B shows a small portion of APD traces from the analysis of a clinical sample (Sample #16). The event at 183 ms has peaks in both the EpCAM and cytokeratin channels without any significant signal in the CD45 channel, indicating that there was a tumor cell flowing through the detection window at that moment.

Imaging results (Figure 5.1C) show a cultured MCF-7 cell labeled with anti-EpCAM and anti-cytokeratin in the microfluidic channel. The bright field image shows that the MCF-7 cell was in the channel surrounded by numerous blood cells and could not be identified in this context. However, using epi-fluorescence imaging, the cell had strong yellow (PE-anti-EpCAM) and red (Alexa647-anti-cytokeratin) emission, which made it distinguishable from the blood cells in the channel.

While the initial signal to noise (S/N) ratio (> 20) of the fluorescence detection was high at the experimental flow rate (50 to 60 μL/min), it was important to optimize the data analysis so that the

system could be operated at the highest throughput and would be robust enough to handle the variability found in patient samples undergoing different clinical treatments. For example, to eliminate cross talk between different wavelength bands, spectral un-mixing is used in the MATLAB script to analyze the data. To reduce the noise and smooth the baseline, a sigmoidal burst detection filter was applied in the script for data analysis (Figure 5.2).

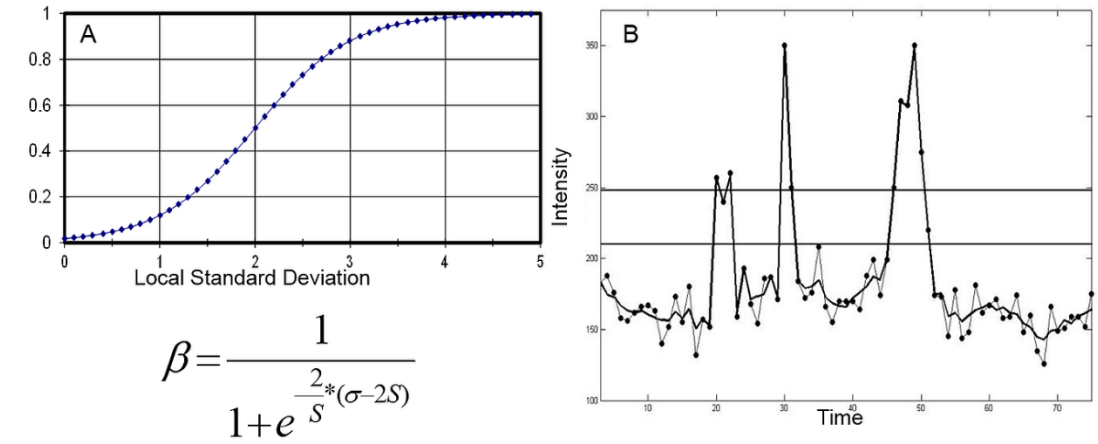

$$\beta = \frac{1}{1 + e^{\frac{2}{S} * (\sigma - 2S)}}$$

Figure 5.2 Sigmoidal burst filtering to improve the S/N. (A) A sigmoidal function based on the deviation of the intensity for a time bin from the local median intensity. (B) An example APD trace showing the uncorrected (dots and thin line) and corrected (dark line) data. The corrected data has significantly reduced noise, allowing for a lower threshold value in identifying CTCs without changing the intensity of the identified CTCs.

When the flow rate was increased, the mean time for a cancer cell to pass the detection region decreased, thus the S/N was lowered accordingly. To ensure that the S/N value was high enough (>10) to detect CTCs in whole blood with a flow rate between 50 to 80 μL/min, we measured S/N values for both spiked-in cells and clinical samples. Figure 5.3 shows the distribution of S/N values from a clinical sample (Sample ID 77) tested using EpCAM and cytokeratin as positive markers and CD45 as a negative marker. Over 95% of the data points have a S/N value higher

than 20, which is high enough to identify peaks. For this sample, the average and median values of S/N in EpCAM channel are 56 and 44, respectively; the average and median values of S/N in cytokeratin channel are 29 and 24, respectively.

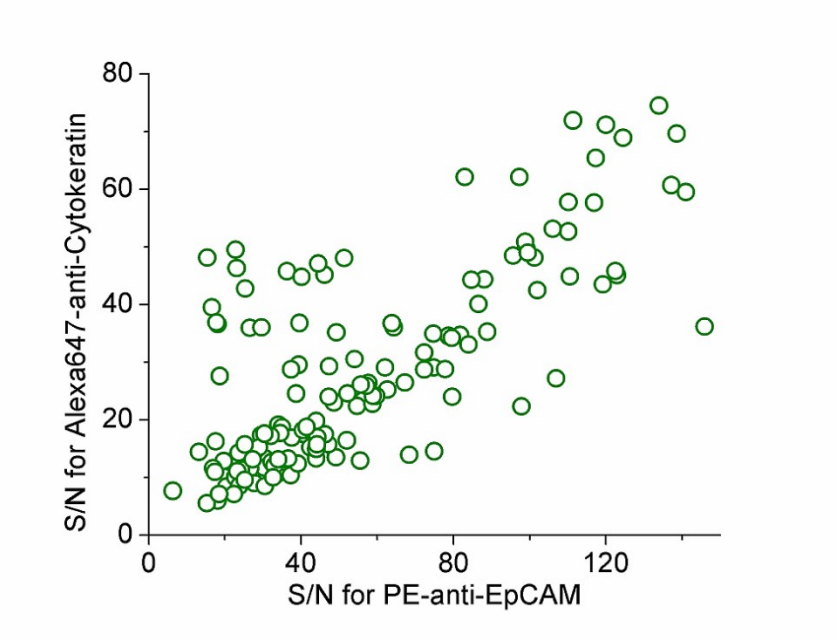

Figure 5.3 The distribution of signal-to-noise ratio (S/N) of a breast-cancer sample analyzed by the EpCAM/cytokeratin/CD45 method. All the data points were two-color events (EpCAM positive, Cytokeratin positive, and CD45 negative), which were considered to be CTCs.

5.2.2 Background Level of Detected CTCs from Healthy donors and the Recovery Performance of the Flow Counting Method

Blood is a highly complex biological fluid, so it is necessary to evaluate the background levels for any method designed to detect CTCs. In this study, 10 samples of whole blood from healthy donors were analyzed under the experimental conditions used for clinical samples. Each sample had an initial volume of 0.5 mL and the results were normalized to 1mL of blood. Similar to many other CTC detection methods, which have reported a non-zero background level [20, 67, 103, 107-

108], this method has an average background level for healthy donor blood samples of 1.2 counts/mL (Figure 5.4A). This value is slightly lower than, for example, a recently developed CTC capture hip that has an average background level of 2.2 cells/mL with a range of 0 to 12 cells/mL [108].

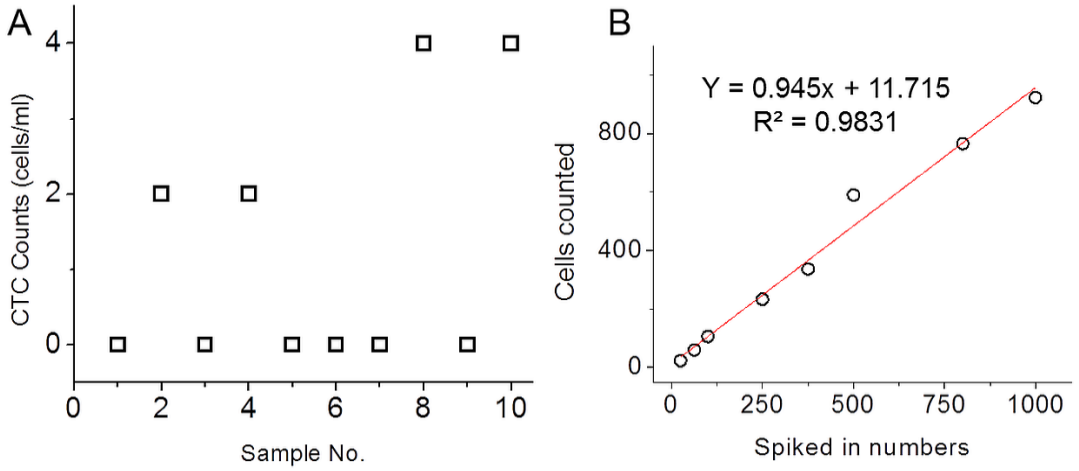

Figure 5.4 False positive and recovery performance. (A) On average 1.2 cells were found per mL of healthy donor blood with 60% of the samples reporting zero cells. (B) MCF-7 cells with known numbers were spiked into a healthy donor's blood, which was then labeled with PE-anti-EpCAM, Alexa647-anti-cytokeratin, and FITC-anti-CD45. Enumeration results showed an average 94% recovery.

Background CTC counts may result from several different sources. It could be caused by the process of measurement. For example, similar to flow cytometry, antibodies in solution can form aggregates due to random co-localization, which lead to false positive signals. Antibody aggregation may be more prone to occur when the blood samples are fixed and permeabilized. This issue can be addressed by using more biomarkers with more fluorescent colors, thus lowering the probability of detecting a random event, i.e., antibody aggregates, with the desired combination of colors. Indeed, this type of multi-parameter analysis has been used to significantly reduce false positive rates in flow cytometry [109]. Alternatively, background levels may be false positive

events that resulted from fluorescent dust particles in blood samples that show relatively wide emission spectra compared to labeled cells. However, the possibility of this occurring in our experiment was relatively low, because we require that the green channel (CD45; FITC) be non-fluorescent. Finally, it is possible that the background level was caused by the fact that some circulating epithelial cells are present in healthy individuals [10]. While this scenario is possible, we believe it is unlikely based on our previous studies33 and as long as the first tube of drawn blood is discarded to avoid contamination of epithelial cells during the venipuncture process. In any case, as long as the background levels are much fewer than in cancer patients, it should not affect the assay.

Because the background was above zero, accurate fast screening of CTCs in actual clinical practice will require a threshold to be determined by statistical analysis of the experimentally measured background, i.e., the sample is considered as CTC-positive only if the number of events is higher than that threshold. This type of threshold is used in conventional flow cytometry [110]. It is also applied in other published works for the enumeration of CTCs. For example39, Stott, SL et al. showed their method has a mean background level of 3 cells/mL, ranging from 0 to 8 cells/mL, in their analysis of samples from healthy donors. As a result, they set up a cut-off value at 10 cells/mL to prevent false positive detection. If the sample count falls below the threshold in our method, it can be further analyzed by a zero-false-positive method such as eDAR (0 CTCs/mL, n=9) 33, because the labeled sample is not damaged during the flow detection test.

To determine the recovery efficiency of this method, 25 to 1000 SKBr-3 cells were spiked into 8 blood samples (1 mL for each sample) from healthy donors and then analyzed using the same

preparation procedure used for patient samples. The average recovery was about 94% with a R2 value of 0.9831 (Figure 3B). A similar recovery rate was observed for MCF-7 cells (data not shown). This value is consistent with the recovery value of eDAR (93%), and is acceptable for screening CTCs from clinical samples.

5.2.3 Alternative Labeling and Detection Schemes

We have also tested other possible labeling and detection schemes. Because Her2 is a widely used biomarker in breast cancer studies (~ 25% of breast cancer patients are Her2 positive) and is the target of the monoclonal antibody trastuzumab, we designed a scheme to enumerate Her2 positive CTCs from breast cancer patients. In this scheme, the blood sample was labeled with PE-anti-EpCAM, Alexa647-anti-Her2, and FITC-anti-CD45, so a Her2 positive CTC should be positive for EpCAM but negative for CD45 (Figure 5.5).

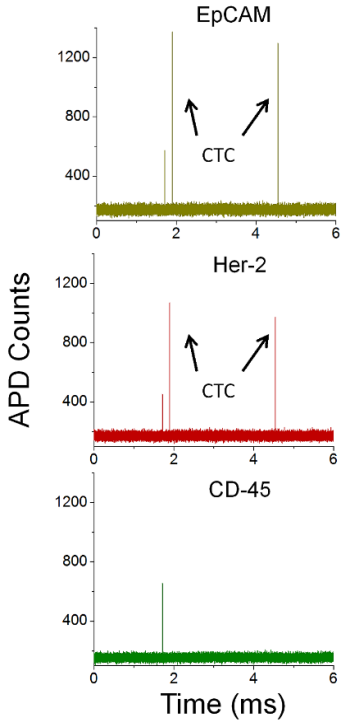

Figure 5.5 Example of APD data for the detection scheme using EpCAM, Her2 and CD45 as biomarkers.

In this figure, there were 3 detectable events in 5 ms, and the first event at 1.7 ms was not a CTC event, because it had a strong CD45 signal together with the EpCAM and Her2 responses. The last two events are defined as CTCs, because both EpCAM and Her2 expression are high without any significant CD45 signals. This experiment shows that the Her2 positive CTCs could be counted using the current labeling and detection scheme.

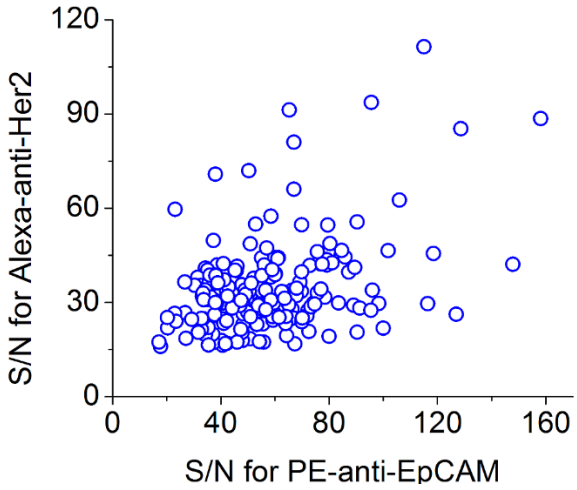

Figure 5.6 The distribution of signal-to-noise ratio (S/N) of a breast-cancer sample analyzed by EpCAM\Her2\CD45 method. All the data points were two-color events (EpCAM positive, Her2 positive, and CD45 negative).

To test the applicability of this scheme, we did an analysis on the distribution of S/N values for another patient sample (Sample ID 103) analyzed by EpCAM/Her2/CD45, which had average S/N ratios of 57 and 35 for EpCAM and Her2 channels, respectively (Figure 5.6). False positive studies were also performed using 1 mL of whole blood as the initial volume of each sample (n=5). No CTCs were found in 3 (60%) samples, and 1 CTC per 1 mL of whole blood was found in the other 2 (40%) samples. The average background value of this scheme is about 0.4 cells/mL. The

difference between the false positive values of the two strategies (EpCAM+/Her2+/CD45- and EpCAM+/Cytokeratin+/CD45-) was possibly due to the difference in the sample preparation procedure. Since Her2 is a surface antibody, the blood does not need to be fixed and permeabilized for labeling. This gave us a generally higher signal-to-noise value and a lower false positive rate, which indicates that if we use cell surface markers instead of cytoplasmic markers, we can reduce the false positive rate as well.

To demonstrate the flexibility of our labeling scheme, we also enumerated circulating cells that were CD44+/CD24-/EpCAM+, because CD44+/CD24- is a marker that has been used to identify stem cell like CTCs. CD44+ can also be present on some blood cells, however, and our enumeration relied on a single marker, EpCAM+, to distinguish CTCs that were CD44+/CD24- from these blood cells. Therefore, to more definitively confirm these are indeed cancer stem cells, one would need to use additional markers (e.g. CD45- and Cytokeratin+) to minimize the possibility of false positives. At present, our setup is only capable of detecting 3 markers and thus this experiment also shows the advantage of being able to monitor additional markers by adding more detectors and by utilizing fluorophores with narrower emission spectra to facilitate multiplexing.

5.2.4 Results of Clinical Samples

Over a two-year period, we collected 90 blood samples from 24 patients with stage IV metastatic breast cancer and performed a side-by-side study comparing the high-throughput flow detection method with the FDA-approved CellSearch system (Figure 4). CTCs in all the 90 samples reported in this paper were identified as EpCAM+/cytokeratin+/CD45-, similar to the criteria used in

CellSearch analysis, which has one more nuclear stain (DAPI) marker, and does not image the EpCAM expression of the captured cells.

CTC positive events were found using the high-throughput flow detection method in 82 samples (91%), ranging from 15 to 3375 counts per 7.5 mL of blood, with an average CTC level of 305 counts per 7.5 mL of blood, and a median value of 90 counts/7.5 mL. The CellSearch system found CTCs in 44% of samples, ranging from 1 to 846 cells per 7.5 mL of blood, with an average CTC level of 36 cells per 7.5 mL of blood, and a median value of 0 cells/7.5 mL. Previous studies proposed that the relevant prognostic cutoff level of CTCs in metastatic breast cancer is 5 cells per 7.5 mL of blood as determined by the CellSearch method. In our study, only 22% of the samples had the level of CTCs higher than that threshold using the CellSearch system.

However, considering our current background level (1.2 counts/mL), it is necessary to set a threshold with a certain confidence level, so we can exclude the data points that might represent false positive signals. As we discussed previously, there are several different approaches we can follow to set this threshold.

For example, we might use a simple threshold that is above the range of the detected background level as reported previously. The mean background level of our method is 1.2 counts/mL, ranging from 0 to 4 counts/mL. Similar to the other published works [108], we may set up a threshold at 5 counts/mL as a cut off value to distinguish the CTC events from the background. After the normalization to 7.5 mL, this threshold would be 38 counts/7.5 mL.

Another possibility is to use a threshold that is the mean background count plus 2 standard deviations, a method reported in the flow cytometry literature [110]. The mean background level of our method is 1.2 counts/mL with a standard deviation of 1.6 counts/mL. As a result, the corresponding threshold would be 4.4 counts/mL. For 7.5 mL of the blood, the threshold would be 33 counts/7.5 mL.

The third approach is to use one-sided Z-test to determine a threshold with a particular confidence level. The false positive data (Figure 5.4A) has an average value of 0.6 cells per sample (0.5 mL), and a standard deviation of 0.8 cells per sample (0.5 mL). Because there was only one measurement per clinical sample, we assume Poisson distributed error for the clinical samples. For the Z test,

$$Z = \frac{S - B}{\sqrt{\sigma_S^2 + \sigma_B^2}}$$

Where S is the counts in the clinical sample and B = 0.60 is the average counts in the blank and is the variance in the blank. For the clinical sample can be approximated by S, so we get

$$Z = \frac{S - 0.6}{\sqrt{S + 0.64}}$$

For S = 4.2, Z = 1.63, which is a 90% confidence interval. For 7.5 mL, we have 4.2 × 15 = 63. Any sample with S > 4 will have a confidence level > 90% for a two-tail test, and > 95% for a one-tail test. Since a sample cannot have a negative number of counts, we should use the one-tail test. As a result, this threshold (63 counts/7.5mL) would be used for a one-sided test with a confidence level higher than 95%.

Based on this more stringent threshold, our method found that 60% of the patient samples were positive to CTCs with a 95% confidence level. A detailed list of all the patient samples and CTC counts using CellSearch and our method is provided in supporting information (Table 5.1). Figure 5.7 shows the result and the corresponding thresholds set using the three methods described above.

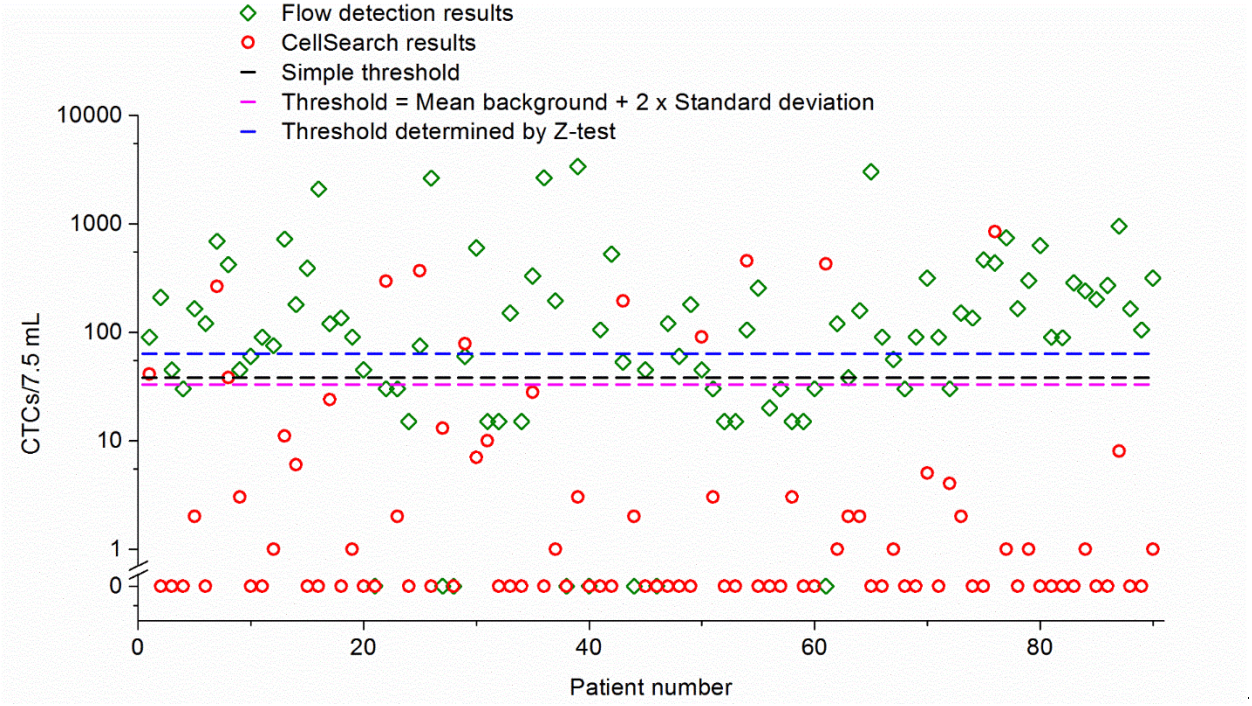

Figure 5.7 Clinical results from the CTC flow counting system and CellSearch. Our method found a median of 90 CTCs per 7.5 mL of blood compared to a median of zero for the CellSearch system. The black dashed line is a simple threshold (38 counts/7.5 mL) set based on the range of detected CTCs in healthy donors. The magenta dashed line is the threshold (33 counts/7.5 mL) set using the mean background level plus two times of its standard deviation. The blue dashed line is the threshold (63 counts/7.5 mL) determined by Z-test with a 95% confidence level.

Of the 90 patient samples, 30 were additionally analyzed using EpCAM and CD44 as positive markers, as well as CD24 as a negative marker to enumerate CTCs with stem cell characteristics. Figure 5.8 shows the side by side comparison of the stem cell counts and regular CTC numbers

enumerated by the flow detection method, as well as the CTC numbers determined by CellSearch method. EpCAM+/CD44+/CD24- events were found in 90% of the samples with average and median values of 150 cells/7.5mL and 53 cells/7.5 mL, respectively.

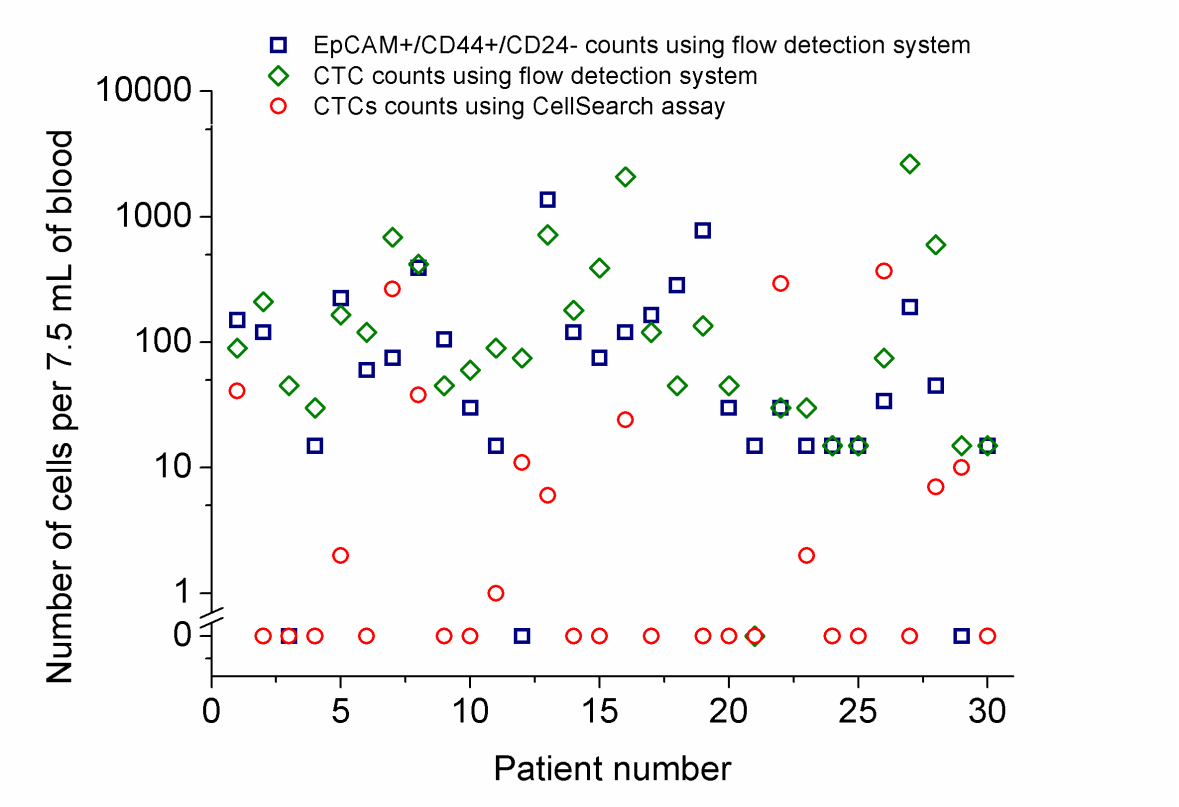

Figure 5.8 Side-by-side clinical results for regular CTCs and circulating cells with EpCAM+ / CD44+ / CD24- expression from the CTC flow detection system and CellSearch. Normal CTCs were determined by both flow detection and CellSearch method. The average number of the EpCAM+/CD44+/CD24- cells for these 30 patient samples is 150 cells/7.5mL.

It is also interesting to compare this flow detection method with eDAR. CTC counts collected from the eDAR approach (n=22, from 9 patients) [76] and the flow detection approach (n=40, from the same 9 patients) were analyzed with Analysis of Variance (ANOVA). Figure 5.9 shows the boxplots and histograms for each dataset. The dataset from flow detection averaged 102 CTCs/7.5 mL, whereas that from eDAR averaged 52 CTCs/7.5 mL. However, given the large variance in

the flow detection dataset, eDAR and flow detection are not significantly different ($p = 0.14$, $\alpha = 0.05$, ANOVA test). This consistency is due to the similarity of fluidics and fluorescence detection schemes between the two methods.

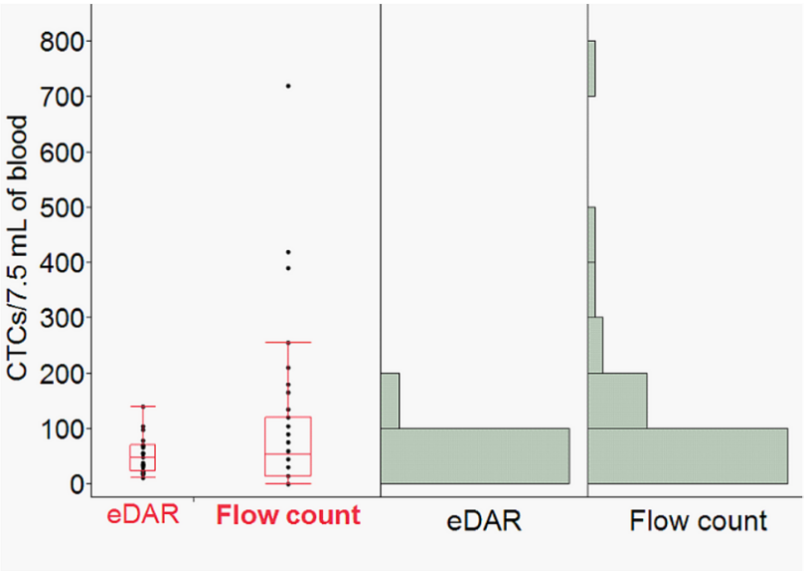

Figure 5.9 Comparison of the CTC enumeration results from the same set of patients using eDAR and flow detection system. The left part is the box plots that show the smallest observation, lower quartile, median, upper quartile, and the largest observation of the two data sets (eDAR vs Flow count), respectively. The right part shows the histograms of the two data sets.

Sample ID	CTC counts by flow detection /7.5 mL	CTC counts by CellSearch /7.5 mL	Sample ID	CTC counts by flow detection /7.5 mL	CTC counts by CellSearch /7.5 mL
1	90	41	46	0	0
2	210	0	47	120	0
3	45	0	48	60	0
4	30	0	49	180	0
5	165	2	50	45	90
6	120	0	51	30	3
7	690	265	52	15	0
8	420	38	53	15	0
9	45	3	54	105	457
10	60	0	55	255	0
11	90	0	56	20	0
12	75	1	57	30	0
13	720	11	58	15	3
14	180	6	59	15	0
15	390	0	60	30	0
16	2085	0	61	0	426
17	120	24	62	120	1
18	135	0	63	38	2
19	90	1	64	158	2
20	45	0	65	3015	0
21	0	0	66	90	0
22	30	294	67	56	1
23	30	2	68	30	0
24	15	0	69	90	0
25	75	368	70	315	5
26	2637	0	71	90	0
27	0	13	72	30	4
28	0	0	73	150	2
29	60	78	74	135	0
30	600	7	75	465	0
31	15	10	76	435	846
32	15	0	77	743	1
33	150	0	78	165	0
34	15	0	79	300	1
35	330	28	80	630	0
36	2655	0	81	90	0
37	195	1	82	89	0
38	0	0	83	285	0
39	3375	3	84	240	1
40	0	0	85	200	0
41	105	0	86	270	0
42	525	0	87	950	8
43	53	194	88	165	0
44	0	2	89	105	0
45	45	0	90	315	1

Table 5.1 High-throughput flow detection and CellSearch results obtained for 90 breast-cancer patient samples. The side-by-side comparison between the commercial CellSearch system and our eDAR platform using blood samples drawn from Stage IV metastatic breast cancer patients.

5.3 Materials and Methods

5.3.1 Design and Fabrication of Microfluidic Devices

The microfluidic channel was 200 μm wide, 50 μm tall, and 3 cm long. The polydimethylsiloxane (PDMS) device was prepared by photolithography and replica molding methods described previously. The features were designed in AutoCAD 2010 (Autodesk, San Rafael, CA), and then written to a transparency mask (FineLine imaging, Colorado springs, CO). To create masters for replica molding, silicon wafers were spin-coated with SU-8 3050 (MicroChem, Newton, MA), forming a 50-μm thick film. The features were developed and then silanized with tridecafluoro-1,1,2,2-tetrahydrooctyl-1-trichlorosilane (Sigma-Aldrich, St. Louis, MO) to prevent PDMS from sticking to the wafer. Uncured PDMS was poured onto the surface of the master, and then incubated at 75 °C for 4 hours. The PDMS chip was sealed to a No. 4 cover glass (Thermo Fisher Scientific, Portsmouth, NH) by oxygen plasma bonding.

5.3.2 Biological and clinical materials

Isoton buffer, purchased from Beckman Coulter (Miami, FL), was used in all experiments. Prior to use, the buffer was filtered using a 50 mL Steri-flip filter (Milipore, Billerica, MA). Two breast cancer cell lines, MCF-7 and SKBr-3, were purchased from American Type Culture Collection

(ATCC). Both were used to characterize and optimize the continuous flow system. Cells were maintained and cultured in the recommended culture media (McCoy's 5A or EMEM), which contained 2 mM L-glutamine, 10% fetal bovine serum (FBS) (ATCC), and 50 μg/mL penicillin/streptomycin (ATCC) at 37 °C with 5% CO2 in a humidified environment.

Human whole blood, individually drawn from healthy donors, was provided by Plasma Lab International (Everett, WA) and stored at 4°C upon arrival. Each 20-mL draw was collected into four 5 mL Vacutainer tubes coated with EDTA as anti-coagulant. The first tube of each draw was discarded to avoid potential contamination from skin cells.

Clinical samples were collected from Stage IV metastatic breast cancer patients according to a protocol approved by University of Washington's institutional review board. Blood was drawn at the Seattle Cancer Care Alliance and multiple tubes were collected in each draw. One tube was collected in a Veridex CellSave tube for enumeration of CTCs by the CellSearch system (Veridex, Raritan, NJ). The second one was collected in a Vacutainer tube containing EDTA for the flow detection analysis. The sample was stored at 4°C after the draw and analyzed within 4 h.

5.3.3 Line-confocal Detection Scheme

To detect a single CTC in a background of nanoliters of blood, we developed a line-confocal detection scheme34-35 with a probe volume that spanned the width (200 μm) and height (50 μm) of the micro-channel. Our system had two lasers (488 nm and 633 nm), whose outputs were shaped by cylindrical lenses and focused into a 20× objective to form a 200 μm by 5 μm line (Fig. 1a). Fluorescence from this region was collected through a rectangular confocal aperture and a series

of dichroics and filters to fiber-coupled avalanche photodiodes (APDs) (Excelitas Technologies, Waltham, MA), operating in the single-photon counting mode. In our current setup, APD1 detected the yellow fluorescence (560-590 nm) from the monoclonal antibody labeled with phycoerythrin (PE); APD2 was used as a negative control for the green wavelength range, such as fluorescein isothiocyanate (FITC) (500-550 nm) to eliminate false positives from broadly emitting fluorescent contaminants or the antibody conjugated with FITC; and APD3 detected the antibody labeled with Alexa-647 in the red wavelength band (640-690 nm).

5.3.4 Sample Preparation and Experimental Procedures

Antibodies were centrifuged (14000 rpm, 5 min) to remove possible aggregates before any labeling procedure. In each clinical run, 0.5 to 1 mL of blood was added to a 15-mL polypropylene conical centrifuge tube (Becton Dickinson, Franklin Lakes, NJ). 60 μL of PE-anti-epithelial cell adhesion molecule (EpCAM) (BioLegend, San Diego, CA, Catalog # 324206), 80 μL of Alexa-647-anti-Cytokeratin (Cell Signalling technologies, Danvers, MA, Catlog # 4528), and 20 μL of FITC-anti-CD45 (BioLegend, San Diego, CA, Catolog # 304006) were added to the blood in the dark and incubated at room temperature for half an hour. When cytokeratin was used as the second positive marker for breast cancer cells, the blood was fixed before labeling. 84 μL paraformaldehyde (PFA) (20%) were used to fix the blood at room temperature for 15 minutes. Then 44 μL of Surfynol 465 (Air product, Allentown, PA) were added to help anti-cytokeratin penetrate the cell membrane. When Her2 was used as the second positive marker, there was no fixing step before labeling. 10 μL of Alexa-647-anti-Her2 (BioLegend, San Diego, CA, Catolog # 324412) were added to blood

with the same amount of anti-EpCAM and anti-CD45 as described above. The labeling parameters were characterized and optimized in chapter 2.

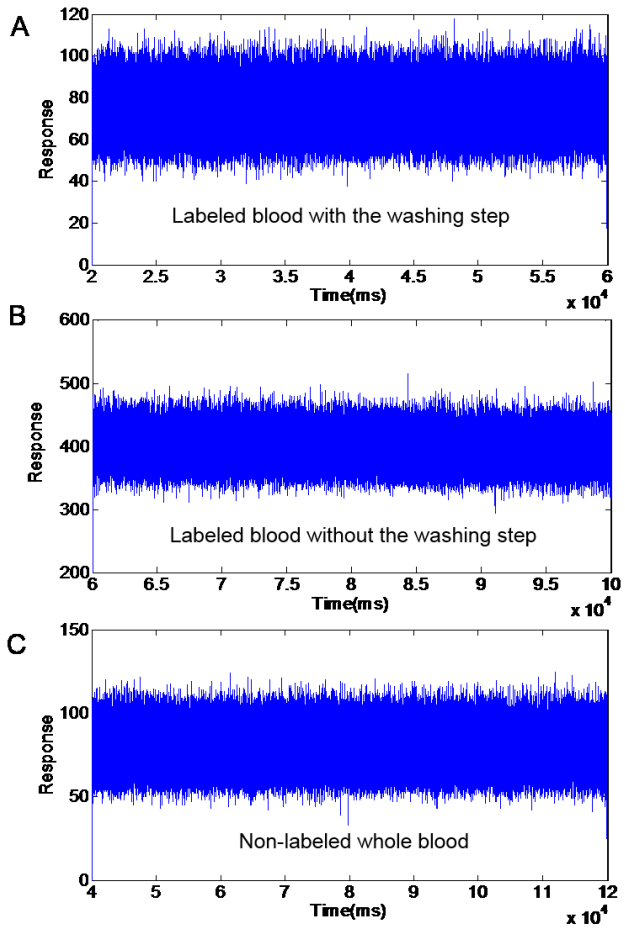

Figure 5.10 Fluorescence background levels in PE (phycoerythrin) detection channel, when we flow, (A) healthy blood sample labeled with anti-EpCAM-PE with the same washing step used in this paper, (B) healthy blood sample labeled with anti-EpCAM-PE without any washing step, and (C) healthy blood sample without any labeling and washing steps. The average level of background in (A), (B) and (C) is 79.4, 397.4 and 74.6, respectively.

The labeled blood was diluted to 14 mL and then centrifuged (500 rpm, 10 minutes) to remove the free antibodies. This dilution factor was optimized to get the lowest background counts. Figure 5.10 showing the background measurement of 3 different samples in the PE (phycoerythrin)

detection channel. When we labeled the blood with anti-EpCAM-PE, and then washed it using the same procedure described in the manuscript, the average background level would be 79.4 counts (Figure 5.10A). If the same blood sample labeled with anti-EpCAM-PE, but did not have a washing step, the fluorescent background would increase to 397.4 counts on average (Figure 5.10B). We also injected unlabeled whole blood as a control, and figure 5.10C shows that the average fluorescence background was 74.6 counts. It proves that our washing step is efficient in removing most of the free antibodies in the blood.

The final volume was adjusted to be the same as the initial volume for both clinical and control samples. After that, the sample was loaded into the microfluidic chip pneumatically and analyzed using the home-built line confocal system. The flow rate was controlled by the gas pressure regulator and measured by an electrical scale (ACCULAB Measurement Standards, Danvers, MA), which was controlled by a custom LabVIEW (National Instruments, Austin, TX) program. APD traces were collected by a PCI data acquisition card (PCI 6602, National Instruments, Austin, TX) and analyzed by a MATLAB (MathWorks, Natick, MA) script developed in-house. The threshold of signal-to-noise ratio for all the 3 channels was set to 5 to ensure the highest possible sensitivity.

5.4 Conclusion

The enumeration of CTCs is an important component of monitoring cancer progression, and the reported CTC flow counting system is an automated, quick, and sensitive method. Additionally, the system is very flexible in the sense that it can be used with a variety of markers and any user-defined fluorescence-based criterion for enumerating cells of interest can be designed. We demonstrated the ability to enumerate spiked-in cancer cells from whole blood with a high

recovery efficiency of 94%. A side-by-side clinical study of 90 patient samples showed that our method is sensitive and efficient for CTC detection in patients with stage IV metastatic breast cancer. Flow detection technique is free of enrichment steps, which are required in most CTC analysis techniques, so the sample preparation is minimized and the detection and enumeration analysis is fully automated. Moreover, because it is a non-destructive analysis technique (samples simply flowed through a straight channel), samples can be re-analyzed and verified using other CTC methods. This compatibility would be ideal for a high-throughput screening application, because the positive samples may need to be further tested by other techniques to obtain more cellular and molecular information. In summary, we believe this simple, fast, and robust method is useful for the enumeration of CTCs from patient blood, and it may be potentially used for other rare-cell enumeration studies.

Chapter 6 Conclusion and Perspective

The ultimate goal of this dissertation is to develop an ideal method to analyze rare cells, especially CTCs from whole blood, with a high sensitivity, throughput and flexibility. I report three methods for CTC analysis, two generations of eDAR and an automated counting method. We can always improve these methods and incorporate them with other methods. For example, one possible future improvement could be redesigning the microfluidic structure, so eDAR can select multiple populations of rare cells from the same sample simultaneously. Although filtration worked well in the reported method as a further purification method, it is also possible to develop the subsequent purification unit based on other schemes. For example, we can directly couple two eDAR designs sequentially, so the second one would serve as a further purification unit for the first eDAR, which would improve the enrichment ratio and thus the purity significantly.

Understanding the molecular and cellular characters of captured CTCs are the ultimate goal of any CTC technologies in the future. eDAR has a great flexibility of downstream analyses, and we have finalized the methods for protein analysis and single-cell manipulation. In the future, more subsequent analyses methods should be integrated onto the eDAR platform. For example, after we pick up the isolated CTCs from the microfluidic chip, we can perform single-cell PCR experiments on the isolated CTCs easily. In situ investigation of genes could also be performed by using FISH methods. Many other assays could be performed too, such as single-cell proteomics. If we can lyse the captured CTCs in a small volume, it may be possible to analyze it using proteomics methods, so we will not be limited by the immuno-staining techniques to understand the expression of proteins.

References

1. Jemal, A., Bray, F., Center, M. M., Ferlay, J., Ward, E., Forman, D., *CA-Cancer J. Clin.* **2011**, *61*. 69-90.
2. Parkin, D. M., Pisani, P., Ferlay, J., *CA-Cancer J. Clin.* **1999**, *49*. 33-64.
3. Gupta, G. P., Massague, J., *Cell* **2006**, *127*. 679-695.
4. Pantel, K., Alix-Panabieres, C., Riethdorf, S., *Nat. Rev. Clin. Oncol.* **2009**, *6*. 339-351.
5. Steeg, P. S., *Nat. Med.* **2006**, *12*. 895-904.
6. Chaffer, C. L., Weinberg, R. A., *Science* **2011**, *331*. 1559-1564.
7. Husemann, Y., Geigl, J. B., Schubert, F., Musiani, P., Meyer, M., Burghart, E., Forni, G., Eils, R., Fehm, T., RiethmUller, G., Klein, C. A., *Cancer Cell* **2008**, *13*. 58-68.
8. Mego, M., Mani, S. A., Cristofanilli, M., *Nat. Rev. Clin. Oncol.* **2010**, *7*. 693-701.
9. Mocellin, S., Keilholz, U., Rossi, C. R., Nitti, D., *Trends Mol. Med* **2006**, *12*. 130-139.
10. Paterlini-Brechot, P., Benali, N. L., *Cancer Lett.* **2007**, *253*. 180-204.
11. Mostert, B., Sleijfer, S., Foekens, J. A., Gratama, J. W., *Cancer Treatment Reviews* **2009**, *35*. 463-474.
12. Fidler, I., *Nature Reviews Cancer* **2003**, *3*. 453-458.
13. Fokas, E., Engenhart-Cabillic, R., Daniilidis, K., Rose, F., An, H. X., *Cancer Metastasis Rev.* **2007**, *26*. 705-715.
14. Allard, W., Matera, J., Miller, M., Repollet, M., Connelly, M., Rao, C., Tibbe, A., Uhr, J., Terstappen, L., *Clin. Cancer Res.* **2004**, *10*. 6897-6904.
15. Aurilio, G., Sciandivasci, A., Munzone, E., Sandri, M. T., Zorzino, L., Cassatella, M. C., Verri, E., Rocca, M. C., Nole, F., *Expert Rev. Anticancer Ther* **2012**, *12*. 203-214.
16. Theodoropoulos, P. A., Polioudaki, H., Agelaki, S., Kallergi, G., Saridaki, Z., Mavroudis, D., Georgoulias, V., *Cancer Lett.* **2010**, *288*. 99-106.
17. Hou, J. M., Krebs, M., Ward, T., Sloane, R., Priest, L., Hughes, A., Clack, G., Ranson, M., Blackhall, F., Dive, C., *Am. J. Pathol.* **2011**, *178*. 989-996.
18. Maheswaran, S., Sequist, L., Nagrath, S., Ulkus, L., Brannigan, B., Collura, C., Inserra, E., Diederichs, S., Iafrate, A., Bell, D., *New England Journal of Medicine* **2008**, *359*. 366-377.

19. Khoja, L., Backen, A., Sloane, R., Menasce, L., Ryder, D., Krebs, M., Board, R., Clack, G., Hughes, A., Blackhall, F., Valle, J. W., Dive, C., *British Journal of Cancer* **2012**, *106*. 508-516.

20. Marrinucci, D., Bethel, K., Kolatkar, A., Luttgen, M. S., Malchiodi, M., Baehring, F., Voigt, K., Lazar, D., Nieva, J., Bazhenova, L., Ko, A. H., Korn, W. M., Schram, E., Coward, M., Yang, X., Metzner, T., Lamy, R., Honnatti, M., Yoshioka, C., Kunken, J., Petrova, Y., Sok, D., Nelson, D., Kuhn, P., *Physical Biology* **2012**, *9*.

21. Kirby, B. J., Jodari, M., Loftus, M. S., Gakhar, G., Pratt, E. D., Chanel-Vos, C., Gleghorn, J. P., Santana, S. M., Liu, H., Smith, J. P., Navarro, V. N., Tagawa, S. T., Bander, N. H., Nanus, D. M., Giannakakou, P., *Plos One* **2012**, *7*.

22. Danila, D. C., Fleisher, M., Scher, H. I., *Clin. Cancer Res.* **2011**, *17*. 3903-3912.

23. Vona, G., Estepa, L., Beroud, C., Damotte, D., Capron, F., Nalpas, B., Mineur, A., Franco, D., Lacour, B., Pol, S., Brechot, C., Paterlini-Brechot, P., *Hepatology* **2004**, *39*. 792-797.

24. Silva, J. M., Rodriguez, R., Garcia, J. M., Munoz, C., Silva, J., Dominguez, G., Provencio, M., Espana, P., Bonilla, F., *Gut* **2002**, *50*. 530-534.

25. Vidaurreta, M., Sastre, J., Teresa Sanz-Casla, M., Luisa Maestro, M., Rafael, S., Diaz-Rubio, E., *Medicina Clinica* **2007**, *129*. 333-334.

26. Nakagawa, T., Martinez, S. R., Goto, Y., Koyanagi, K., Kitago, M., Shingai, T., Elashoff, D. A., Ye, X., Singer, F. R., Giuliano, A. E., Hoon, D. S. B., *Clin. Cancer Res.* **2007**, *13*. 4105-4110.

27. Hartkopf, A. D., Banys, M., Krawczyk, N., Wallwiener, M., Schneck, H., Neubauer, H., Fehm, T., *Geburtshilfe Frauenheilkd.* **2011**, *71*. 1067-1072.

28. Lianidou, E. S., Markou, A., Strati, A., *Cancer Metastasis Rev.* **2012**, *31*. 663-671.

29. Andreopoulou, E., Cristofanilli, M., *Expert Rev. Anticancer Ther* **2010**, *10*. 171-177.

30. Bidard, F.-C., Hajage, D., Bachelot, T., Delaloge, S., Brain, E., Campone, M., Cottu, P., Beuzeboc, P., Rolland, E., Mathiot, C., Pierga, J.-Y., *Breast Cancer Res.* **2012**, *14*.

31. Cristofanilli, M., Budd, G., Ellis, M., Stopeck, A., Matera, J., Miller, M., Reuben, J., Doyle, G., Allard, W., Terstappen, L., *New England Journal of Medicine* **2004**, *351*. 781-791.

32. Riethdorf, S., Fritsche, H., Mueller, V., Rau, T., Schindibeck, C., Rack, B., Janni, W., Coith, C., Beck, K., Jaenicke, F., Jackson, S., Gornet, T., Cristofanilli, M., Pantel, K., *Clin. Cancer Res.* **2007**, *13*. 920-928.

33. Krebs, M. G., Sloane, R., Priest, L., Lancashire, L., Hou, J.-M., Greystoke, A., Ward, T. H., Ferraldeschi, R., Hughes, A., Clack, G., Ranson, M., Dive, C., Blackhall, F. H., *J. Clin. Oncol.* **2011**, *29*. 1556-1563.

34. Cohen, S. J., Punt, C. J. A., Iannotti, N., Saidman, B. H., Sabbath, K. D., Gabrail, N. Y., Picus, J., Morse, M., Mitchell, E., Miller, M. C., Doyle, G. V., Tissing, H., Terstappen, L., Meropol, N. J., *J. Clin. Oncol.* **2008**, *26*. 3213-3221.

35. Lucci, A., Hall, C. S., Lodhi, A. K., Bhattacharyya, A., Anderson, A. E., Xiao, L., Bedrosian, I., Kuerer, H. M., Krishnamurthy, S., *Lancet Oncology* **2012**, *13*. 688-695.

36. Pierga, J.-Y., Bidard, F.-C., Mathiot, C., Brain, E., Delaloge, S., Giachetti, S., de Cremoux, P., Salmon, R., Vincent-Salomon, A., Marty, M., *Clin. Cancer Res.* **2008**, *14*. 7004-7010.

37. Alunni-Fabbroni, M., Sandri, M. T., *Methods* **2010**, *50*. 289-297.

38. Budd, G. T., Cristofanilli, M., Ellis, M. J., Stopeck, A., Borden, E., Miller, M. C., Matera, J., Repollet, M., Doyle, G. V., Terstappen, L. W. M. M., Hayes, D. F., *Clin. Cancer Res.* **2006**, *12*. 6403-6409.

39. Liu, M. C., Shields, P. G., Warren, R. D., Cohen, P., Wilkinson, M., Ottaviano, Y. L., Rao, S. B., Eng-Wong, J., Seillier-Moiseiwitsch, F., Noone, A.-M., Isaacs, C., *J. Clin. Oncol.* **2009**, *27*. 5153-5159.

40. Punnoose, E. A., Atwal, S. K., Spoerke, J. M., Savage, H., Pandita, A., Yeh, R.-F., Pirzkall, A., Fine, B. M., Amler, L. C., Chen, D. S., Lackner, M. R., *Plos One* **2010**, *5*.

41. Yu, M., Ting, D. T., Stott, S. L., Wittner, B. S., Ozsolak, F., Paul, S., Ciciliano, J. C., Smas, M. E., Winokur, D., Gilman, A. J., Ulman, M. J., Xega, K., Contino, G., Alagesan, B., Brannigan, B. W., Milos, P. M., Ryan, D. P., Sequist, L. V., Bardeesy, N., Ramaswamy, S., Toner, M., Maheswaran, S., Haber, D. A., *Nature* **2012**, *487*. 510-U130.

42. Yu, M., Bardia, A., Wittner, B. S., Stott, S. L., Smas, M. E., Ting, D. T., Isakoff, S. J., Ciciliano, J. C., Wells, M. N., Shah, A. M., Concannon, K. F., Donaldson, M. C., Sequist, L. V., Brachtel, E., Sgroi, D., Baselga, J., Ramaswamy, S., Toner, M., Haber, D. A., Maheswaran, S., *Science* **2013**, *339*. 580-584.

43. Ashworth, T. R., *Aust. Med. J.* **1869**, *14*. 2.

44. Dharmasiri, U., Witek, M. A., Adams, A. A., Soper, S. A., *Annual Review of Analytical Chemistry* **2010**, *3*. 409-431.

45. Zieglschmid, V., Hollmann, C., Bocher, O., *Crit. Rev. Clin. Lab. Sci.* **2005**, *42*. 155-196.

46. Gross, H. J., Verwer, B., Houck, D., Hoffman, R. A., Recktenwald, D., *Proceedings of the National Academy of Sciences of the United States of America* **1995**, *92*. 537-541.

47. Patriarca, C., Macchi, R. M., Marschner, A. K., Mellstedt, H., *Cancer Treatment Reviews* **2012**, *38*. 68-75.

48. Yu, M., Stott, S., Toner, M., Maheswaran, S., Haber, D. A., *Journal of Cell Biology* **2011**, *192*. 373-382.

49. Krebs, M. G., Hou, J.-M., Sloane, R., Lancashire, L., Priest, L., Nonaka, D., Ward, T. H., Backen, A., Clack, G., Hughes, A., Ranson, M., Blackhall, F. H., Dive, C., *Journal of Thoracic Oncology* **2012**, *7*. 306-315.

50. Lara, O., Tong, X. D., Zborowski, M., Chalmers, J. J., *Exp Hematol* **2004**, *32*. 891-904.

51. Balasubramanian, P., Yang, L. Y., Lang, J. C., Jatana, K. R., Schuller, D., Agrawal, A., Zborowski, M., Chalmers, J. J., *Molecular Pharmaceutics* **2009**, *6*. 1402-1408.

52. Balasubramanian, P., Lang, J. C., Jatana, K. R., Miller, B., Ozer, E., Old, M., Schuller, D. E., Agrawal, A., Teknos, T. N., Summers, T. A., Jr., Lustberg, M. B., Zborowski, M., Chalmers, J. J., *Plos One* **2012**, *7*.

53. Farace, F., Massard, C., Vimond, N., Drusch, F., Jacques, N., Billiot, F., Laplanche, A., Chauchereau, A., Lacroix, L., Planchard, D., Le Moulec, S., Andre, F., Fizazi, K., Soria, J. C., Vielh, P., *British Journal of Cancer* **2011**, *105*. 847-853.

54. Zheng, S., Lin, H., Liu, J. Q., Balic, M., Datar, R., Cote, R. J., Tai, Y. C., *J. Chromatogr. A* **2007**, *1162*. 154-161.

55. Xu, T., Lu, B., Tai, Y., Goldkorn, A., *Cancer Research* **2010**, *70*. 6420-6428.

56. Lin, H. K., Zheng, S., Williams, A. J., Balic, M., Groshen, S., Scher, H. I., Fleisher, M., Stadler, W., Datar, R. H., Tai, Y.-C., Cote, R. J., *Clin. Cancer Res.* **2010**, *16*. 5011-5018.

57. Hosokawa, M., Hayata, T., Fukuda, Y., Arakaki, A., Yoshino, T., Tanaka, T., Matsunaga, T., *Anal. Chem.* **2010**, *82*. 6629-6635.

58. Muller, V., Stahmann, N., Riethdorf, S., Rau, T., Zabel, T., Goetz, A., Janicke, F., Pantel, K., *Clin. Cancer Res.* **2005**, *11*. 3678-3685.

59. Wang, N., Shi, L., Li, H., Hu, Y., Du, W., Liu, W., Zheng, J. e., Huang, S., Qu, X., *Tumor Biology* **2012**, *33*. 561-569.

60. Gupta, V., Jafferji, I., Garza, M., Melnikova, V. O., Hasegawa, D. K., Pethig, R., Davis, D. W., *Biomicrofluidics* **2012**, *6*.

61. Sun, J. S., Li, M. M., Liu, C., Zhang, Y., Liu, D. B., Liu, W. W., Hu, G. Q., Jiang, X. Y., *Lab Chip* **2012**, *12*. 3952-3960.

62. Gossett, D. R., Weaver, W. M., Mach, A. J., Hur, S. C., Tse, H. T. K., Lee, W., Amini, H., Di Carlo, D., *Anal. Bioanal. Chem.* **2010**, *397*. 3249-3267.

63. Sieuwerts, A. M., Kraan, J., Bolt, J., van der Spoel, P., Elstrodt, F., Schutte, M., Martens, J. W. M., Gratama, J. W., Sleijfer, S., Foekens, J. A., *J. Natl. Cancer Inst.* **2009**, *101*. 61-66.

64. Riethdorf, S., Mueller, V., Zhang, L., Rau, T., Loibl, S., Komor, M., Roller, M., Huober, J., Fehm, T., Schrader, I., Hilfrich, J., Holms, F., Tesch, H., Eidtmann, H., Untch, M., von Minckwitz, G., Pantel, K., *Clin. Cancer Res.* **2010**, *16*. 2634-2645.

65. Hoshino, K., Huang, Y.-Y., Lane, N., Huebschman, M., Uhr, J. W., Frenkel, E. P., Zhang, X., *Lab Chip* **2011**, *11*. 3449-3457.

66. Nagrath, S., Sequist, L. V., Maheswaran, S., Bell, D. W., Irimia, D., Ulkus, L., Smith, M. R., Kwak, E. L., Digumarthy, S., Muzikansky, A., Ryan, P., Balis, U. J., Tompkins, R. G., Haber, D. A., Toner, M., *Nature* **2007**, *450*. 1235-1239.

67. Stott, S. L., Hsu, C. H., Tsukrov, D. I., Yu, M., Miyamoto, D. T., Waltman, B. A., Rothenberg, S. M., Shah, A. M., Smas, M. E., Korir, G. K., Floyd, F. P., Gilman, A. J., Lord, J. B., Winokur, D., Springer, S., Irimia, D., Nagrath, S., Sequist, L. V., Lee, R. J., Isselbacher, K. J., Maheswaran, S., Haber, D. A., Toner, M., *Proceedings of the National Academy of Sciences of the United States of America* **2010**, *107*. 18392-18397.

68. Wang, S. T., Liu, K., Liu, J. A., Yu, Z. T. F., Xu, X. W., Zhao, L. B., Lee, T., Lee, E. K., Reiss, J., Lee, Y. K., Chung, L. W. K., Huang, J. T., Rettig, M., Seligson, D., Duraiswamy, K. N., Shen, C. K. F., Tseng, H. R., *Angew. Chem.-Int. Edit.* **2011**, *50*. 3084-3088.

69. Gleghorn, J. P., Pratt, E. D., Denning, D., Liu, H., Bander, N. H., Tagawa, S. T., Nanus, D. M., Giannakakou, P. A., Kirby, B. J., *Lab Chip* **2010**, *10*. 27-29.

70. Gorges, T. M., Tinhofer, I., Drosch, M., Rose, L., Zollner, T. M., Krahn, T., von Ahsen, O., *BMC Cancer* **2012**, *12*.

71. Alix-Panabieres, C., Pantel, K., *Clin. Chem.* **2013**, *59*. 110-118.

72. Guetta, E., Simchen, M. J., Mammon-Daviko, K., Gordon, D., Aviram-Goldring, A., Rauchbach, N., Barkai, G., *Stem Cells Dev.* **2004**, *13*. 93-99.

73. Oudejans, C. B. M., Tjoa, M. L., Westerman, B. A., Mulders, M. A. M., Van Wijk, I. J., Van Vugt, J. M. G., *Prenat. Diagn.* **2003**, *23*. 111-116.

74. Al-Hajj, M., Wicha, M. S., Benito-Hernandez, A., Morrison, S. J., Clarke, M. F., *Proceedings of the National Academy of Sciences of the United States of America* **2003**, *100*. 3983-3988.

75. Reya, T., Morrison, S. J., Clarke, M. F., Weissman, I. L., *Nature* **2001**, *414*. 105-111.

76. Schiro, P. G., Zhao, M., Kuo, J. S., Koehler, K. M., Sabath, D. E., Chiu, D. T., *Angew. Chem.-Int. Edit.* **2012**, *51*. 4618-4622.

77. Lorenz, R. M., Fiorini, G. S., Jeffries, G. D. M., Lim, D. S. W., He, M., Chiu, D. T., *Anal. Chim. Acta* **2008**, *630*. 124-130.

78. Edgar, J. S., Milne, G., Zhao, Y. Q., Pabbati, C. P., Lim, D. S. W., Chiu, D. T., *Angew. Chem.-Int. Edit.* **2009**, *48*. 2719-2722.

79. Jeffries, G. D. M., Lorenz, R. M., Chiu, D. T., *Anal. Chem.* **2010**, *82*. 9948-9954.

80. Kahn, H. J., Presta, A., Yang, L. Y., Blondal, J., Trudeau, M., Lickley, L., Holloway, C., McCready, D. R., Maclean, D., Marks, A., *Breast Cancer Res. Treat.* **2004**, *86*. 237-247.

81. Zhao, Y., Schiro, P. G., Kuo, J., Ng, L., Chiu, D. T., *Anal. Chem.* **2008**, *81*. 1285-1290.

82. Aktas, B., Tewes, M., Fehm, T., Hauch, S., Kimmig, R., Kasimir-Bauer, S., *Breast Cancer Res.* **2009**, *11*.

83. Balasubramanian, P., Yang, L., Lang, J. C., Jatana, K. R., Schuller, D., Agrawal, A., Zborowski, M., Chalmers, J. J., *Molecular Pharmaceutics* **2009**, *6*. 1402-1408.

84. Jaggupilli, A., Elkord, E., *Clinical & Developmental Immunology* **2012**.

85. Schiro, P. G., Kuyper, C. L., Chiu, D. T., *Electrophoresis* **2007**, *28*. 2430-2438.

86. Fiorini, G. S., Chiu, D. T., *Biotechniques* **2005**, *38*. 429-446.

87. Hulme, S. E., Shevkoplyas, S. S., Whitesides, G. M., *Lab Chip* **2009**, *9*. 79-86.

88. Lee, S., Goedert, M., Matyska, M., Ghandehari, E., Vijay, M., Pesek, J., *Journal of Micromechanics and Microengineering* **2008**, *18*.

89. Li, P., Stratton, Z. S., Dao, M., Ritz, J., Huang, T. J., *Lab Chip* **2013**, *13*. 602-609.

90. Ozkumur, E., Shah, A. M., Ciciliano, J. C., Emmink, B. L., Miyamoto, D. T., Brachtel, E., Yu, M., Chen, P.-i., Morgan, B., Trautwein, J., Kimura, A., Sengupta, S., Stott, S. L., Karabacak, N. M., Barber, T. A., Walsh, J. R., Smith, K., Spuhler, P. S., Sullivan, J. P., Lee, R. J., Ting, D. T., Luo, X., Shaw, A. T., Bardia, A., Sequist, L. V., Louis, D. N., Maheswaran, S., Kapur, R., Haber, D. A., Toner, M., *Science Translational Medicine* **2013**, *5*. 179ra147.

91. Payne, R. E., Yaguee, E., Slade, M. J., Apostolopoulos, C., Jiao, L. R., Ward, B., Coombes, R. C., Stebbing, J., *Pharmacogenomics* **2009**, *10*. 51-57.

92. Zhao, M., Schiro, P. G., Kuo, J. S., Koehler, K. M., Sabath, D. E., Popov, V., Feng, Q., Chiu, D. T., *Anal. Chem.* **2013**, *85*. 2465-2471.

93. Martin, R. M., Leonhardt, H., Cardoso, M. C., *Cytometry Part A* **2005**, *67A*. 45-52.

94. Singh, R., Bandyopadhyay, D., *Cancer Biol. Ther.* **2007**, *6*. 481-486.

95. Holz, C., Niehr, F., Boyko, M., Hristozova, T., Distel, L., Budach, V., Tinhofer, I., *Radiotherapy and Oncology* **2011**, *101*. 158-164.

96. Alsalameh, S., Amin, R., Gemba, T., Lotz, M., *Arthritis and Rheumatism* **2004**, *50*. 1522-1532.

97. Issadore, D., Chung, J., Shao, H., Liong, M., Ghazani, A. A., Castro, C. M., Weissleder, R., Lee, H., *Science Translational Medicine* **2012**, *4*.

98. Adams, A. A., Okagbare, P. I., Feng, J., Hupert, M. L., Patterson, D., Goettert, J., McCarley, R. L., Nikitopoulos, D., Murphy, M. C., Soper, S. A., *Journal of the American Chemical Society* **2008**, *130*. 8633-8641.

99. Dharmasiri, U., Njoroge, S. K., Witek, M. A., Adebiyi, M. G., Kamande, J. W., Hupert, M. L., Barany, F., Soper, S. A., *Anal. Chem.* **2011**, *83*. 2301-2309.

100. Hsieh, H. B., Marrinucci, D., Bethel, K., Curry, D. N., Humphrey, M., Krivacic, R. T., Kroener, J., Kroener, L., Ladanyi, A., Lazarus, N., Kuhn, P., Bruce, R. H., Nieva, J., *Biosens. Bioelectron.* **2006**, *21*. 1893-1899.

101. Cima, I., Yee, C. W., Iliescu, F. S., Phyo, W. M., Lim, K. H., Iliescu, C., Tan, M. H., *Biomicrofluidics* **2013**, *7*.

102. Dong, Y., Skelley, A. M., Merdek, K. D., Sprott, K. M., Jiang, C., Pierceall, W. E., Lin, J., Stocum, M., Carney, W. P., Smirnov, D. A., *Journal of Molecular Diagnostics* **2013**, *15*. 149-157.

103. Goda, K., Ayazi, A., Gossett, D. R., Sadasivam, J., Lonappan, C. K., Sollier, E., Fard, A. M., Hur, S. C., Adam, J., Murray, C., Wang, C., Brackbill, N., Di Carlo, D., Jalali, B., *Proceedings of the National Academy of Sciences of the United States of America* **2012**, *109*. 11630-11635.

104. Schiro, P. G., Gadd, J. C., Yen, G. S., Chiu, D. T., *J. Phys. Chem. B* **2012**, *116*. 10490-10495.

105. Shirasaki, Y., Tanaka, J., Makazu, H., Tashiro, K., Shoji, S., Tsukita, S., Funatsu, T., *Anal. Chem.* **2006**, *78*. 695-701.

106. Yagublu, V., Ahmadova, Z., Hafner, M., Keese, M., *In Vivo* **2012**, *26*. 599-607.

107. Krivacic, R. T., Ladanyi, A., Curry, D. N., Hsieh, H. B., Kuhn, P., Bergsrud, D. E., Kepros, J. F., Barbera, T., Ho, M. Y., Chen, L. B., Lerner, R. A., Bruce, R. H., *Proceedings of the National Academy of Sciences of the United States of America* **2004**, *101*. 10501-10504.

108. Stott, S. L., Lee, R. J., Nagrath, S., Yu, M., Miyamoto, D. T., Ulkus, L., Inserra, E. J., Ulman, M., Springer, S., Nakamura, Z., Moore, A. L., Tsukrov, D. I., Kempner, M. E., Dahl, D. M., Wu, C.-L., Iafrate, A. J., Smith, M. R., Tompkins, R. G., Sequist, L. V., Toner, M., Haber, D. A., Maheswaran, S., *Science Translational Medicine* **2010**, *2*.

109. Daugherty, P. S., Iverson, B. L., Georgiou, G., *Journal of Immunological Methods* **2000**, *243*. 211-227.

110. Bottcher, S., Ritgen, M., Pott, C., Bruggemann, M., Raff, T., Stilgenbauer, S., Dohner, H., Dreger, P., Kneba, M., *Leukemia* **2004**, *18*. 1637-1645.

Vita

2008-2012 Graduate student

Department of Chemistry, University of Washington, Seattle

2006-2008 M.S.

Department of Chemistry, Tsinghua University, Beijing

2002-2006 B.S.

Department of Chemistry, Tsinghua University, Beijing

Publication since 2008

[1] **Zhao, M**., Schiro, P. G., Kuo, J. S., Koehler, K. M., Sabath, D. E., Popov, V., Feng, Q., Chiu, D. T., *Anal. Chem.* 2013, *85*. 2465-2471.

Highlighed by:

C&EN April 2013 91 (15) 28-29.

C&EN Febuary 2013: http://cen.acs.org/articles/91/web/2013/02/Counting-Cancer-Cells-Quickly.html

[2] Schiro, P. G.*, **Zhao, M**.*, Kuo, J. S., Koehler, K. M., Sabath, D. E., Chiu, D. T., *Angew. Chem. Int. Edit.* 2012, *51*. 4618-4622. (* These authors contributed equally to this work.)

VIP paper and cover story

Press release: http://www.wiley.com/WileyCDA/PressRelease/pressReleaseId-102699.html

Highlighed by:

C&EN April 2013 91 (15) 28-29.

Science, 335, 1410.